CONFIDENTIAL

NACA

RESEARCH MEMORANDUM

THE ROLLING MOMENT DUE TO SIDESLIP OF SWEPT WINGS AT SUBSONIC AND TRANSONIC SPEEDS

By Edward C. Polhamus and William C. Sleeman, Jr.

Langley Aeronautical Laboratory
Langley Field, Va.

NATIONAL ADVISORY COMMITTEE
FOR AERONAUTICS

WASHINGTON

March 8, 1955

CONFIDENTIAL

NACA RM L54L01

NATIONAL ADVISORY COMMITTEE FOR AERONAUTICS

RESEARCH MEMORANDUM

THE ROLLING MOMENT DUE TO SIDESLIP OF SWEPT WINGS AT SUBSONIC AND TRANSONIC SPEEDS

By Edward C. Polhamus and William C. Sleeman, Jr.

SUMMARY

A summary and analysis has been made of results obtained in a systematic research program concerned with the effects of wing sweep, aspect ratio, taper ratio, and dihedral on the rolling moment due to sideslip characteristics of wing-fuselage configurations up to Mach numbers of about 0.95. Other test results are presented to show trends of rolling moment due to sideslip with Mach number for a few wings in the transonic and supersonic speed range.

In view of the need for reliable procedures for estimating rolling moment due to sideslip at high subsonic speeds, new methods have been derived and design charts are presented for estimating the effects of compressibility and wing geometry. The overall agreement between estimated and experimental results indicated that the effects of wing aspect ratio, taper ratio, sweep, and dihedral on the rolling moment due to sideslip of wing-fuselage configurations for sideslip angles up to $\pm 5^{\circ}$ could be estimated with reasonable accuracy up to the force-break Mach number at low lift coefficients.

INTRODUCTION

A systematic research program has been conducted in the Langley high-speed 7- by 10-foot tunnel to study effects of wing geometry on the aerodynamic characteristics of wing-body combinations at high subsonic speeds. This program included effects of sweepback, aspect ratio, taper ratio, and geometric dihedral on the lateral aerodynamic characteristics for Mach numbers up to about 0.95. In order to expedite publication of these data, each series was published separately (refs. 1 to 6) with only a limited analysis of the data. However, these limited analyses indicated, as does reference 7, the need for more reliable methods of

predicting the rolling moment due to sideslip which, for wings of current interest, may be the most important of the lateral derivatives. The purpose of this paper therefore is to summarize and analyze the results for the rolling moment due to sideslip of the aforementioned general research program and to develop new methods of estimating the derivative. In addition, experimental data from other sources will be utilized where needed.

COEFFICIENTS AND SYMBOLS

The stability system of axes (axes yaw but do not pitch with model) was used and moments are referred to the quarter-chord point of the mean aerodynamic chord.

C_L lift coefficient, Lift/qS

C_l rolling-moment coefficient, Rolling moment/qSb

c_l section lift coefficient

q dynamic pressure, $\rho V^2/2$, lb/sq ft

V free-stream velocity, ft/sec

ρ mass density of air, slugs/cu ft

S wing area, sq ft

b wing span, ft

α angle of attack, radians (except where noted)

β angle of sideslip, radians (except where noted)

Γ dihedral angle, deg; also circulation strength (appendix B)

Λ angle of sweepback of quarter-chord line, deg (except where noted)

M Mach number

R Reynolds number

A wing aspect ratio, b^2/S

λ wing taper ratio, Tip chord/Root chord

$$a_o = \frac{\partial c_l}{\partial \alpha}$$

$$C_{L_\alpha} = \frac{\partial C_L}{\partial \alpha}$$

C_{l_β} rolling moment due to sideslip, $\frac{\partial c_l}{\partial \beta}$

$$C_{l_{\beta_{C_L}}} = \frac{\partial\left(\frac{\partial c_l}{\partial \beta}\right)}{\partial C_L}$$

$$C_{l_{\beta_\Gamma}} = \frac{\partial\left(\frac{\partial c_l}{\partial \beta}\right)}{\partial \Gamma}$$

$$K_{\Gamma/p} = C_{l_{\beta_\Gamma}} \Big/ C_{l_p}$$

$$C_{l_p} = \frac{\partial c_l}{\partial\left(\frac{pb}{2V}\right)}$$

p rolling velocity, radians/sec

D maximum fuselage diameter, ft

l_f fuselage length ahead of wing-tip half-chord point, ft

t wing airfoil thickness, ft

c wing chord, ft

y spanwise distance to lateral center of pressure, ft

y_b spanwise distance to sweep discontinuity, ft

y' spanwise distance to center of horseshoe vortex, ft

$B = \sqrt{1 - M^2}$

Subscripts:

w	wing alone
wf	wing-fuselage combination
R	right wing panel
L	left wing panel
Λ	portion due to sweep
A	portion due to aspect ratio
Γ	portion due to geometric dihedral

SCOPE OF EXPERIMENTS AND ANALYSIS

The range of wing plan forms investigated in the Langley high-speed 7- by 10-foot tunnel over a Mach number range from 0.40 to approximately 0.95 is shown in figure 1 and a photograph showing one of the models mounted on the support sting is given as figure 2. In addition to the plan-form variations indicated in figure 1, results are presented for wings of aspect ratio 4 and taper ratio 0.6 having quarter-chord sweep angles of 3.6° and 45° for which the dihedral was varied over a range of $\pm 10^\circ$. Except where noted, all wings had NACA 65A006 airfoil sections in the stream direction. All the wings were tested on the same fuselage and, with the exception of the aspect-ratio-4 60° swept wing, (ref. 1) were positioned on the fuselage such that the 25-percent mean aerodynamic chord was at the same fuselage station. The variation with Mach number of mean test Reynolds number based on the mean aerodynamic chord for these investigations is given in figure 3. Details of the models and tests can be found in references 1 to 6.

The scope of composite M- and W-wing plan forms tested at low speed in the Langley 300-MPH 7- by 10-foot tunnel is given in figure 4. The basic results of this plan form study are unpublished. Results of some high-speed tests of an M-wing plan form presented in this paper were obtained from reference 8.

Results from other test facilities have been included in this paper for comparison with estimates at low speed and for indicating trends that would be expected near a Mach number of unity where theoretical

estimates would not be expected to be reliable. Reference to these results will be made as they are discussed. A summary of geometric characteristics of the wing plan forms included in the experimental results is presented in table I.

Comparison of the test results presented in references 1 to 5 with estimates based on existing theory has shown the need for more reliable methods of predicting the rolling moment due to sideslip with regard to both the magnitude and variation with Mach number. This paper presents design charts and a summary of methods for estimating the various component effects contributing to the overall rolling moment due to sideslip based on existing relationships where applicable and on new methods derived herein. Inasmuch as the discussion of test results at low lift is concerned to a large extent with the comparison with estimated results, the development of theoretical estimates will be treated prior to the discussion of the experimental results.

THEORETICAL METHODS

The rolling moment due to sideslip is considered to be composed of several parts and since estimates of all these parts are not included in this paper, the overall expression will be summarized first for convenience and the reader is referred to the references and following sections for evaluation and discussion of the various components. For example, the present paper is concerned only with midwing arrangements inasmuch as the experimental results summarized herein consisted entirely of midwing configurations. The effect of wing height can be estimated by use of references 7 and 9.

The rolling moment due to sideslip for a midwing configuration (no tail contribution included) is considered to be composed of the components appearing in the following expression:

$$C_{l_\beta} = C_L\left[\left(C_{l_{\beta_{C_L}}}\right)_\Lambda K_{M_\Lambda} K_f + \left(C_{l_{\beta_{C_L}}}\right)_A\right] + \Gamma\left(C_{l_{\beta_\Gamma}} K_{M_\Gamma} + \Delta C_{l_{\beta_\Gamma}}\right)$$

where

$\left(C_{l_{\beta_{C_L}}}\right)_\Lambda$ component primarily associated with wing sweep (fig. 6)

K_{M_Λ} compressibility correction to sweep contribution (fig. 11)

K_f fuselage effect (fig. 7)

$\left(C_{l_{\beta_{C_L}}}\right)_A$ aspect-ratio effect at zero sweep (fig. 8)

$C_{l_{\beta_\Gamma}}$ dihedral effect (ref. 10 or 11)

K_{M_Γ} compressibility correction to dihedral effect (fig. 12)

$\Delta C_{l_{\beta_\Gamma}}$ effect of fuselage on transverse flow (eq.(5))

All the design charts presented in this paper concerned with effects of wing sweep are given as a function of the half-chord sweep angle to minimize effects of taper ratio as shown in appendix A. Since the most commonly used sweep reference line is the quarter chord, a chart has been prepared from which the half-chord sweep can be easily obtained from the quarter-chord sweep, aspect ratio, and taper ratio. For convenience in locating this chart, it has been placed at the end of the figures (fig. 29).

Effect of Sweep Angle

Infinite aspect ratio.- In the analysis of effects of wing sweep on the rolling moment due to sideslip, determination of the expression for an infinite-aspect-ratio wing is of interest as a limiting case for wings of finite aspect ratio. The sweep effect on rolling moment due to sideslip for a wing of infinite aspect ratio can be assumed to arise entirely from lift increments associated with the difference in effective sweep angle on the leading and trailing wing panels in sideslip. The leading wing is considered to have a lower effective sweep $(\Lambda - \beta)$ and, consequently, a higher lift slope; conversely, the trailing wing panel has a higher effective sweep $(\Lambda + \beta)$ and a lower lift slope than at zero sideslip. The rolling moment due to sideslip for an infinite-aspect-ratio swept wing may be derived by replacing the sweep angle with effective sweep angle $(\Lambda \pm \beta)$ and differentiating the expression for lift with respect to sideslip. The total rolling moment can be expressed as

$$C_l = \left(c_l \frac{y}{b}\right)_L + \left(c_l \frac{y}{b}\right)_R$$

where

$$(c_l)_L = \frac{2\pi\alpha \cos(\Lambda + \beta)}{2}$$

and

$$(c_l)_R = \frac{2\pi\alpha \cos(\Lambda - \beta)}{2}$$

and angles are in radians. The expressions for c_l represent one-half the lift of two infinite-aspect-ratio swept wings having sweep angles of $(\Lambda + \beta)$ and $(\Lambda - \beta)$. For small angles of sideslip, $\sin \beta \approx \beta$ and $\cos \beta \approx 1$; then

$$(c_l)_L = \frac{2\pi\alpha(\cos \Lambda - \beta \sin \Lambda)}{2}$$

$$(c_l)_R = \frac{2\pi\alpha(\cos \Lambda + \beta \sin \Lambda)}{2}$$

Differentiating with respect to β gives

$$(c_{l_\beta})_{L,R} = \mp \frac{2\pi\alpha \sin \Lambda}{2}$$

Then

$$C_{l_\beta} = 2\pi\alpha\left[-\left(\frac{\sin \Lambda}{2}\frac{y}{b}\right)_L + \left(\frac{\sin \Lambda}{2}\frac{y}{b}\right)_R\right]$$

Since the lift acts at the midsemispan and y/b is positive for the left panel and negative for the right panel,

$$C_{l_\beta} = 2\pi\alpha\left(-\frac{\sin \Lambda}{4}\right)$$

Substituting $c_l/2\pi \cos \Lambda$ for α and converting angles to degrees gives

$$C_{l_\beta} = -c_l \frac{\tan \Lambda}{4(57.3)} \tag{1}$$

Equation (1) is the well-known expression for the infinite-aspect-ratio case. This relationship can also be obtained by differentiation of the lift expression with respect to sweep angle since C_{l_β} for infinite aspect ratio is due only to lift differences associated with the different sweep angles on the leading and trailing wing panels. Inasmuch as this procedure is not applicable to the finite-aspect-ratio case because the lift differences are associated with both the panel sweep and aspect ratio, it was not used in the two-dimensional case.

It can be easily shown furthermore that equation (1) can be obtained by differentiating the lift expression for either wing panel (for example $c_l = 2\pi\alpha \cos(\Lambda + \beta)$) with proper regard for moment-arm sign conventions and this procedure will be used for simplicity in the derivation for the finite-aspect-ratio case.

Finite aspect ratio.- For the determination of the effect of sweep on finite-aspect-ratio wings, the same concepts regarding effective sweep angle of the leading and trailing wing panels in sideslip may be used as for the infinite-aspect-ratio case; however, other factors must be considered. The loss in lift, for example, on the trailing wing panel in sideslip occurs not only from the increased sweep $(\Lambda + \beta)$ on this panel but also from the reduced geometric panel aspect ratio $\frac{A \cos^2(\Lambda + \beta)}{\cos^2\Lambda}$ relative to the unyawed wing panel. Furthermore, because the increment of lift distribution resulting from sideslip is antisymmetrical, the aerodynamic induction effects would be similar to a wing having half the panel aspect ratio of the yawed panel. It is therefore assumed that the lift on the trailing panel of a swept wing in sideslip is the same as the lift (C_L^*) of a wing at zero sideslip whose aspect ratio and sweep are given by

$$A^* = \frac{A}{2} \frac{\cos^2(\Lambda + \beta)}{\cos^2\Lambda}$$

$$\Lambda^* = \Lambda + \beta$$

Derivation of the rolling moment due to sideslip for the finite-aspect-ratio case is made in the same manner as for the infinite-aspect-ratio case with the aforementioned additional effects considered.

The derivation of a very simple expression for the lift-curve slope of finite-aspect-ratio wings is described in appendix A which gives results that are in excellent agreement with lifting-surface solutions. Equation A6 of appendix A is therefore used in the rolling-moment derivation for finite-aspect-ratio wings. At zero Mach number equation (A6) becomes

$$C_{L_\alpha} = \frac{2\pi A}{2 + \sqrt{4 + \left(\frac{A}{\cos \Lambda}\right)^2}} \tag{2}$$

By accounting for effects of sideslip on the aspect ratio, sweep, and induction effects of a trailing wing panel, an expression for the lift can be obtained from equation (2).

$$C_L{}^* = \frac{\alpha 2\pi A^*}{2 + \sqrt{4 + \left(\frac{A^*}{\cos \Lambda^*}\right)^2}}$$

Substituting A^* and Λ^* into the preceding expression gives

$$C_L{}^* = \frac{\alpha 2\pi \frac{A}{2} \frac{\cos^2(\Lambda + \beta)}{\cos^2 \Lambda}}{2 + \sqrt{4 + \frac{A^2}{4} \frac{\cos^2(\Lambda + \beta)}{\cos^4 \Lambda}}}$$

which reduces to

$$C_L{}^* = \frac{\alpha 2\pi \frac{A}{2}\left(1 - 2\beta \tan \Lambda\right)}{2 + \sqrt{4 + \frac{A^2}{4}\left(\frac{1}{\cos^2 \Lambda} - \frac{2\beta \tan \Lambda}{\cos^2 \Lambda}\right)}} \tag{3}$$

by dropping second-order terms of β and taking $\sin \beta \approx \beta$ and $\cos \beta \approx 1$. The quantity C_L^* is considered the lift coefficient of a fictitious wing whose sweep angle is Λ^* and whose aspect ratio is A^*. As pointed out in the derivation for infinite aspect ratio, the rolling moment can be derived from the lift expression for either wing panel in sideslip and differentiation of equation (3) therefore gives the following expression:

$$C_{L_\beta}{}^* = -\frac{2\pi \frac{A}{2} \alpha}{2 + \sqrt{4 + \frac{A^2}{4 \cos^2 \Lambda}}} \left[2 \tan \Lambda - \frac{\frac{A^2 2 \tan \Lambda}{4 \cos^2 \Lambda}}{2\sqrt{4 + \frac{A^2}{4 \cos^2 \Lambda}} \left(2 + \sqrt{4 + \frac{A^2}{4 \cos^2 \Lambda}} \right)} \right]$$

Substituting for angle of attack by using the relationships of equation (2) for the complete wing gives

$$C_{L_\beta}{}^* = -C_L \tan \Lambda \frac{2 + \sqrt{4 + \left(\frac{A}{\cos \Lambda} \right)^2}}{2 + \sqrt{4 + \frac{1}{4}\left(\frac{A}{\cos \Lambda} \right)^2}} \left[1 - \frac{\frac{1}{8}\left(\frac{A}{\cos \Lambda} \right)^2}{4 + \frac{1}{4}\left(\frac{A}{\cos \Lambda} \right)^2 + 2\sqrt{4 + \frac{1}{4}\left(\frac{A}{\cos \Lambda} \right)^2}} \right]$$

The rolling moment due to sideslip associated with wing sweep is then

$$\left(C_{l_{\beta C_L}} \right)_\Lambda = -\frac{1}{2} \tan \Lambda \frac{y}{b/2} \frac{2 + \sqrt{4 + \left(\frac{A}{\cos \Lambda} \right)^2}}{2 + \sqrt{4 + \frac{1}{4}\left(\frac{A}{\cos \Lambda} \right)^2}} \left[1 - \frac{\frac{1}{8}\left(\frac{A}{\cos \Lambda} \right)^2}{4 + \frac{1}{4}\left(\frac{A}{\cos \Lambda} \right)^2 + 2\sqrt{4 + \frac{1}{4}\left(\frac{A}{\cos \Lambda} \right)^2}} \right] \quad (4)$$

Where $\frac{y}{b/2}$ is the spanwise lateral center of pressure which, if small angles of sideslip are assumed, can be estimated from reference 12.

Estimates of the sweep contribution to rolling moment due to sideslip are presented in the upper portion of figure 5 for wings of aspect ratio 4 as a function of sweep angle and in the lower portion of figure 5 for 60° swept wings of various aspect ratios. Estimated effects of sweep are compared with results obtained from 20-vortex, modified lifting-line solutions described in appendix B and the estimated variation with aspect ratio is compared with wing-alone experimental results for the 60° swept wings of reference 13. These experimental points in the lower portion of figure 5 were obtained by subtracting the theoretical values (of aspect-ratio contribution) for unswept wings given in figure 23 of reference 14 from the experimental values given in reference 13 for the 60° swept wings.

Comparison of the estimated results of equation (4) and reference 14 in figure 5 indicates rather large differences between the two methods for aspect-ratio-4 wings having appreciable sweep and at all aspect ratios for the 60° swept wings. Estimates obtained from equation (4) are in fairly good agreement with experiment for the 60° swept wing whereas estimates from reference 14 predicted only about two-thirds the value for this wing at a given aspect ratio. The same observations can be made regarding the two estimates when they are compared with the 20-vortex solutions for the aspect-ratio-4 wings.

Inasmuch as the method developed in this paper appears to afford reliable estimates of the sweep contribution to rolling moment due to sideslip, design charts presented in figure 6 have been prepared by using equation (4) and values of the lateral center of pressure from reference 12. The sweep of the half chord was used in figure 6 in order to minimize any effects other than the effect on the lateral center of pressure that taper ratio might have (taper effects on lift-curve slopes are discussed more fully in appendix A).

The rather large differences shown between the present estimates and those of reference 14 appear to be associated with the basic assumptions regarding effects of asymmetrical panel aspect ratio on the yawed wing. In reference 14 this effect was assumed to apply only to the increment of lift on each panel due to sideslip whereas in equation (4) the asymmetrical panel aspect-ratio effect was assumed to apply to the total lift loading rather than only the lift increment due to sideslip. The two assumptions are illustrated in the following sketches:

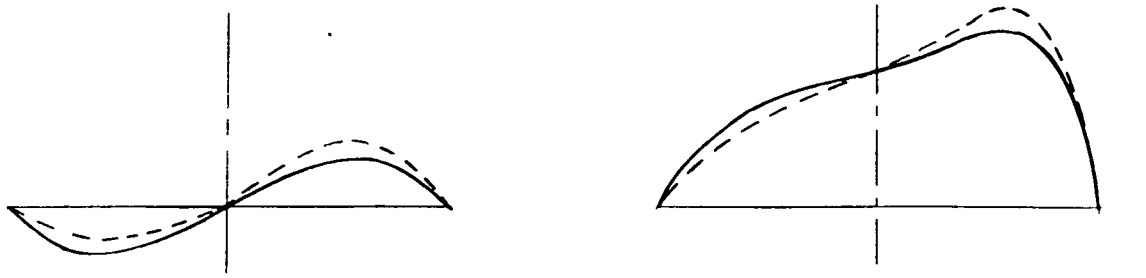

(a) Incremental load distribution due to sideslip.

(b) Total load distribution in sideslip.

In both sketches, the aspect-ratio effect tends to increase the loading on the leading wing (wing panel with the highest aspect ratio) and decrease the loading on the trailing wing in sideslip. Effects of these loading changes on rolling moment are different, however, for the incremental (sketch (a)) and the total loading (sketch (b)). In the derivations of reference 14, the effects of asymmetric panel aspect ratio on incremental loading were found negligible and therefore terms associated with this effect were dropped. Sketch (a) shows that even if these aspect-ratio effects on the incremental loading of each panel were large, they would counteract each other. It would seem reasonable, however, that any change in effective panel aspect ratio would produce changes in the loads associated with both total angle of attack and sideslip (sketch (b)) and not just the antisymmetrical load associated with sideslip. When this aspect-ratio effect is applied to the total load, the effect on each panel is, of course, greater since the total load is greater than the load due to sideslip and they are additive as illustrated in sketch (b). This effect accounts for the larger values of $Cl_{\beta C_L}$ given by the present method when compared with those of reference 14.

Effect of fuselage flow field.- The preceding theoretical determination of $\left(C_{l_{\beta C_L}}\right)_\Lambda$ was for the sweep contribution of the wing alone; however, experimental results with and without a fuselage consistently indicated smaller values of rolling moment due to sideslip even when the wing was mounted on the fuselage center line. Therefore, in addition to the well-known effect of wing height (refs. 7 and 9), there appears to be an additional effect of the fuselage. A possible explanation of this additional fuselage effect is indicated in figure 7(a) which illustrates the possible reduction in effective sideslip angle over the wing caused by the presence of the fuselage. For the wing alone, each wing panel would be at an effective sideslip equal to the geometric sideslip angle as in the top portion of figure 7(a) whereas for the wing-fuselage configuration the fuselage would be expected to aline the flow field in the direction to decrease the effective sideslip. An attempt to correct for this fuselage effect has been made by using experimental data from references 15, 16, and 17, and the results are presented in figure 7(b) as a function of the ratio of fuselage length ahead of the wing-tip half chord to wing span. The relationship used to derive K_f and a summary of pertinent model geometry with appropriate references are also given in figure 7(b). The fuselage length was considered the main variable in the determination of K_f inasmuch as the only systematic investigation available (ref. 17) indicated that the fuselage length had a fairly large effect on the rolling moment due to sideslip. Other parameters such as the ratio of fuselage diameter to wing span should also be important; however, the range of this parameter studied is too limited to evaluate adequately. With regard to use of the wing-tip half-chord point in the correlation of figure 7, selection of this point was rather arbitrary and was based only on the importance of the half-chord sweep and the fact that the load at the wing tip has the longest moment arm. The most accurate correlation point undoubtedly would be a function of wing plan form and fuselage shape and probably would be located somewhat inboard of the tip; however, these refinements could not be determined from the limited data available. Considerably more research is needed with regard to fuselage effects and the correlation presented in figure 7 should be regarded as only an approximate indication of these effects.

Effect of Aspect Ratio

In addition to the effect of aspect ratio on the sweep contribution to the rolling moment due to sideslip, there is an additional aspect-ratio effect which occurs at zero sweep and is assumed to be relatively invariant with sweep angle. This increment, which is designated $\left(C_{l_{\beta C_L}}\right)_A$ in this paper, has been treated theoretically by Weissinger for unswept

wings (see ref. 18). Weissinger's results indicated that $\left(C_{l_{\beta C_L}}\right)_A$ increased approximately linearly with $1/A$ and decreased somewhat with taper. Values of $\left(C_{l_{\beta C_L}}\right)_A$ were determined from reference 18 for a large number of wing plan forms and when combined with the sweep contribution (from fig. 6) showed fair agreement with experiment. The lack of consistently good agreement between the aforementioned estimates and experimental results for wing alone suggested that greater accuracy might be obtained by correlating a large amount of experimental data to obtain $\left(C_{l_{\beta C_L}}\right)_A$. (The difference between experiment and theoretical $\left(C_{l_{\beta C_L}}\right)_A$ was considered to be the aspect-ratio effect $\left(C_{l_{\beta C_L}}\right)_A$. Results of such a correlation obtained from references 13, 19, 20, and 21 and presented in table II and in the upper part of figure 8 for 14 untapered wings of various aspect ratios and sweep angles appear to substantiate the linearity of $\left(C_{l_{\beta C_L}}\right)_A$ with $1/A$ and the assumption that sweep has little effect. The mean line has been replotted for convenience in the lower part of figure 8 as a function of aspect ratio. Also presented is the mean line for zero taper which was obtained in a similar manner.

Effect of Geometric Dihedral

A large number of solutions pertaining to the effect of geometric dihedral on the rolling moment due to sideslip have been obtained by the Weissinger modified lifting-line method and are presented in design charts in terms of $C_{l_{\beta_\Gamma}}$ in references 10 and 11 and therefore will not be repeated here. These solutions are, however, for the wing alone and a correction factor is needed to account for effects of the transverse flow over the yawed fuselage when applying these solutions to wing-fuselage configurations. Now, the effect of this fuselage flow field on the rolling moment of wings without geometric dihedral is well known; however an additional effect is introduced for wings having dihedral. This additional effect is associated with the fact that the vertical position of a wing having dihedral varies along the span relative to the fuselage. A method is suggested in reference 9 by which estimates may be made for a wing with dihedral by replacing it with a wing without dihedral at some effective height relative to the fuselage and evaluating the fuselage flow effect for this equivalent wing. The results of reference 9 show that the equivalent wing will have approximately the same rolling moment due to sideslip if its vertical position relative to the fuselage

coincides with the wing with dihedral at the spanwise position equal to $1.4D/b$ as illustrated in the following sketch.

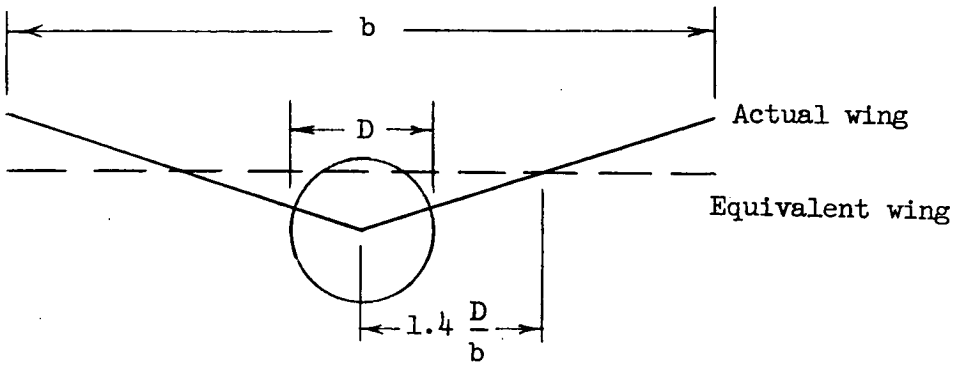

The spanwise position of $1.4D/b$ is considered applicable only for wings with dihedral that intersect the vertical plane of symmetry at or near the midfuselage height. For estimates regarding high- and low-wing configurations, the reader is referred to figure 4 of reference 9.

Inasmuch as the aforementioned fuselage effect is relatively small when compared with the effect of the isolated wing, use of the simple expression for the effect of wing height given in reference 7 should give satisfactory results. This expression for fuselages of circular cross section is

$$\Delta C_{l_\beta} = -1.2 \sqrt{A} \frac{z_w}{b} \frac{2D}{b} \frac{1}{57.3}$$

where z_w is the height above the fuselage center line of an actual wing without dihedral or of an equivalent wing at a height corresponding to the height of the $1.4D/b$ spanwise station of a wing with dihedral as mentioned previously. Therefore, for wings having dihedral

$$z_w = \frac{b}{2} \frac{\Gamma}{57.3} \frac{1.4D}{b}$$

and by substitution

$$\Delta C_{l_{\beta\Gamma}} = -0.0005\sqrt{A}\left(\frac{D}{b}\right)^2 \qquad (5)$$

where β and Γ are in degrees.

Effect of Mach Number

Very little theoretical work has been done with regard to the effects of compressibility on rolling moment due to sideslip at subsonic speeds. Application of the Prandtl-Glauert plan-form transformation which has been useful in determining compressibility effects for other parameters from available incompressible solutions presents difficulties for C_{l_β} because of the resulting asymmetrical wings (transformation must be applied in the sideslip condition) for which incompressible solutions are not readily available. Compressibility corrections for C_{l_β} which are presented in reference 22 appear to be the only theoretical corrections available for this derivative. The results of reference 22 indicate, however, that rolling moment due to sideslip decreases with Mach number for a given lift coefficient; whereas available experimental data indicate an increase with Mach number. (See refs. 1 to 5.) This decrease shown by the theory of reference 22 apparently arises from the fact that only the aerodynamic induction factors were corrected for compressibility effects. However, even for a two-dimensional swept wing where there is no aerodynamic induction, it can be shown that there is a rather large effect of compressibility on the rolling moment due to sideslip. Since the compressibility corrections of reference 22 do not appear to give results consistent with experimental results, new relationships accounting for compressibility effects on rolling moment due to sideslip have been derived for infinite- and finite-aspect-ratio wings in the same manner as for the incompressible case previously discussed.

Infinite aspect ratio.- As shown previously, the rolling moment due to sideslip for an infinite-aspect-ratio wing arises from lift increments associated with differences in effective sweep angle of the leading and trailing wing panels in sideslip. This compressibility effect is due to the fact that the rate of change of lift with sweep angle increases with increasing Mach number. This effect is illustrated in figure 9 where the lift coefficient for unit angle of attack is plotted as a function of sweep angle for Mach numbers of 0 and 0.9. For convenience, the curve representing a Mach number of 0.9 has been reduced proportionally (equivalent to an angle-of-attack change) so that the lift coefficient is independent of Mach number at a sweep angle of 30° (see dashed line in fig. 9). Now, the rolling moment due to sideslip is proportional to the rate of change of lift coefficient with sweep angle and therefore the rolling moment due to sideslip (fig. 9) is considerably higher at a Mach number of 0.9 than at zero Mach number. From another viewpoint, since

the lift on the leading and trailing wing panels are dependent on the Mach number normal to their respective leading edges, the leading wing has a greater compressibility effect $\left(1/\sqrt{1 - M^2\cos^2(\Lambda - \beta)}\right)$ than the trailing wing $\left(1/\sqrt{1 - M^2\cos^2(\Lambda + \beta)}\right)$. Based on the above concepts, effects of compressibility can be included in the derivation of $C_{l_{\beta C_L}}$ for infinite-aspect-ratio swept wings and appropriate compressibility corrections obtained thereby. If the same approach as for the incompressible case, including the effect of Mach number on lift, is made, the following relationships are obtained:

$$\left(c_l\right)_M = \frac{2\pi\alpha \cos(\Lambda + \beta)}{\sqrt{1 - M^2\cos^2(\Lambda + \beta)}} \tag{6}$$

$$\left(c_l\right)_M = \frac{2\pi\alpha(\cos \Lambda - \beta \sin \Lambda)}{\sqrt{1 - M^2\left(\cos^2\Lambda - 2 \cos \Lambda\, \beta\sin\Lambda\right)}}$$

Differentiating with respect to β gives

$$\left(c_{l_\beta}\right)_M = -\frac{2\pi\alpha \sin \Lambda}{\sqrt{1 - M^2\left(\cos^2\Lambda - 2 \cos \Lambda\, \beta\sin\Lambda\right)}}\left[\frac{1 - M^2\cos \Lambda\, \beta\sin\Lambda}{1 - M^2\left(\cos^2\Lambda - 2 \cos \Lambda\, \beta\sin\Lambda\right)}\right]$$

Substituting $\frac{c_l\sqrt{1 - M^2\cos^2\Lambda}}{2\pi \cos \Lambda}$ for α and letting β approach zero as a limit gives

$$\left(c_{l_\beta}\right)_M = \frac{-c_l \tan \Lambda}{1 - M^2\cos^2\Lambda}$$

and

$$\left(C_{l_\beta}\right)_M = -c_l \frac{\tan \Lambda}{4(57.3)\left(1 - M^2\cos^2\Lambda\right)} \tag{7}$$

Comparison of equations (1) and (7) shows that the compressible value differs from the incompressible value for $C_{l_{\beta_{c_l}}}$ by the factor $\frac{1}{1 - M^2\cos^2\Lambda}$ and this factor is plotted in figure 10 to show the large compressibility correction to $C_{l_{\beta_{C_L}}}$ for infinite aspect ratio especially at the lower sweep angles.

As mentioned previously in connection with the incompressible case, $\left(C_{l_\beta}\right)_M$ as given in equation (7) can be easily obtained by differentiating the compressible lift expression (eq. (6) with $\beta = 0$) with respect to sweep; however, the preceding derivation is given in order to be consistent with the finite-aspect-ratio derivation.

Finite aspect ratio.- Derivation of the compressible case for C_{l_β} for finite aspect ratio is treated in the same manner as for the incompressible case. When the same substitutions were made as for the incompressible case in equation (A6) and the Mach number terms included, the compressible counterpart to equation (3) becomes

$$\left(C_L^*\right)_M = \frac{\alpha 2\pi \frac{A}{2}\left(1 - 2\beta \tan \Lambda\right)}{2 + \sqrt{4 + \frac{A^2}{4}\left(\frac{1}{\cos^2\Lambda} - \frac{2\beta \tan \Lambda}{\cos^2\Lambda}\right) - (AM)^2(1 - 2\beta \tan \Lambda)^2}}$$

By differentiation and substitution as before,

$$\left[\left(C_{l_{\beta_{C_L}}}\right)_{\Lambda}\right]_M = -\frac{1}{2}\tan\Lambda\,\frac{y}{b/2}\left(\frac{2+\sqrt{4+\left(\frac{A}{\cos\Lambda}\right)^2}}{2+\sqrt{4+\frac{1}{4}\left(\frac{A}{\cos\Lambda}\right)^2-\frac{1}{4}(AM)^2}}\right)\left[1-\frac{\frac{1}{8}\left(\frac{A}{\cos\Lambda}\right)^2-\frac{1}{4}(AM)^2}{4+\frac{1}{4}\left(\frac{A}{\cos\Lambda}\right)^2-\frac{1}{4}(AM)^2+2\sqrt{4+\frac{1}{4}\left(\frac{A}{\cos\Lambda}\right)^2-\frac{1}{4}(AM)^2}}\right] \quad (8)$$

The compressibility factor for $\left(C_{l_{\beta_{C_L}}}\right)_{\Lambda}$ for finite aspect ratio is obtained from the ratio of equation (8) for a given Mach number to this expression with the terms involving Mach number omitted (eq. 4). Figure 11 presents the compressibility factors thus obtained as a function of the sweep of the half chord and aspect ratio for several Mach numbers. The compressibility effects for finite-aspect-ratio wings presented in figure 11 indicate that $\left(C_{l_{\beta_{C_L}}}\right)_{\Lambda}$ increases appreciably with Mach number for aspect ratios greater than 3 or 4 and moderate sweep angles.

It is interesting to note that results obtained by substituting finite values of sideslip β rather than differentiating with respect to β indicate little effect of sideslip on the compressibility correction, the value for 15° sideslip differing from that for vanishingly small sideslips only by about 4 percent.

Dihedral effect.- Although the effect of compressibility on the rolling moment due to sideslip associated with dihedral $C_{l_{\beta_\Gamma}}$ can be determined by applying the three-dimensional Prandtl-Glauert transformation to the incompressible results presented in references 10 and 11, charts similar to those in figure 6 for $\left(C_{l_{\beta_{C_L}}}\right)_{\Lambda}$ are considerably more convenient to use. Because the span loading due to combined sideslip and dihedral is antisymmetrical, the aerodynamic induction effects, and therefore the compressibility factors, are approximately the same as those for the lift-curve slope of a wing having one-half the aspect ratio. Compressibility factors for $C_{l_{\beta_\Gamma}}$ can therefore be determined by

substituting $A/2$ for A in equation (A6) of appendix A. This substitution gives the following relation:

$$\frac{\left(C_{l_{\beta_\Gamma}}\right)_M}{\left(C_{l_{\beta_\Gamma}}\right)_{M=0}} = \frac{2 + \sqrt{4 + \left(\frac{A}{2 \cos \Lambda}\right)^2}}{2 + \sqrt{4 + \left(\frac{A}{2 \cos \Lambda}\right)^2 - \left(\frac{AM}{2}\right)^2}}$$

Compressibility factors thus obtained are presented in figure 12 as a function of half-chord sweep and aspect ratio for several Mach numbers and have been found to be in good agreement with those obtained by applying the Prandtl-Glauert transformation to the results presented in references 10 and 11. (These corrections, of course, can also be used for the lift-curve slope by using values corresponding to an aspect ratio that is twice that of the wing in question.)

At present, no theory and little or no experimental data are available in the transonic speed range relative to $C_{l_{\beta_\Gamma}}$. In view of this deficiency, it has been suggested in reference 23 that estimates of $C_{l_{\beta_\Gamma}}$ for transonic speeds be made by applying a correction factor to transonic damping in roll results $\left(C_{l_p}\right)$ which are available from rocket-propelled model tests. This correction factor, designated herein as $K_{\Gamma/p}$, is considered equal to the ratio of theoretical values of $C_{l_{\beta_\Gamma}}$ to C_{l_p} and, therefore,

$$C_{l_{\beta_\Gamma}} = C_{l_p} K_{\Gamma/p}$$

Values of $K_{\Gamma/p}$ determined by various methods are presented in figure 13 as a function of taper ratio since taper ratio is the only parameter accounted for in the strip theory (ref. 23). In addition to strip theory (which, of course, neglects induction effects), subsonic results obtained by the Weissinger modified lifting-line method (ref. 11) and results from supersonic linearized theory for a wide range of aspect ratio and sweep (refs. 24 and 25) are also presented. The results of figure 13 show the strip theory to be slightly low and it is recommended that the solid line of figure 13 (average of the more exact solutions) be used to convert experimental C_{l_p} to $C_{l_{\beta_\Gamma}}$.

RESULTS AND DISCUSSION

Characteristics in the Low Lift Range

Inasmuch as the rolling moment due to sideslip C_{l_β} usually varies linearly with lift coefficient up to a C_L value of at least 0.2, and since the effect of geometric dihedral is usually constant over the same lift range, the parameters $C_{l_{\beta C_L}}$ and $C_{l_{\beta_\Gamma}}$ are used in this section of the report to define the low-lift characteristics. The characteristics at moderate and high lift are presented subsequently.

Effect of sweep angle.- The variation of experimental $C_{l_{\beta C_L}}$ with Mach number for various sweep angles is presented in figure 14(a) for aspect-ratio-4 wings. Also shown are estimated results for these wings obtained by methods outlined in "Theoretical Methods" of this report.

The experimental results indicate an increase in $C_{l_{\beta C_L}}$ with sweep which, at low Mach numbers, can be estimated fairly accurately. With regard to Mach number, both the estimated and experimental results indicate an increase up to the force break although the experimental result rises somewhat more rapidly. There is an abrupt decrease in the experimental results above the force-break Mach number. This decrease may be explained from the consideration that the force break would be expected to occur earlier on the leading wing since that wing is carrying more lift than the trailing wing. In addition, for the swept wings, the leading wing would be expected to have a lower critical Mach number than the trailing wing because of its lower effective sweep.

Effect of aspect ratio.- The variation of $C_{l_{\beta C_L}}$ with Mach number for various values of aspect ratio for wings having 45° sweep is presented in figure 14(b). The experimental results indicate that $C_{l_{\beta C_L}}$ increases with decreasing aspect ratio and that $C_{l_{\beta C_L}}$ can be estimated reasonably well for Mach numbers below force break.

Effect of taper ratio.- Experimental results showing effects of taper ratio on $C_{l_{\beta C_L}}$ for aspect-ratio-4 45° swept wings are given in figure 14(c). These results indicate a reduction in $C_{l_{\beta C_L}}$ with

increasing taper (decrease in taper ratio) and the estimated curves are in fairly good agreement with experiment below the force-break Mach number. In general, the variations of $C_{l_{\beta_{C_L}}}$ with Mach number between 0.85 and 0.95 were more pronounced as the taper was increased.

Delta plan forms.- Results of experimental investigations on two delta-wing plan forms are presented in figure 14(d) showing the variation of experimental and estimated $C_{l_{\beta_{C_L}}}$ with Mach number. The results indicate a decrease in $C_{l_{\beta_{C_L}}}$ as the aspect ratio was increased from 2.31 to 4.0 and the estimated curves are in reasonably good agreement with experiment except in the Mach number range between 0.80 and 0.92 for the aspect-ratio-4 wing. The large variation of $C_{l_{\beta_{C_L}}}$ at Mach numbers near the force break for the aspect-ratio-4 wing is in accord with the observed trends mentioned previously with regard to taper effects.

The experimental results just discussed are limited to a Mach number of about 0.95 because of the choking limitations of the solid throat of the Langley high-speed 7- by 10-foot tunnel. Figure 15 has been prepared to provide an indication of the characteristics that might be expected at higher transonic speeds for two delta wings. Experimental results at subsonic speeds for the aspect-ratio-4 wing (NACA 65A006 airfoil sections) were obtained from reference 5 and the data point at $M = 1.4$ was obtained from reference 26 (for $A = 4$ wing having NACA 0005-63 airfoil sections). Test results for the aspect-ratio-2 wing (NACA 0003-63 airfoil sections) were obtained from reference 26. Also shown is the subsonic theory (wing + fuselage) of this paper and the supersonic theory (wing-alone) of reference 27.

Test results for both the delta wings in figure 15 show a much larger effect of Mach number in the transonic and low supersonic range than would be expected from supersonic theory for subsonic leading edges. For both the aspect-ratio-4 and aspect-ratio-2 wings, supersonic theory for subsonic leading edges indicates a constant value of $C_{l_{\beta_{C_L}}}$ for Mach numbers up to that for which the leading edge becomes supersonic where there is a sudden change in sign. The experimental results, however, indicate a gradual reduction in $C_{l_{\beta_{C_L}}}$ with Mach number at supersonic speeds. This difference between theory and experiment may be due, at least in part, to the tendency of the fuselage flow field to reduce the effective sideslip angle of the wing, as discussed earlier for subsonic flow. This

fuselage effect, which, of course, is not included in the supersonic wing-alone theory, might be expected to cover a large portion of the wing for the subsonic-leading-edge case at supersonic speeds. Although the tests were not extended to the supersonic leading-edge case for either wing, the trends with Mach number indicate that the positive values of $C_{l_{\beta_{C_L}}}$ predicted by theory may be realized. Additional test results are needed, however, to determine the degree of correlation for supersonic leading edges.

Effect of geometric dihedral.- Figure 16 summarizes the variation with Mach number of the effect of geometric dihedral on rolling moment due to sideslip $C_{l_{\beta_\Gamma}}$ for an unswept and swept wing (ref. 6). The test results indicate very little effect of sweep on $C_{l_{\beta_\Gamma}}$ for the configurations investigated and that the effect of dihedral can be satisfactorily estimated at subcritical Mach numbers by use of the incompressible results of reference 10 or 11, the compressibility factor from figure 12, and the fuselage effect of equation 5.

Inasmuch as experimental results pertaining to effects of geometric dihedral at transonic speeds are not available, damping-in-roll test results obtained from rocket-propelled model tests at transonic speeds have been converted to $C_{l_{\beta_\Gamma}}$ by use of the factor $K_{\Gamma/p}$ given in figure 13. Figure 17 has been prepared as an example of this method of estimating $C_{l_{\beta_\Gamma}}$ and to indicate the trends with Mach number that would be expected for several wings. These results are compared with theoretical estimates obtained for subsonic speeds from this paper and from reference 27 for supersonic speeds. Experimental results for three wings were selected from a summary of a large number of transonic damping-in-roll results presented in reference 28.

Results for 6-percent-thick wings having delta- and rectangular-plan-form wings are presented in the upper part of figure 17 and results for a 9-percent-thick rectangular wing are given in the lower part of the figure. For the delta wing, subsonic theory is in good agreement with experiment and supersonic theory predicts slightly higher values of $C_{l_{\beta_\Gamma}}$. Test results for the 6-percent-thick rectangular wing indicate a smooth transition from subsonic theory to the supersonic theory, whereas results for the 9-percent-thick wing do not indicate a gradual variation of $C_{l_{\beta_\Gamma}}$ at transonic speeds. Instead, the characteristic "bucket" type of transonic behavior encountered in the lift-curve slopes of wings of this thickness (see ref. 29) occurs. In general, the results

obtained from the damping-in-roll tests gave somewhat lower values than indicated by the estimated curves. The damping-in-roll results of reference 28 were obtained from tests using three wing panels and, although the total wing area was used in determining damping coefficients, the results are still probably somewhat lower than results for two panels because of interference. For example, in reference 28, the damping in roll for four panels was slightly less than that for three panels particularly for the thick unswept wing. This interference effect may account for the differences in $C_{l_{\beta_\Gamma}}$ as determined from the rocket-propelled-model damping in roll and from the theory which is, of course, for two wing panels.

Variation With Lift Coefficient

In the preceding section only the low lift characteristics, which could be represented by the parameters $C_{l_{\beta C_L}}$ and $C_{l_{\beta_\Gamma}}$, were considered. In this section the variation of C_{l_β} with lift coefficient, through the stall in most cases, is discussed.

Effect of sweep at low speed.- Some typical low-speed results for an unswept and a sweptback wing are given in figure 18 to illustrate the effect of wing sweep on the variation of C_{l_β} with lift coefficient. Results of flow studies made by means of surface tufts are also shown for several selected lift coefficients to illustrate the different stall progression for the swept and unswept wing. Results for the unswept wing were obtained from reference 19 and results for the swept wing were obtained from reference 15. The effect of sweep at low lift shows the increase in C_{l_β} with sweep which would be expected from theory as discussed previously and the variation of C_{l_β} with lift coefficient is linear for both wings up to $C_L = 0.6$. At higher lift coefficients, C_{l_β} for the swept wing begins to decrease and changes sign, whereas that for the unswept wing remains fairly linear up to stall and then increases. Inasmuch as the data for the unswept wing (ref. 19) were limited in the angle-of-attack range covered, data for a similar wing (ref. 13) are presented by the dashed lines to show the characteristics above the stall. The difference in high lift characteristics of the swept and unswept wings is shown clearly.

Some insight into the different C_{l_β} variations for these wings may be obtained from the sketches of the flow studies. For the unswept

wing at the higher lift coefficients the flow studies indicate that the trailing wing stalls first (possibly because of spanwise boundary-layer flow) and results, of course, in an increase in C_{l_β}. For the swept wing, however, the stall appears to begin at the leading edge, is more extensive on the leading wing (probably because of the higher angle of attack normal to the sweep line for this panel), and results in a reduction in C_{l_β}.

These test results were obtained for a low-sideslip-angle range ($\beta = \pm 5^\circ$) and may not necessarily be indicative of the characteristics for large values of sideslip ($\beta = \pm 10^\circ$). For example, the reduction in lift-curve slope associated with the higher sweep of the trailing wing panel for large sideslip angles could result in lift values lower than that of the stalled leading wing panel and therefore positive dihedral effect is regained. (For example, see fig. 22(c) of ref. 15.)

Effect of leading-edge radius and Reynolds number.- In the preceding section, the reduction in C_{l_β} at the higher lift coefficients for the swept wing was found to be associated with stalling of the leading wing which began at the leading edge. The variation of C_{l_β} for swept wings at high lift therefore would be expected to be dependent to a large extent on the airfoil leading-edge radius and the Reynolds number. Results of two systematic investigations are summarized in figure 19 showing the effect of airfoil profile (refs. 30 and 31) and Reynolds number (ref. 32) on C_{l_β}. For both a delta and swept wing, use of an airfoil of large leading-edge radius (NACA 0012) afforded substantial increases in effective dihedral at higher lift coefficients compared with the airfoil section of extremely small leading-edge radius (12-percent biconvex). This effect is, of course, due to the fact that the round-nose airfoils are less susceptible to laminar separation at the leading edge than sharp-nose profiles.

Effects of Reynolds number and leading-edge roughness are indicated in the lower portion of figure 19 for a 40° swept wing having NACA 64_1-112 airfoil sections (ref. 32). These results indicate, for the model without leading-edge roughness, that an increase in Reynolds number from 1.7×10^6 to 5.3×10^6 extended the linear range of C_{l_β} from a lift coefficient of about 0.6 to about 0.9. Addition of leading-edge roughness for the higher Reynolds number condition, however, essentially nullified this Reynolds number effect. The overall results of figure 19 indicate that, although the high lift characteristics of these swept wings may be modified by changes in airfoil profile and Reynolds number, the results appear to be mainly that of delaying the break in C_{l_β} to higher lift.

As will be discussed later in more detail, the nature of the variation

of C_{l_β} at high lift for plain wings appears to be associated (for a given Mach number) primarily with wing sweep.

Effect of Mach number.- Before considering experimental data on the effects of Mach number on the variation of C_{l_β} with lift coefficient, a first-order indication of these effects may be obtained from the wing lift characteristics presented in figure 20. Results are presented for aspect-ratio-4 wings having 35° and 45° sweepback at subsonic and transonic speeds (refs. 33 and 34). For the present purpose, these results can be considered indicative of the lift characteristics of the leading (Λ = 35°) and trailing (Λ = 45°) wing panels of a 40° swept wing at 5° sideslip. As was previously discussed, the leading wing panel begins to stall first at low Mach numbers and results in a decrease in C_{l_β} at high angles of attack. For the higher Mach numbers, however, the lift on the leading wing (Λ = 35°) is greater than that for the trailing wing and therefore the reversal in C_{l_β} which was present at low Mach numbers would not be expected to occur. This effect of Mach number on the high lift variation of C_{l_β} is consistently evident in the experimental results of figure 21 for wings of 45° and 32.6° sweep. For the 60° swept wing the Mach number effect is considerably less pronounced as might be expected for this highly swept configuration (fig. 21(a)). Results for the 3.6° swept wing show that the increase in C_{l_β} at higher lift for low Mach numbers did not persist as the Mach number was increased to 0.91 but C_{l_β} gradually decreased with lift coefficient above C_L of about 0.6. This behavior may be associated with increased compressibility effects on the force break of the more highly loaded leading wing, as mentioned previously in connection with the low-lift characteristics. In figures 21(b) and 21(c) similar comparisons are made for systematic variations of aspect ratio and taper ratio and a similar effect of Mach number will be noted. In general, the results of figure 21 indicate that sweep and Mach number have the greatest influence on the type of variation with lift.

Boundary separating two types of variation with lift.- The type of variation of rolling moment due to sideslip with lift coefficient has been shown in figure 21 to depend primarily upon the sweep angle and Mach number. Changes in taper and aspect ratio affected only minor variations and airfoil profile and Reynolds number changes affected mainly the lift coefficient at which the breaks in C_{l_β} occurred. These observations suggest the possibility that a boundary separating desirable and marginal characteristics from undesirable variations of C_{l_β} with lift could be determined from considerations of only wing sweep and Mach number. Results of such a correlation are presented in figure 22 as a function of Mach

number and half-chord sweep and show combinations of these variables for which the indicated variations of C_{l_β} with C_L would be expected. The results of figure 22 should be considered preliminary inasmuch as relatively little data at high speeds and high lift are available. It appears, however, that conditions of decreasing C_{l_β} with increasing lift coefficient occur above sweep angles of approximately 20° and below Mach numbers of about 0.95.

Composite wing plan forms.- The sweep effect on rolling moment due to sideslip for sweptforward wings has been found opposite in sign from that for sweptback wings. The possibility would therefore appear that the unfavorable variations of rolling moment due to sideslip with lift for sweptback wings illustrated in the preceding sections could be improved by utilizing combinations of sweepback and sweepforward on each wing panel and still retain at least a large part of the favorable sweep effect on performance. Two such types of composite plan forms which are commonly referred to as M and W plan forms are shown in figure 4. Low-speed test results obtained from a systematic investigation of the effects of spanwise location of the sweep discontinuity are presented in figure 23 along with a comparison of M and W plan forms with the basic sweptback wing from which these composite plan forms were derived. The basic 45° sweptback wing had an aspect ratio of 6, a taper ratio of 0.6, and NACA 65A009 airfoil sections parallel to the plane of symmetry. In this low-speed study, the midspan location of sweep discontinuity was considered the basic break location and the direction of the break was moved for each wing in a direction to reduce the structural divergence tendency.

The test results, in general, show trends that would be expected in that the characteristics of the M wing are similar to those of the sweptback wing since the part of the wing having the greatest moment arm is sweptback on the M wing. In like manner, the characteristics of the W wing are more like those for a sweptforward wing. The different characteristics indicated for the different plan forms and break locations suggest that attainment of desirable C_{l_β} variations with lift could be achieved by judicious combinations of break location and sweep of the outboard and inboard portions of the wing panels. Differences in the magnitude of break-location effects shown in figure 23 for the M and W wings is believed to be associated with the direction the break was moved for each wing. For the M wing, which showed relatively small effects of break location, the break progressed inboard from the basic location (because of structural divergence considerations) and therefore the areas involved in the changes had relatively small moment arms.

Results of some high-speed tests on an aspect-ratio-4 45° sweptback wing having 0.3 taper ratio and NACA 65A006 airfoil sections (ref. 8)

are compared in figure 24 with a corresponding M wing having a break location at 40-percent semispan. These results indicate that this composite plan form did not effect any very large change in the variation of C_{l_β} with lift and the results of the M wing generally became nonlinear at a lower lift coefficient than for the sweptback wing.

Effect of geometric dihedral.- The variation of $C_{l_{\beta_\Gamma}}$ with lift coefficient for an essentially unswept wing and a 45° sweptback wing (ref. 6) is presented in figure 25 for two Mach numbers. In all cases $C_{l_{\beta_\Gamma}}$ decreased fairly rapidly at high lift and the lift coefficient for which $C_{l_{\beta_\Gamma}}$ becomes zero occurred earlier at the higher Mach number, particularly for the swept wing. Inasmuch as the combination of sideslip and dihedral results in a change in angle of attack of the wing panel ($\Delta\alpha = \beta \sin \Gamma$), the decrease in $C_{l_{\beta_\Gamma}}$ with lift coefficient would be expected to be associated to a large extent with the decreased lift-curve slope at high angles of attack and the condition of $C_{l_{\beta_\Gamma}} = 0$ corresponds to the peak of the lift curve. If experimental lift results are available for the configuration of interest, the variation of experimental lift-curve slope with angle of attack can therefore be considered indicative of the variation of $C_{l_{\beta_\Gamma}}$ with lift coefficient which can be estimated as follows

$$\left(C_{l_{\beta_\Gamma}}\right)_{C_L} = \left(C_{l_{\beta_\Gamma}}\right)_{C_L=0} \left[\frac{\left(C_{L_\alpha}\right)_{C_L}}{\left(C_{L_\alpha}\right)_{C_L=0}}\right]_{\text{Experiment}} \tag{9}$$

Estimated results using the relationships of equation 9 are in fairly good agreement with experimental results except that estimated values for the swept wing show a delayed and more gradual decrease at high lift. This difference in the estimated and experimental results appears to be due to an inboard shift of the lateral center of pressure as indicated by the pitching-moment data of reference 35 which would not appear in the lift-curve-slope ratios of equation 9. For this reason, the use of lateral center of pressure or root-bending-moment data would be expected to be more reliable for estimates of variations of $C_{l_{\beta_\Gamma}}$ with lift than use of lift-curve slopes. However, since lift results are more generally available than root-bending-moment data, the lift-curve-slope ratio is given in equation 9.

The experimental results of figure 25 indicate furthermore that incorporation of geometric dihedral would be expected to be of little use in attempting to compensate for the loss of effective dihedral on sweptback wings at high lift coefficients. Therefore, it appears that some other scheme such as a chord-extension or nose flap must be employed if it is desired to maintain effective dihedral to higher lifts. No attempts are made in this paper, however, to assess various flow-control devices.

CONCLUDING REMARKS

The experimental and estimated results presented in this paper summarize overall characteristics of the rolling moment due to sideslip of a large number of wing configurations as influenced by wing geometry, lift coefficient, and Mach number. The many comparisons of estimated and experimental results serve to indicate the applicability of estimation procedures developed herein as well as indicating regions where additional experimental results are needed to form a basis for developing more reliable estimation procedures.

The estimated results from the methods developed in this paper, compared with experimental results, indicate that the effects of wing aspect ratio, taper ratio, sweep angle, and dihedral on the rolling moment due to sideslip of wing-fuselage configurations can be determined with reasonable accuracy up to the force-break Mach number at low lift coefficients. No attempt has been made to modify the estimation procedures to account for flow separation effects at moderate and high lift coefficients; however, qualitative relationships have been determined from experimental results which indicate the type of variation with lift coefficient for a large number of wing plan forms as a function of wing geometry and Mach number.

With regard to transonic and supersonic speeds, experimental information is indeed sparse; however, indications of the low lift characteristics have been obtained to show the nature of the variation in rolling moment due to sideslip for some wings in transversing from high subsonic to low supersonic speeds. Considerably more experimental data are needed in this speed range to provide general indications of transonic characteristics and to afford a basis for developing new methods of estimation.

Inasmuch as the range of fuselage shapes and relative size was not comprehensive for the models included in the experimental investigations, the extent of applicability and the limitations of the estimation procedures used relative to fuselage effects is not indicated. More experimental results are needed on effects of fuselage diameter, length, and cross-sectional shape to extend the present fuselage correction factors

to arrangements differing appreciably in fuselage geometry from those of the model configurations presented herein.

Langley Aeronautical Laboratory,
National Advisory Committee for Aeronautics,
Langley Field, Va., November 29, 1954.

APPENDIX A

SIMPLIFIED METHOD OF ESTIMATING C_{L_α}

In the body of this paper the rolling moment due to sideslip is estimated for subsonic Mach numbers by considering the lift-curve slope of the leading and trailing wing panels. The purpose of this appendix is to present the development of a simple expression for the lift-curve slope of swept wings of any aspect ratio and taper ratio.

In reference 36 a simple expression for incompressible C_{L_α} developed from that of reference 37 is presented. For the compressible case, however, the method of reference 36 is rather complicated. The following derivation for the compressible case provides an extremely simple expression. Equation (11) of reference 36 can be written as

$$\left(C_{L_\alpha}\right)_{M=0} = \frac{a_o A}{\frac{a_o}{\pi} + \sqrt{\left(\frac{A}{\cos \Lambda}\right)^2 + \left(\frac{a_o}{\pi}\right)^2}} \tag{A1}$$

By applying the three-dimensional Prandtl-Glauert transformation, the compressible equation becomes

$$\left(C_{L_\alpha}\right)_M = \frac{a_o A}{\frac{a_o}{\pi} + \sqrt{\left(\frac{A^2(1 - M^2)}{\cos^2 \Lambda_M}\right) + \left(\frac{a_o}{\pi}\right)^2}} \tag{A2}$$

where

$$\tan \Lambda_M = \frac{\tan \Lambda}{\sqrt{1 - M^2}}$$

Inasmuch as $\tan \Lambda = \frac{\sqrt{1 - \cos^2\Lambda}}{\cos \Lambda}$,

$$\tan^2\Lambda_M = \frac{1 - \cos^2\Lambda}{\cos^2\Lambda(1 - M^2)} = \frac{1}{\cos^2\Lambda(1 - M^2)} - \frac{1}{1 - M^2}$$

Now

$$\cos^2\Lambda_M = \frac{1}{1 + \tan^2\Lambda_M}$$

and, by substitution,

$$\cos^2\Lambda_M = \frac{1}{1 + \frac{1}{\cos^2\Lambda(1 - M^2)} - \frac{1}{1 - M^2}} \tag{A3}$$

The term $\frac{A^2(1 - M^2)}{\cos^2\Lambda_M}$ in equation (A2), by substituting equation (A3), can be expressed as follows:

$$\frac{A^2(1 - M^2)}{\cos^2\Lambda_M} = A^2(1 - M^2)\left(1 + \frac{1}{\cos^2\Lambda(1 - M^2)} - \frac{1}{1 - M^2}\right) = \left(\frac{A}{\cos \Lambda}\right)^2 - (AM)^2 \tag{A4}$$

By substituting equation (A4) into equation (A2)

$$\left(C_{L_\alpha}\right)_M = \frac{a_o A}{\frac{a_o}{\pi} + \sqrt{\left(\frac{A}{\cos \Lambda}\right)^2 + \left(\frac{a_o}{\pi}\right)^2 - (AM)^2}} \tag{A5}$$

which differs from the incompressible case (eq. (A1)) only by the term $(AM)^2$. Equation (A5) was, of course, obtained by applying the Prandtl-Glauert transformation; however, the same result can be obtained by correcting the section lift-curve slope a_o in equation (A1) for compressibility by using the Mach number normal to the leading edge. Substituting

$\frac{a_o}{\sqrt{1 - M^2\cos^2\Lambda}}$ for a_o in equation (A1) and rearranging the equation results in the following relation:

$$\left(C_{L_\alpha}\right)_M = \frac{A}{\frac{1}{\pi} + \sqrt{\frac{A^2(1 - M^2\cos^2\Lambda)}{a_o{}^2\cos^2\Lambda}}}$$

which reduces to

$$\left(C_{L_\alpha}\right)_M = \frac{a_o A}{\frac{a_o}{\pi} + \sqrt{\left(\frac{A}{\cos\Lambda}\right)^2 + \left(\frac{a_o}{\pi}\right)^2 - (AM)^2}}$$

and is identical with equation (A5). For use in the body of this paper, a_o is replaced by 2π so that the following equation results:

$$\left(C_{L_\alpha}\right)_M = \frac{2\pi A}{2 + \sqrt{4 + \left(\frac{A}{\cos\Lambda}\right)^2 - (AM)^2}} \qquad \text{(A6)}$$

The effect of taper ratio is not included in equation (A6); however, this effect can be essentially accounted for by using the sweep of the half-chord line rather than the quarter-chord line as is usually done. This appears somewhat consistent with the reversibility theorem (ref. 38) and modified lifting-line methods such as Weissinger's (ref. 39). With regard to the reversibility theorem, it will be noted that the only sweep that is common to both the original and reversed flows for a tapered wing is that of the half-chord line which changes only in sign. It will

also be noted that in the Weissinger method the load is assumed to be concentrated along the quarter-chord line and the boundary condition satisfied at the three-quarter chord line so that taper effects are dependent upon the sweep of the three-quarter chord line as well as the quarter-chord line. Therefore if one sweep line is to be used to correlate taper effects, the half chord might seem more logical than the quarter chord. The results of some unpublished Weissinger 15-point solutions are shown in figure 26 plotted against both the sweep of the quarter chord and half chord for taper ratios from 0 to 1.5. These results show that, although there is considerable effect of taper ratio when the quarter-chord line is used, there is essentially no effect of taper when the half chord is used. The simple expression (eq. (A6)) for the lift slope therefore is applicable to all taper ratios if the sweep of the half chord is used.

Equation (A6) at zero Mach number is compared with some of the available lifting-surface solutions (refs. 40-44) in figure 27. The solution for the 60° elliptical wing (unpublished data) was made by Robert S. Swanson by using the electomagnetic analogy method described in reference 45. The results are presented in the form of C_{L_α}/A as a function of $A/\cos \Lambda$ since equation (A6) is a unique function of $A/\cos \Lambda$ for zero Mach number. The comparison of results indicates that equation (A6) is very accurate when the half-chord sweep is used. Furthermore, comparisons with reference 12 indicate that equation (A6) is more accurate than Weissinger's seven-point modified lifting-line method.

Inasmuch as the most commonly used sweep reference line is the quarter chord, a chart (fig. 29) has been prepared from which the half-chord sweep can be easily obtained from the quarter-chord sweep, aspect ratio, and taper ratio.

APPENDIX B

20-VORTEX SOLUTION FOR THE ROLLING MOMENT DUE TO SIDESLIP

In reference 46 a finite-step method of calculating wing span loadings is outlined. In this method the wing is replaced by a system of N horseshoe vortices along the quarter-chord line and the summation of their downwash velocities at N control points along the three-quarter-chord line is equated to the component of free-stream velocity normal to the wing chord. Reference 46 deals only with the symmetrical case for which application of this tangent flow boundary condition provides a set of $N/2$ simultaneous equations in the $N/2$ unknown circulation strengths across the semispan. In the present case, however, the method is to be used for wings in sideslip and, therefore, because of the asymmetry, N simultaneous equations in the N unknown circulation strengths must be used.

The $N = 20$ vortex system was selected and the layout for a 45° sweptback wing is illustrated in figure 28. In order to maintain the same span of the horseshoe vortices a greater number must be placed on the advancing wing than on the retreating wing for the swept-wing solutions. Therefore, sideslip angles were chosen such that there were 11 vortices on the advancing panel and 9 on the retreating panel. (See fig. 28.) The relative position of the various control points with regard to the various horseshoe vortices was then determined and the downwash in terms of the unknown circulation Γ due to each horseshoe vortex was summed at each of the 20 control points and equated to $V \sin \alpha$. This gave 20 simultaneous equations, with 20 unknown circulation strengths, which were solved by an iteration process. (See ref. 46 for details.) The resulting circulation strengths required to satisfy the boundary conditions are presented in table III for several wings. The rolling moment due to sideslip was then computed by the relation:

$$C_{l_\beta C_L} = \frac{\Delta\left(\Sigma\Gamma \frac{y}{b}\right)}{\beta(\Sigma\Gamma)}$$

where $\Delta\left(\Sigma\Gamma \frac{y}{b}\right)$ is the difference between the summation of the circulation times the moment arm for the advancing and retreating wing panels, and $\Sigma\Gamma$ is the sum of the circulation on each panel. The values thus obtained are presented in table III and it will be noted that the value for the unswept wing appears to be somewhat low when compared with experiment or other theories. This is probably due to the fact that the effect of the nonstreamwise tips caused by the sideslip angle has not been accounted for. Inasmuch as this effect would occur on all the wings, it is felt that the increments due to sweep are fairly reliable.

REFERENCES

1. Kuhn, Richard E., and Fournier, Paul G.: Wind-Tunnel Investigation of the Static Lateral Stability Characteristics of Wing-Fuselage Combinations at High Subsonic Speeds - Sweep Series. NACA RM L52G11a, 1952.

2. Fournier, Paul G., and Byrnes, Andrew L., Jr.: Wind-Tunnel Investigation of the Static Lateral Stability Characteristics of Wing-Fuselage Combinations at High Subsonic Speeds. Aspect-Ratio Series. NACA RM L52L18, 1953.

3. Wiggins, James W., and Fournier, Paul G.: Wind-Tunnel Investigation of the Static Lateral Stability Characteristics of Wing-Fuselage Combinations at High Subsonic Speeds - Taper-Ratio Series. NACA RM L53B25a, 1953.

4. Wiggins, James W.: Wind-Tunnel Investigation at High Subsonic Speeds of the Static Longitudinal and Static Lateral Stability Characteristics of a Wing-Fuselage Combination Having a Triangular Wing of Aspect Ratio 2.31 and an NACA 65A003 Airfoil. NACA RM L53G09a, 1953.

5. Fournier, Paul G.: Wind-Tunnel Investigation of the Aerodynamic Characteristics in Pitch and Sideslip at High Subsonic Speeds of a Wing-Fuselage Combination Having a Triangular Wing of Aspect Ratio 4. NACA RM L53G14a, 1953.

6. Kuhn, Richard E., and Draper, John W.: Wind-Tunnel Investigation of the Effects of Geometric Dihedral on the Aerodynamic Characteristics in Pitch and Sideslip of an Unswept- and a 45° Sweptback-Wing—Fuselage Combination at High Subsonic Speeds. NACA RM L53F09, 1953.

7. Campbell, John P., and McKinney, Marion O.: Summary of Methods for Calculating Dynamic Lateral Stability and Response and for Estimating Lateral Stability Derivatives. NACA Rep. 1098, 1952. (Supersedes NACA TN 2409.)

8. Goodson, Kenneth W., and Becht, Robert E.: Wind-Tunnel Investigation at High Subsonic Speeds of the Stability Characteristics of a Complete Model Having Sweptback-, M-, W-, and Cranked-Wing Plan Forms and Several Horizontal-Tail Locations. NACA RM L54C29, 1954.

9. Levacic, I.: Rolling Moment Due to Sideslip. Part III. Rep. No. Aero. 2139, British R.A.E., July 1946.

10. Bird, John D.: Some Theoretical Low-Speed Span Loading Characteristics of Swept Wings in Roll and Sideslip. NACA Rep. 969, 1950. (Supersedes NACA TN 1839.)

11. DeYoung, John: Theoretical Antisymmetric Span Loading for Wings of Arbitrary Plan Form at Subsonic Speeds. NACA Rep. 1056, 1951. (Supersedes NACA TN 2140.)

12. DeYoung, John, and Harper, Charles W.: Theoretical Symmetric Span Loading at Subsonic Speeds for Wings Having Arbitrary Plan Form. NACA Rep. 921, 1948.

13. Goodman, Alex, and Brewer, Jack D.: Investigation at Low Speeds of the Effect of Aspect Ratio and Sweep on Static and Yawing Stability Derivatives of Untapered Wings. NACA TN 1669, 1948.

14. Toll, Thomas A., and Queijo, M. J.: Approximate Relations and Charts for Low-Speed Stability Derivatives of Swept Wings. NACA TN 1581, 1948.

15. Griner, Roland F.: Static Lateral Stability Characteristics of an Airplane Model Having a 47.7° Sweptback Wing of Aspect Ratio 6 and the Contribution of Various Model Components at a Reynolds Number of 4.45×10^6. NACA RM L53G09, 1953.

16. Letko, William, and Wolhart, Walter D.: Effect of Sweepback on the Low-Speed Static and Rolling Stability Derivatives of Thin Tapered Wings of Aspect Ratio 4. NACA RM L9F14, 1949.

17. Queijo, M. J., and Wolhart, Walter D.: Experimental Investigation of the Effect of Vertical-Tail Size and Length and of Fuselage Shape and Length on the Static Lateral Stability Characteristics of a Model With 45° Sweptback Wing and Tail Surfaces. NACA Rep. 1049, 1951. (Supersedes NACA TN 2168.)

18. Weissinger, J.: Der schiebende Tragflügel bei gesunder Strömung-Bericht S 2 der Lilienthal-Gesellschaft für Luftfahrtforschung, 1938-39, pp. 13-51.

19. Jacobs, W.: Systematische Sechskomponentenmessungen an Pfeilflügeln. Bericht 44/21, Aerodynamisches Institut der T. H. Braunschweig, Apr. 9, 1944.

20. Letko, William, and Goodman, Alex: Preliminary Wind-Tunnel Investigation at Low Speed of Stability and Control Characteristics of Swept-Back Wings. NACA TN 1046, 1946.

21. Purser, Paul E., and Spearman, M. Leroy: Wind-Tunnel Tests at Low Speed of Swept and Yawed Wings Having Various Plan Forms. NACA TN 2445, 1951. (Supersedes NACA RM L7D23.)

22. Fisher, Lewis R.: Approximate Corrections for the Effects of Compressibility on the Subsonic Stability Derivatives of Swept Wings. NACA TN 1854, 1949.

23. Purser, Paul E.: An Approximation to the Effect of Geometric Dihedral on the Rolling Moment Due to Sideslip for Wings at Transonic and Supersonic Speeds. NACA RM L52B01, 1952.

24. Tucker, Warren A., and Nelson, Robert L.: Theoretical Characteristics in Supersonic Flow of Constant-Chord Partial-Span Control Surfaces on Rectangular Wings Having Finite Thickness. NACA TN 1708, 1948.

25. Robinson, A., and Hunter-Tod, J. H.: The Aerodynamic Derivatives With Respect to Sideslip for a Delta Wing With Small Dihedral at Zero Incidence at Supersonic Speeds. R. & M. No. 2410, British A.R.C., Dec. 1947.

26. Christensen, Frederik B.: An Experimental Investigation of Four Triangular-Wing-Body Combinations in Sideslip at Mach Numbers 0.6, 0.9, 1.4, and 1.7. NACA RM A53L22, 1954.

27. Jones, Arthur L., and Alksne, Alberta: A Summary of Lateral-Stability Derivatives Calculated for Wing Plan Forms in Supersonic Flow. NACA Rep. 1052, 1951.

28. Stone, David G.: A Collection of Data for Zero-Lift Damping in Roll of Wing-Body Combinations As Determined With Rocket-Powered Models Equipped With Roll-Torque Nozzles. NACA RM L53E26, 1953.

29. Polhamus, Edward C.: Summary of Results Obtained by Transonic-Bump Method on Effects of Plan Form and Thickness on Lift and Drag Characteristics of Wings at Transonic Speeds. NACA RM L51H30, 1951.

30. Jaquet, Byron M., and Brewer, Jack D.: Low-Speed Static-Stability and Rolling Characteristics of Low-Aspect-Ratio Wings of Triangular and Modified Triangular Plan Forms. NACA RM L8L29, 1949.

31. Letko, William, and Jaquet, Byron M.: Effect of Airfoil Profile of Symmetrical Sections on the Low-Speed Static-Stability and Yawing Derivatives of 45° Sweptback Wing Models of Aspect Ratio 2.61. NACA RM L8H10, 1948.

32. Neely, Robert H., and Conner, D. William: Aerodynamic Characteristics of a 42° Sweptback Wing With Aspect Ratio 4 and NACA 64_1-112 Airfoil Sections at Reynolds Numbers From 1,700,000 to 9,500,000. NACA RM L7D14, 1947.

33. Cahill, Jones F. and Gottlieb, Stanley M.: Low-Speed Aerodynamic Characteristics of a Series of Swept Wings Having NACA 65A006 Airfoil Sections. (Revised). NACA RM L50F16, 1950.

34. Turner, Thomas R.: Effects of Sweep on the Maximum-Lift Characteristics of Four Aspect-Ratio-4 Wings at Transonic Speeds. NACA RM L50H11, 1950.

35. Wiggins, James W., and Kuhn, Richard E.: Wind-Tunnel Investigation of the Aerodynamic Characteristics in Pitch of Wing-Fuselage Combinations at High-Subsonic Speeds. Sweep Series. NACA RM L52D18, 1952.

36. Diederich, Franklin W.: A Plan-Form Parameter for Correlating Certain Aerodynamic Characteristics of Swept Wings. NACA TN 2335, 1951.

37. Polhamus, Edward C.: A Simple Method of Estimating the Subsonic Lift and Damping in Roll of Sweptback Wings. NACA TN 1862, 1949.

38. Brown, Clinton E.: The Reversibility Theorem for Thin Airfoils in Subsonic and Supersonic Flow. NACA Rep. 986, 1950. (Supersedes NACA TN 1944.)

39. Weissinger, J.: The Lift Distribution of Sweptback Wings. NACA TM 1120, 1947.

40. Krienes, Klaus: The Elliptic Wing Based on the Potential Theory. NACA TM 971, 1941.

41. Falkner, V. M. (With Appendix by Doris Lehrian): Calculated Loadings Due to Incidence of a Number of Straight and Swept-Back Wings. R. & M. No. 2596, British A.R.C., June 1948.

42. Dickson, R.: Comparison of Two Methods of Calculating Aerodynamic Loadings on an Aerofoil With Large Sweepback and Small Aspect Ratio. R. & M. No. 2353, British A.R.C., June 1946.

43. Schneider, William C.: A Comparison of the Spanwise Loading Calculated by Various Methods With Experimental Loadings Obtained on a 45° Sweptback Wing of Aspect Ratio 8 at a Reynolds Number of 4.0×10^6. NACA RM L51G30, 1952.

44. Jones, Robert T.: Properties of Low-Aspect-Ratio Pointed Wings at Speeds Below and Above the Speed of Sound. NACA Rep. 835, 1946. (Supersedes NACA TN 1032.)

45. Swanson, Robert S., and Crandall, Stewart M.: Lifting-Surface-Theory Aspect-Ratio Corrections to the Lift and Hinge-Moment Parameters for Full-Span Elevators on Horizontal Tail Surfaces. NACA Rep. 911, 1948. (Supersedes NACA TN 1175.)

46. Campbell, George S.: A Finite-Step Method for the Calculation of Span Loadings of Unusual Plan Forms. NACA RM L50L13, 1951.

TABLE I

SUMMARY OF GEOMETRIC CHARACTERISTICS OF MODELS

INCLUDED IN EXPERIMENTAL RESULTS

$\Lambda_{c/4}$ deg	$\Lambda_{c/2}$ deg	Aspect ratio, A	Taper ratio, λ	NACA airfoil section	Reference	Figure
3.6	0	4	0.6	65A006	1, 6	1, 14(a), 21(a), 16, and 25
32.6	30				1	1, 14(a), and 21(a)
45	43.15				1, 6	1, 14(a), 21(a), 16, and 25
60	59.08				1	1, 14(a), and 21(a)
45	36.87	2			2	1, 14(b), and 21(b)
	43.15	4			2	1, 14(b), and 21(b)
	43.78	6			2	1, 14(b), and 21(b)
	40.88	4	.3		3	1, 14(c), and 21(c)
	43.15		.6		3	1, 14(c), and 21(c)
	45		1.0		3	1, 14(c), and 21(c)
52.43	40.93	2.31	0	65A003	4	1 and 14(d)
				65A006	28	17
				12 percent biconvex, 0012	30	19
36.87	26.56	4	0	65A006	5	1, 14(d), and 15
				0005-63	26	15
56.31	45	2	0	0003-63	26	15
0	0	3.7	1.0	65A006	28	17
		4.5		65A009	28	17
		5		23012	19	18
40	36.94	6	.313	64-210	15	19
45	45	2.61	1.0	12 percent biconvex, 65_1-012, 0012	31	19
40	38	4	.625	64_1-112	32	19
30	27.25	4	.6	65A006	33	20
35	32,52				34	20
45	43.15				33, 34	20

TABLE II

TABULATED RESULTS USED IN DETERMINING ASPECT-RATIO CONTRIBUTION TO ROLLING MOMENT DUE TO SIDESLIP FOR UNTAPERED WINGS AT LOW SPEED

Symbol used for data in figure 8	A	1/A	Λ, deg	$C_{l_{\beta C_L}}$ (Experimental)	$\left(C_{l_{\beta C_L}}\right)_\Lambda$ (Theoretical, fig. 6)	$\left(C_{l_{\beta C_L}}\right) - \left(C_{l_{\beta C_L}}\right)_\Lambda = \left(C_{l_{\beta C_L}}\right)_A$	Reference
○	2.60	0.385	60	-0.0112	-0.0082	-0.0030	21
□	1.50	.666	60	-.0124	-.0068	-.0056	21
△	1.34	.746	60	-.0145	-.0072	-.0073	13
▽	2.61	.383	60	-.0115	-.0082	-.0033	13
▽	5.16	.194	60	-.0100	-.0088	-.0012	13
◿	5.16	.194	45	-.0054	-.0048	-.0006	13
◸	2.61	.383	45	-.0075	-.0044	-.0031	13
▱	1.34	.746	45	-.0117	-.0041	-.0076	13
◇	5.00	.200	45	-.0055	-.0048	-.0007	19
◇	5.16	.194	0	-.0012	0	-.0012	13
▱	2.61	.383	0	-.0040	0	-.0040	13
▽	1.34	.746	0	-.0083	0	-.0083	13
▷	5.02	.199	0	-.0011	0	-.0011	20
◁	4.13	.242	0	-.0015	0	-.0015	20

TABLE III

FINITE-STEP VORTEX SOLUTIONS FOR WING LOADINGS IN SIDESLIP

[1] $\frac{y'}{b}$	Γ	$\Gamma \frac{y'}{b}$	[1] $\frac{y'}{b}$	Γ	$\Gamma \frac{y'}{b}$	[1] $\frac{y'}{b}$	Γ	$\Gamma \frac{y'}{b}$
Advancing panel								
19/40	0.4767	0.2264	21/44	0.4934	0.2355	21/44	0.4216	0.2012
17/40	.6795	.2888	19/44	.6791	.2933	19/44	.5398	.2331
15/40	.8122	.3046	17/44	.7780	.3006	17/44	.5972	.2308
13/40	.9101	.2958	15/44	.8382	.2858	15/44	.6330	.2159
11/40	.9861	.2712	13/44	.8763	.2589	13/44	.6571	.1942
9/40	1.0461	.2354	11/44	.9007	.2252	11/44	.6710	.1678
7/40	1.0937	.1914	9/44	.9129	.1868	9/44	.6750	.1381
5/40	1.1314	.1414	7/44	.9130	.1453	7/44	.6676	.1062
3/40	1.1588	.0869	5/44	.9011	.1024	5/44	.6475	.0736
1/40	1.1745	.0294	3/44	.8848	.0603	3/44	.6272	.0428
			1/44	.9008	.0204	1/44	.6529	.0148
Retreating panel								
1/40	1.1780	0.0295	1/36	0.9100	0.0253	1/36	0.6705	0.0186
3/40	1.1632	.0872	3/36	.9091	.0758	3/36	.6762	.0564
5/40	1.1344	.1418	5/36	.8984	.1248	5/36	.6735	.0935
7/40	1.0949	.1916	7/36	.8768	.1705	7/36	.6634	.1290
9/40	1.0439	.2349	9/36	.8427	.2107	9/36	.6460	.1615
11/40	.9797	.2694	11/36	.7868	.2404	11/36	.6212	.1898
13/40	.9009	.2928	13/36	.7365	.2660	13/36	.5862	.2117
15/40	.8004	.3002	15/36	.6417	.2674	15/36	.5304	.2210
17/40	.6669	.2834	17/36	.4670	.2206	17/36	.4127	.1949
19/40	.4651	.2209						

$\Delta\Sigma\Gamma \frac{y'}{b} = -0.0196$

$\Sigma\Gamma = 18.8963$

$C_{l_{\beta C_L}} = \frac{-0.0196}{18.8963(5.00)}$

$= -0.0002$

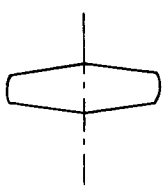

$\Lambda = 36^\circ$

$\beta = 5.00^\circ$

$\Delta\Sigma\Gamma \frac{y'}{b} = -0.5130$

$\Sigma\Gamma = 16.1464$

$C_{l_{\beta C_L}} = \frac{-0.5130}{16.1464(6.06)}$

$= -0.0052$

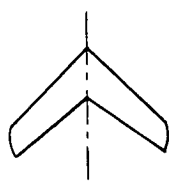

$\Lambda = 45^\circ$

$\beta = 6.06^\circ$

$\Delta\Sigma\Gamma \frac{y'}{b} = -0.3421$

$\Sigma\Gamma = 12.2693$

$C_{l_{\beta C_L}} = \frac{-0.3421}{12.2693(3.10)}$

$= -0.0089$

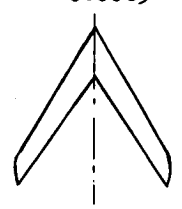

$\Lambda = 60^\circ$

$\beta = 3.10^\circ$

[1] See figure 28.

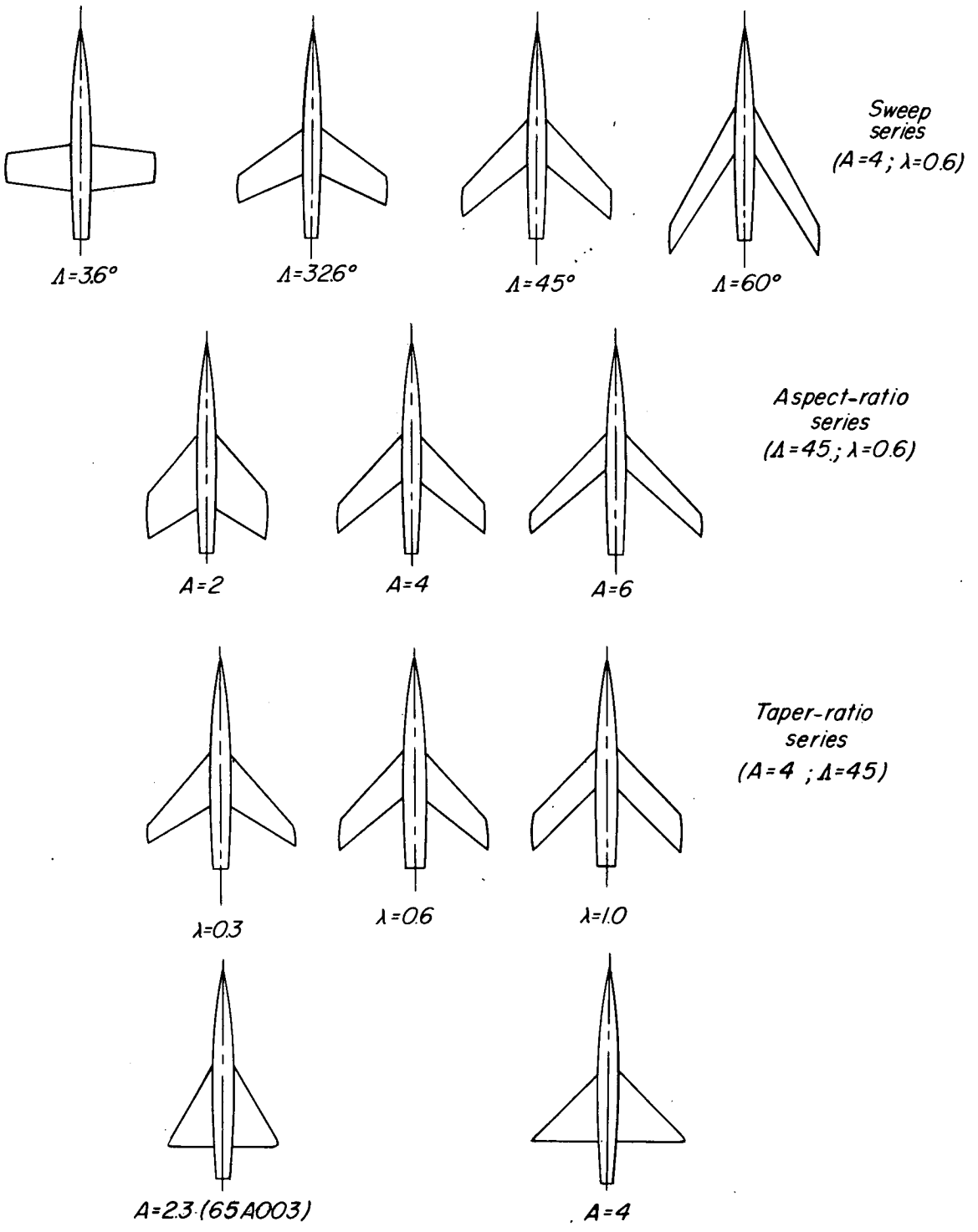

Figure 1.- Wing plan forms tested in the Langley high-speed 7- by 10-foot tunnel. NACA 65A006 airfoil sections except where noted.

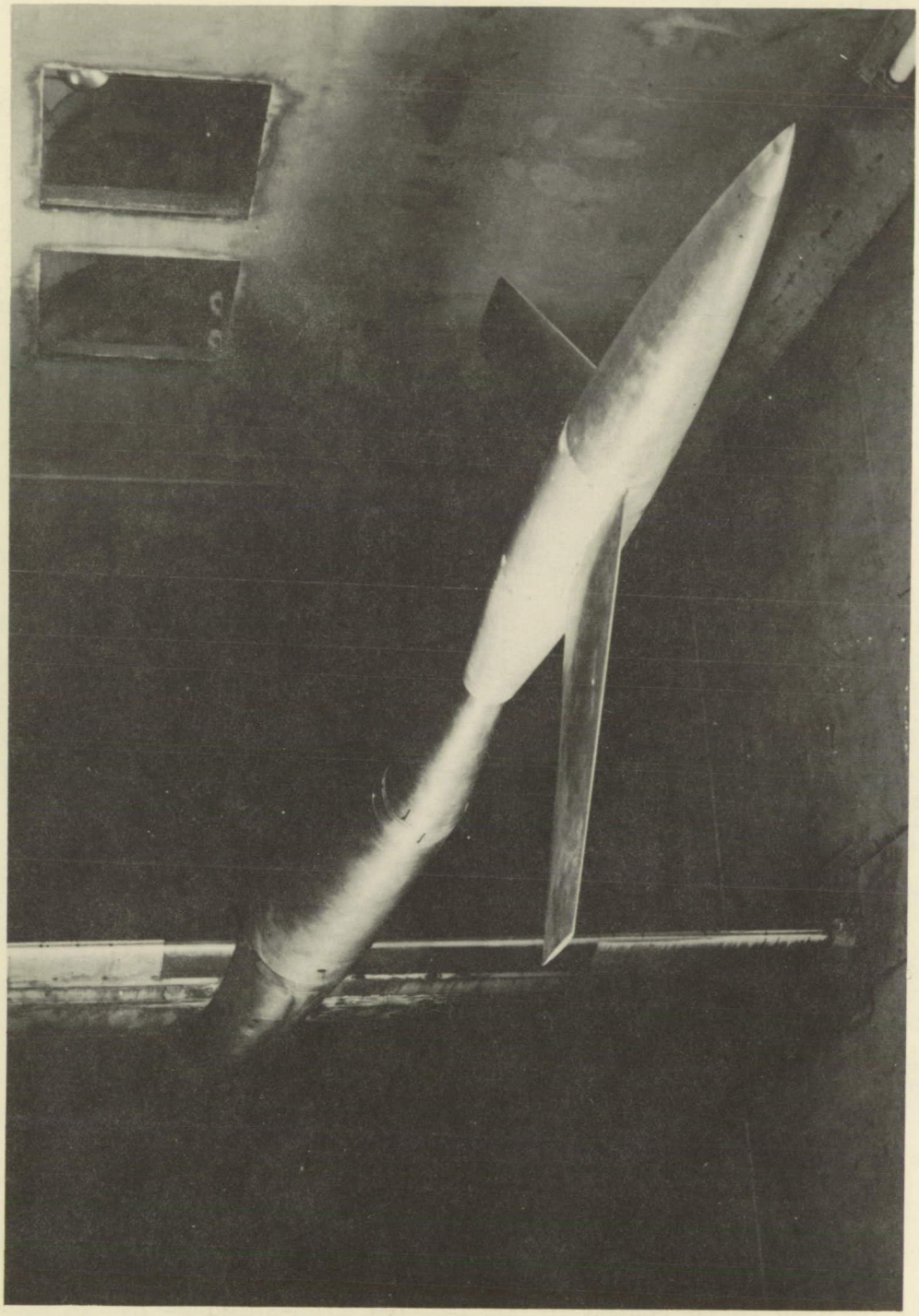

L-72400

Figure 2.- A test model mounted on the sting support in the Langley high-speed 7- by 10-foot tunnel.

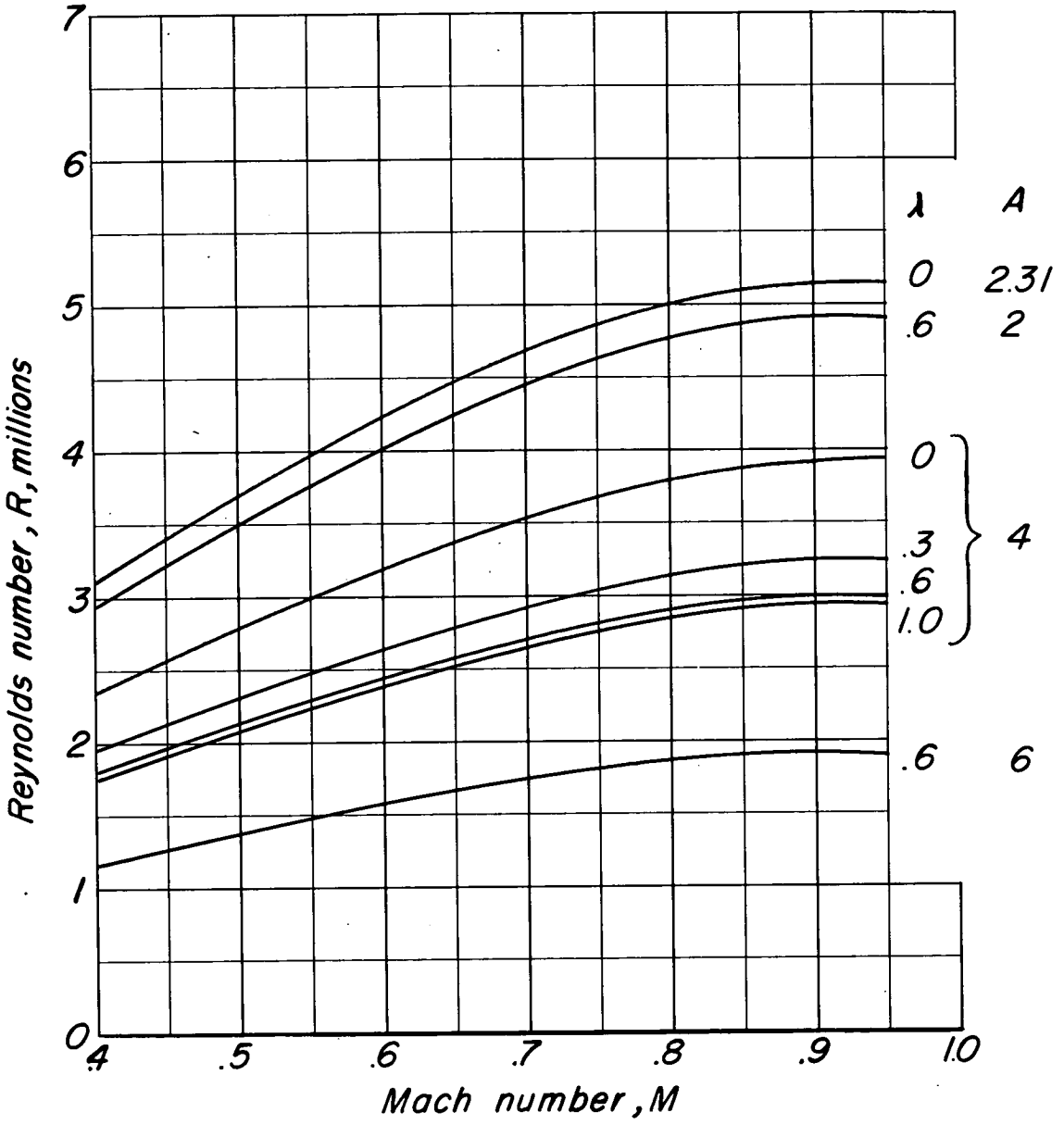

Figure 3.- Variation of mean test Reynolds number with Mach number for the wings tested in the Langley high-speed 7- by 10-foot tunnel.

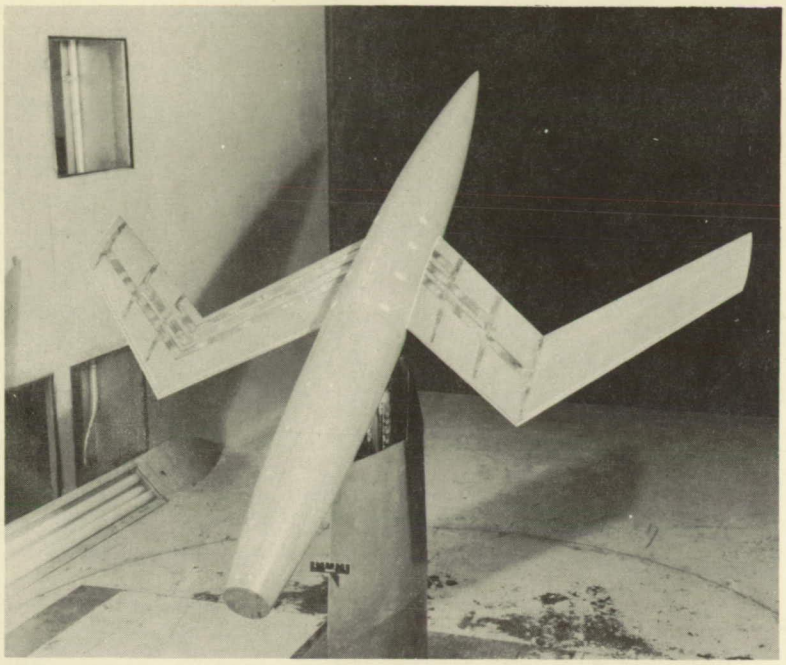

L-67337

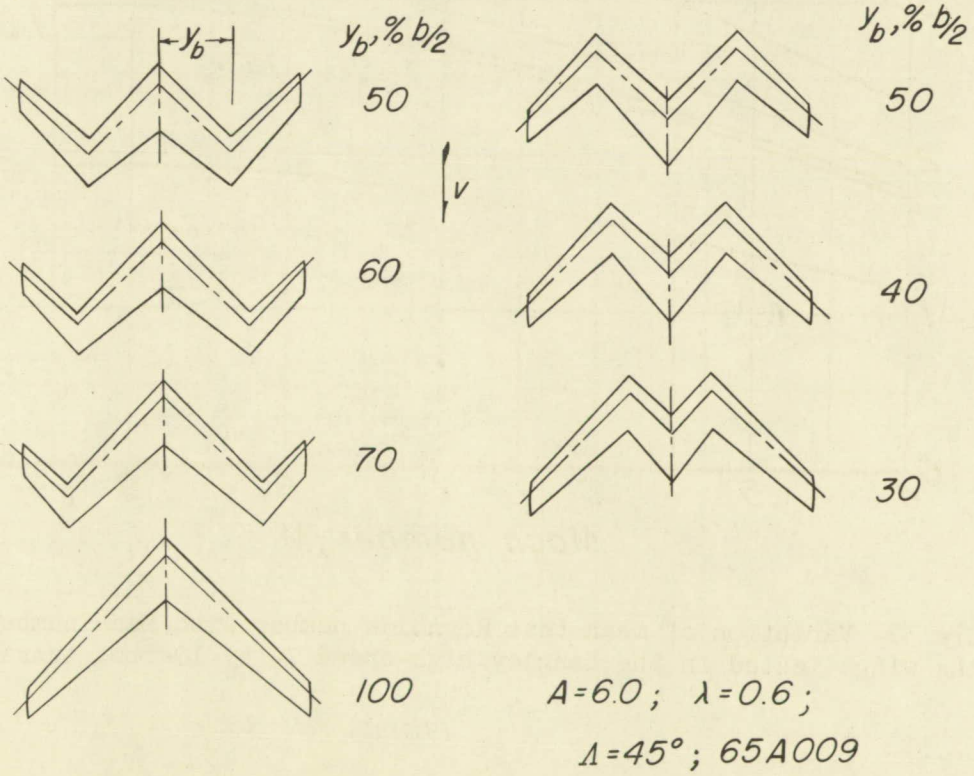

Figure 4.- Composite wing plan forms tested at low speed in the Langley 300 MPH 7- by 10-foot tunnel.

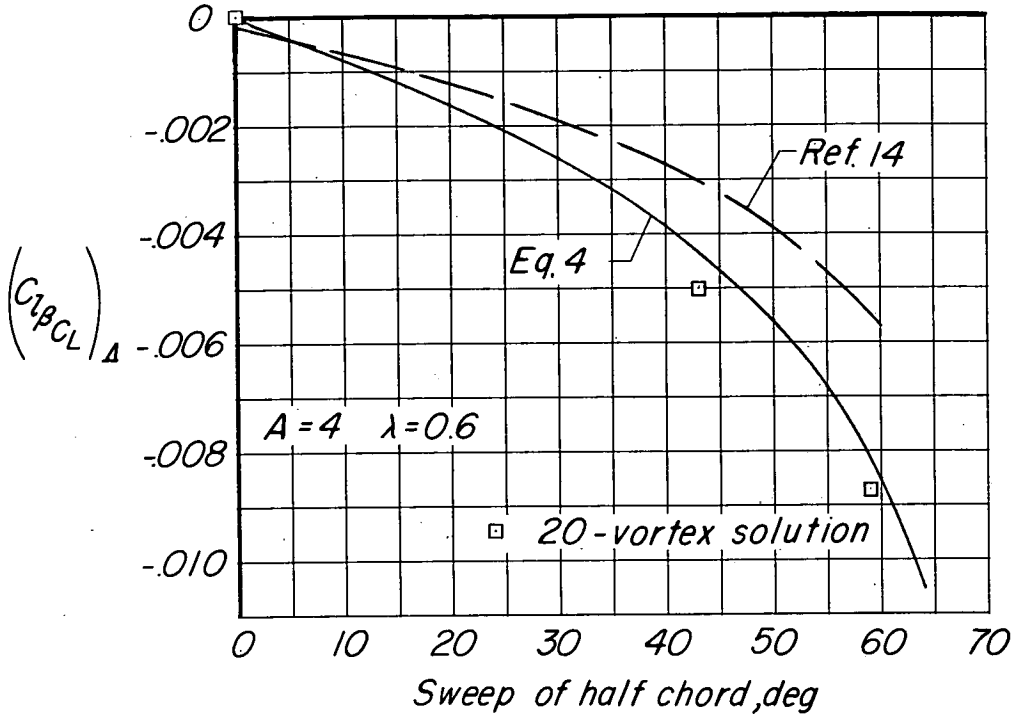

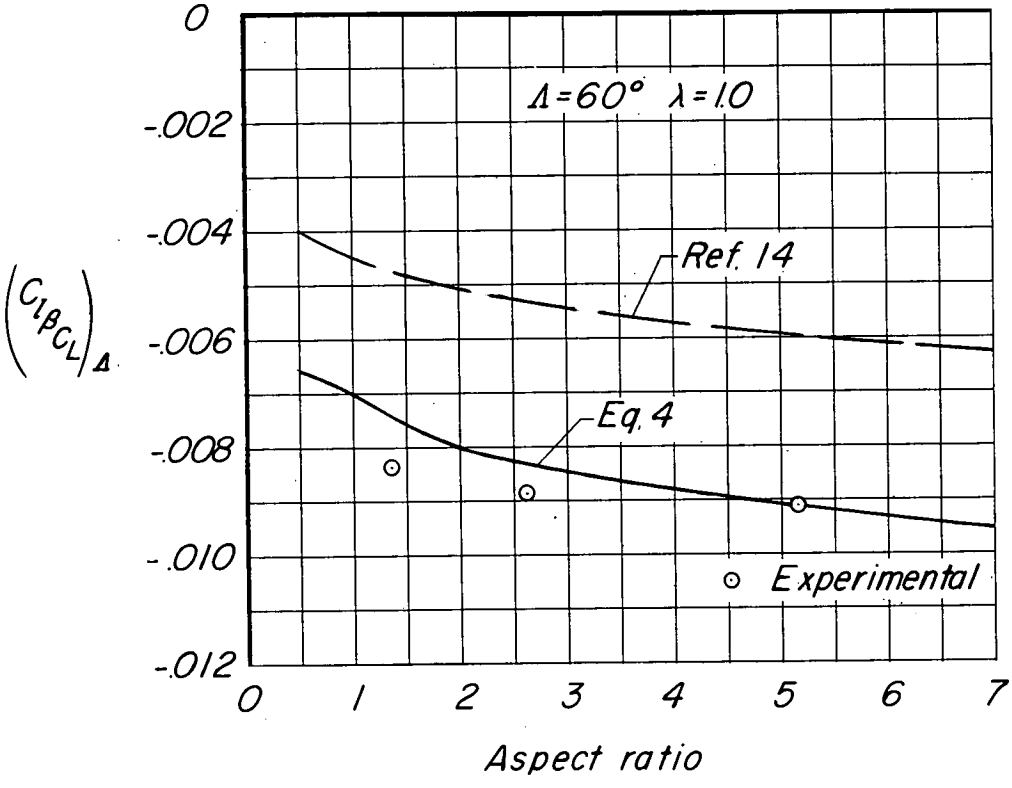

Figure 5.- Comparison of theoretical methods for estimating the wing sweep contribution to rolling moment due to sideslip. (β in degrees.)

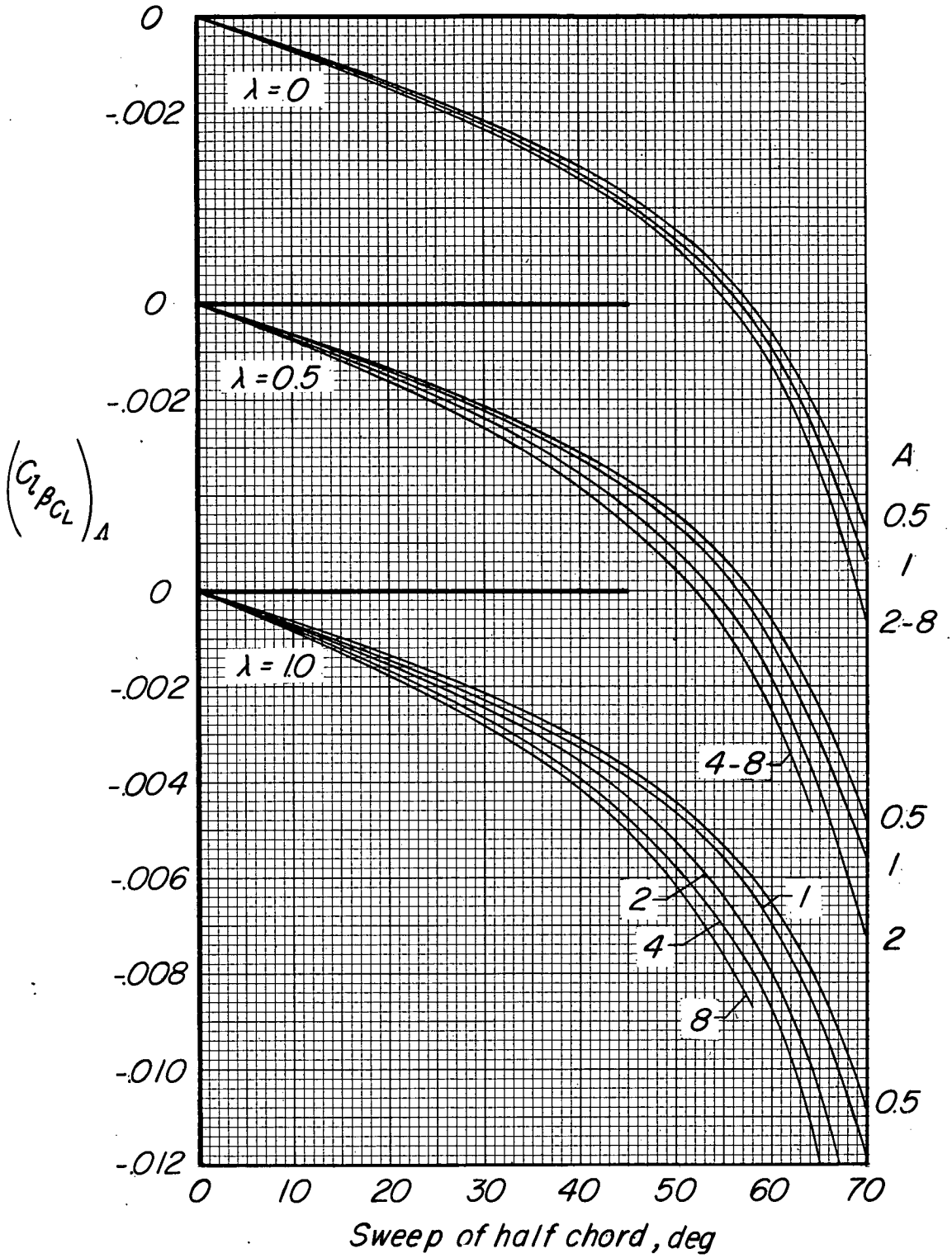

Figure 6.- Charts for determining the contribution of wing sweep to rolling moment due to sideslip as determined from equation (4). (β in degrees.)

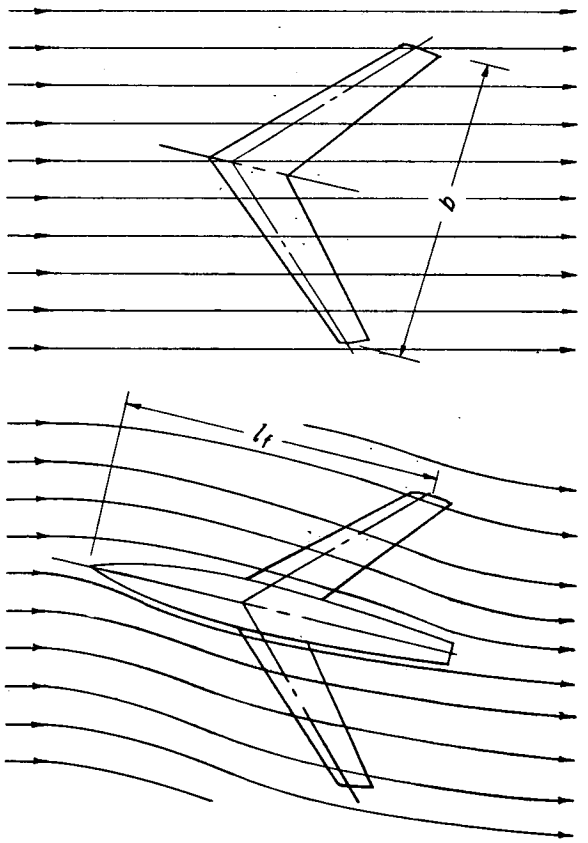

(a) Assumed streamlines illustrating reduction in effective sideslip angle caused by fuselage.

	Δ	A	λ	D/b	Ref
○	45°	4	.60	.167	17
□	46.7°	4	.60	.125	16
◇	45°	6	.31	.101	15

$$K_f = \frac{\left(C_{l\beta_{C_L}}\right)_{WF(exp)} - \left(C_{l\beta_{C_L}}\right)_{A(theory)}}{\left(C_{l\beta_{C_L}}\right)_{W(exp)} - \left(C_{l\beta_{C_L}}\right)_{A(theory)}}$$

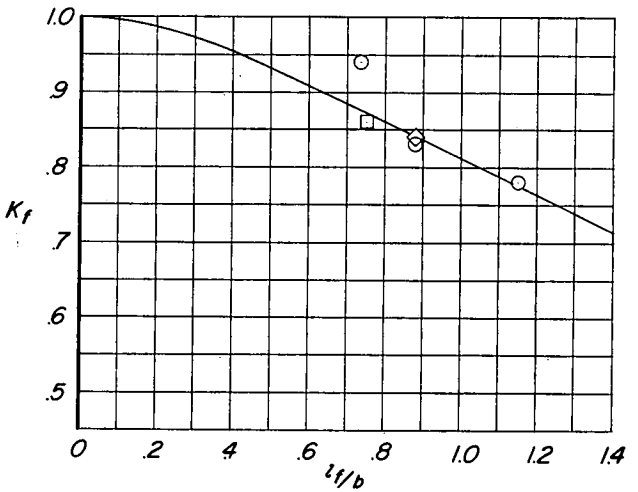

(b) Correlation curve determined from experimental data.

Figure 7.- Fuselage effect on the sweep contribution to rolling moment due to sideslip.

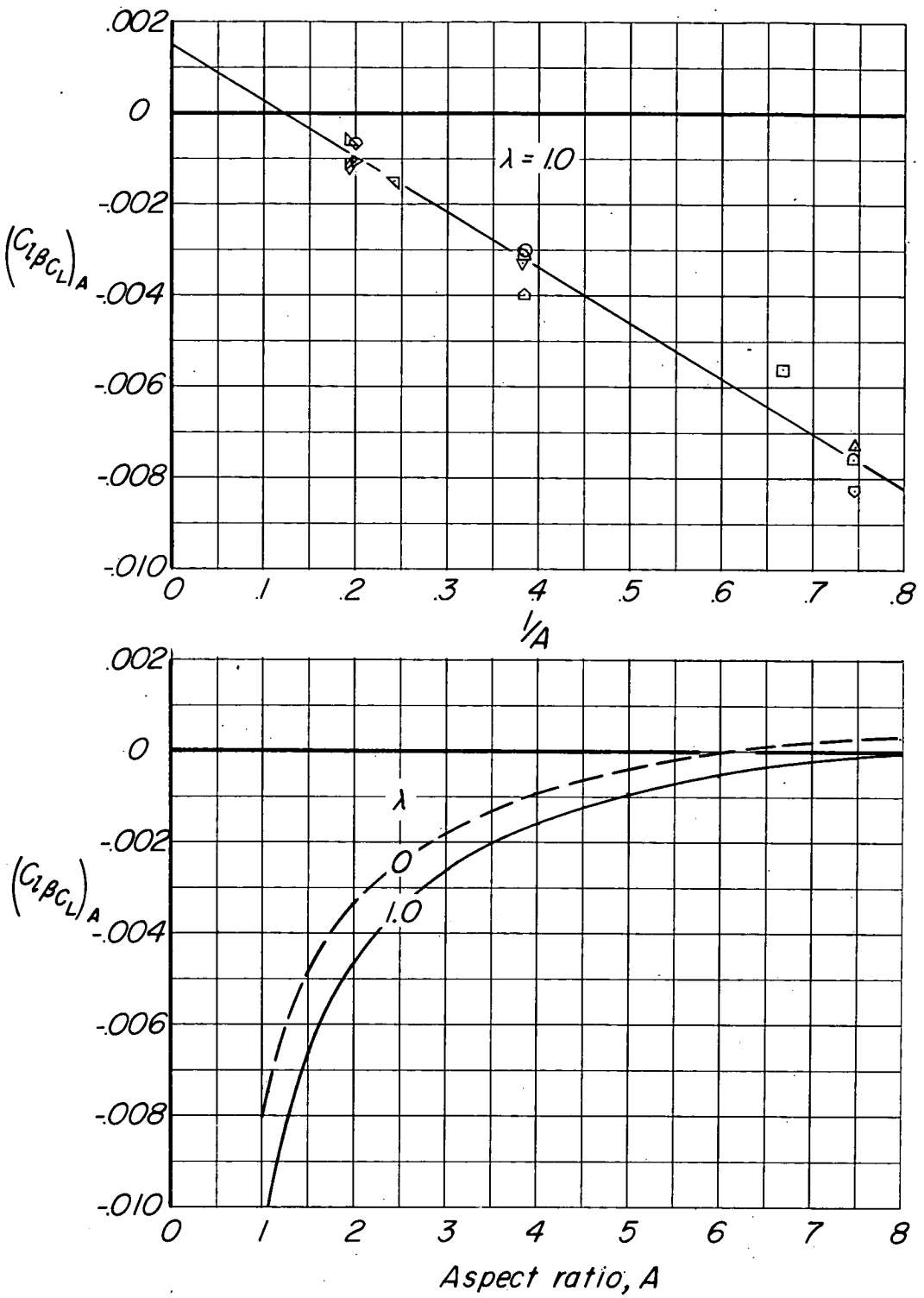

Figure 8.- Chart for determining the aspect-ratio contribution to rolling moment due to sideslip as determined from correlation of experimental data. (β in degrees.)

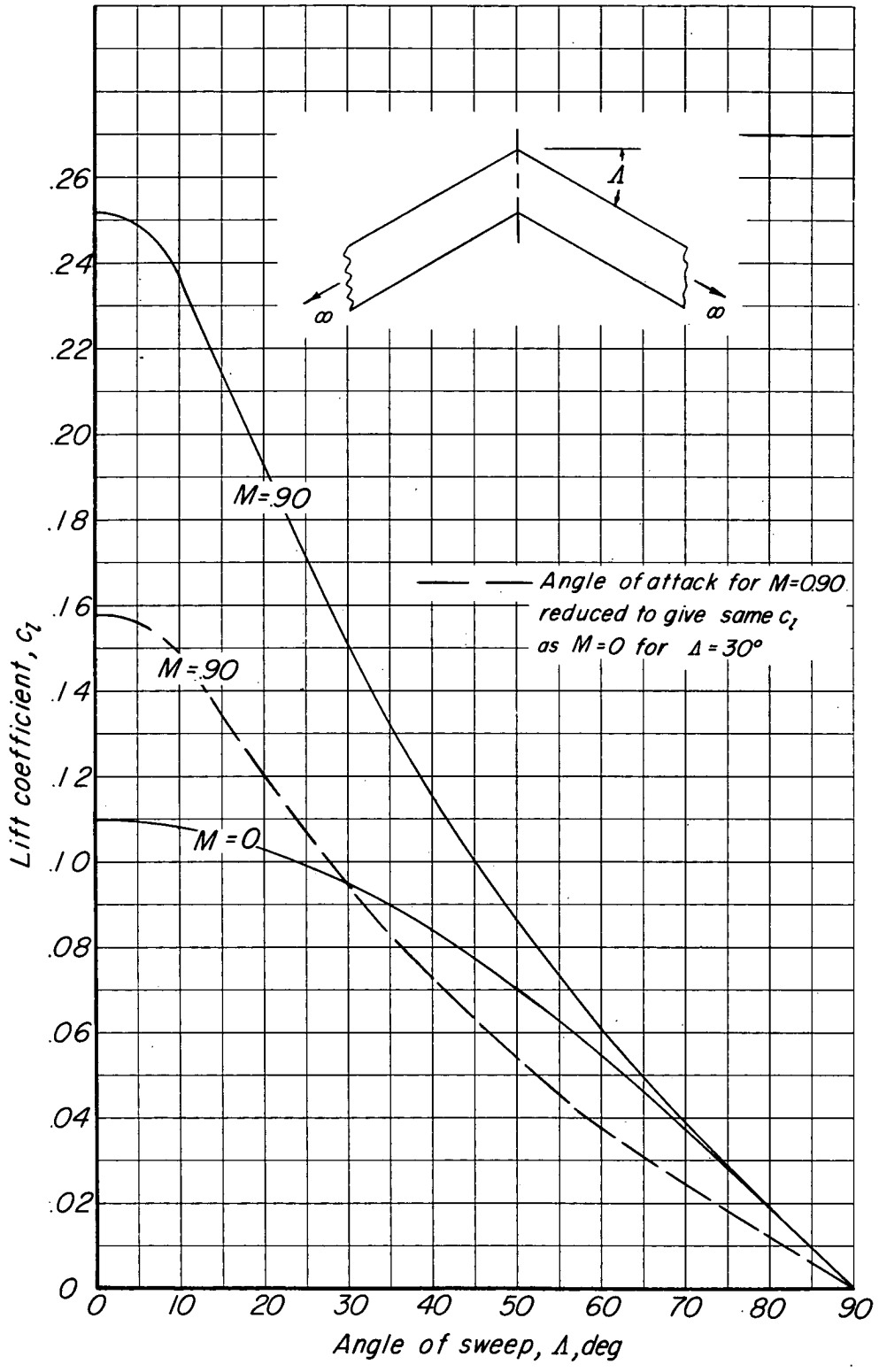

Figure 9.- Illustration of compressibility effects on the variation of section lift coefficient with wing sweep.

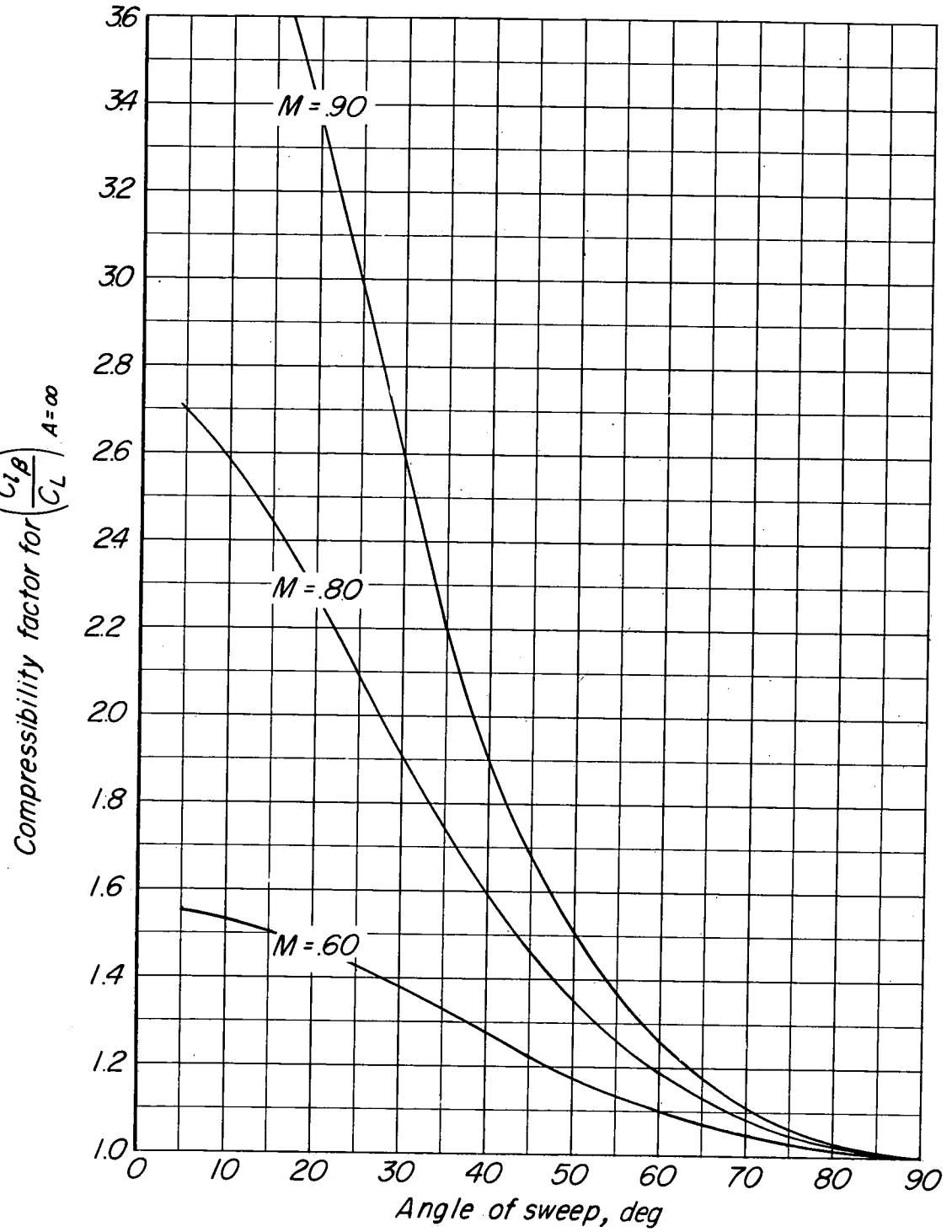

Figure 10.- Compressibility correction factor to the wing sweep contribution to rolling moment due to sideslip for infinite-aspect-ratio wings as determined from equation (7).

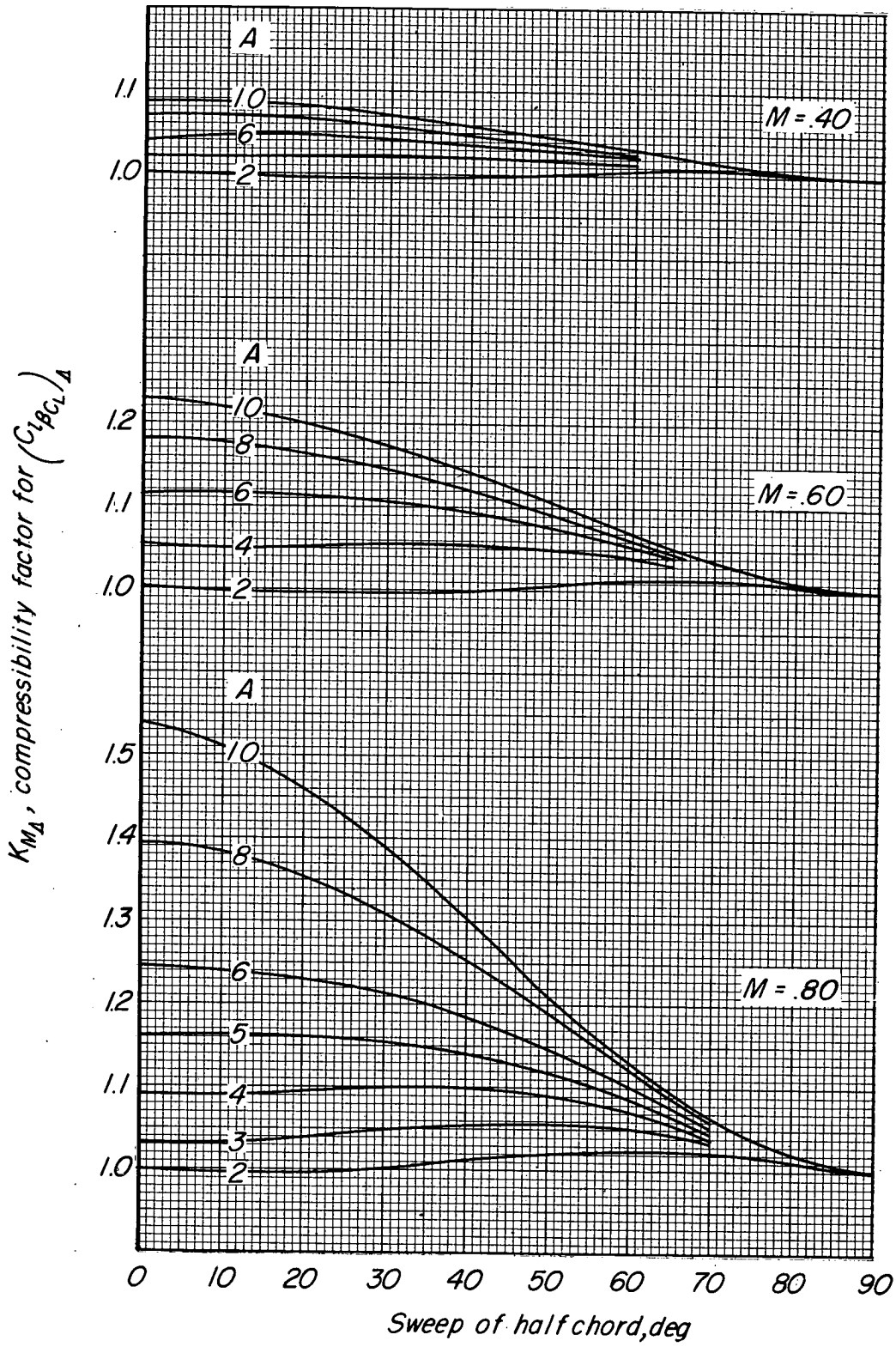

Figure 11.- Compressibility correction factor for the wing sweep contribution to rolling moment due to sideslip for finite-aspect-ratio wings.

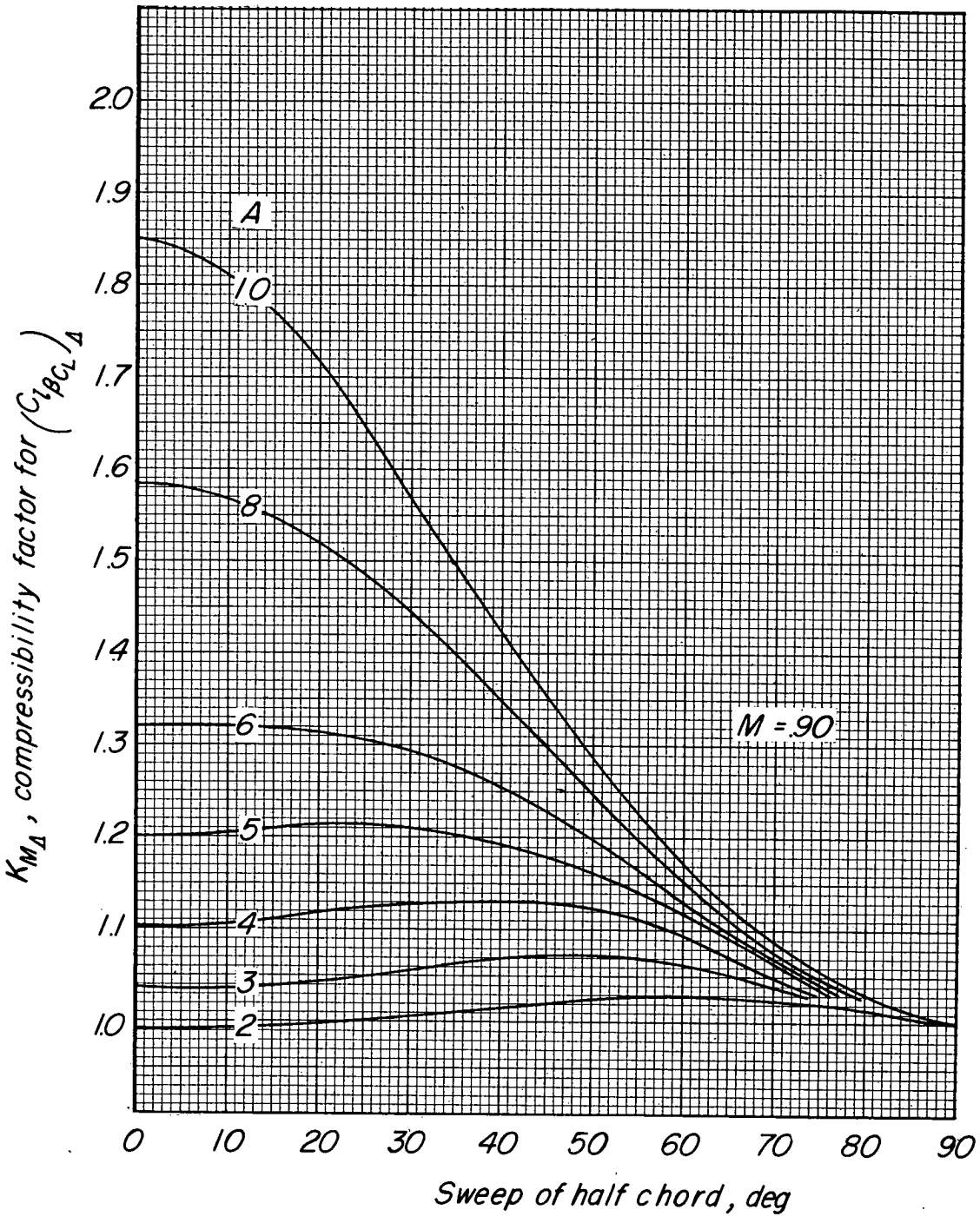

Figure 11.- Continued.

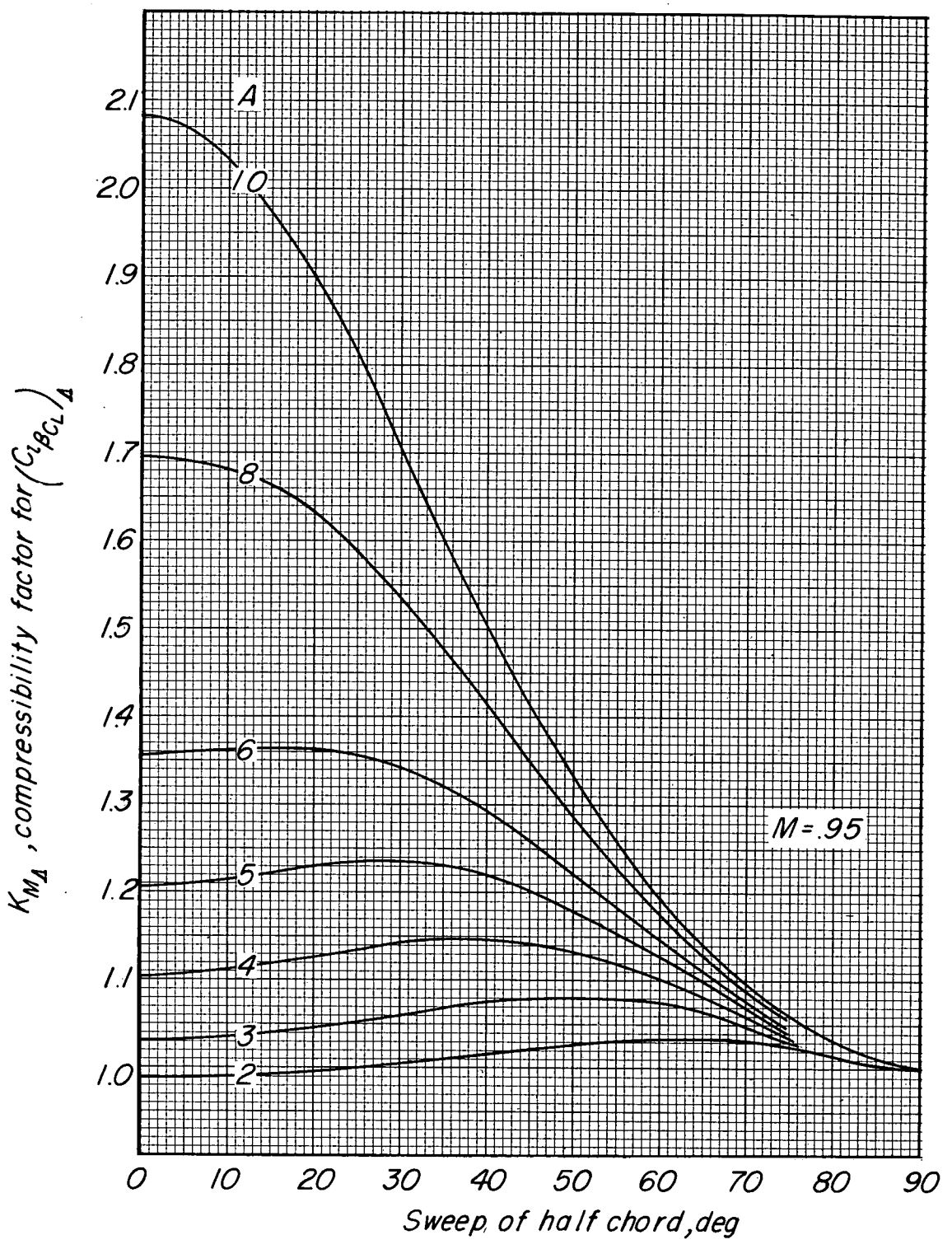

Figure 11.- Concluded.

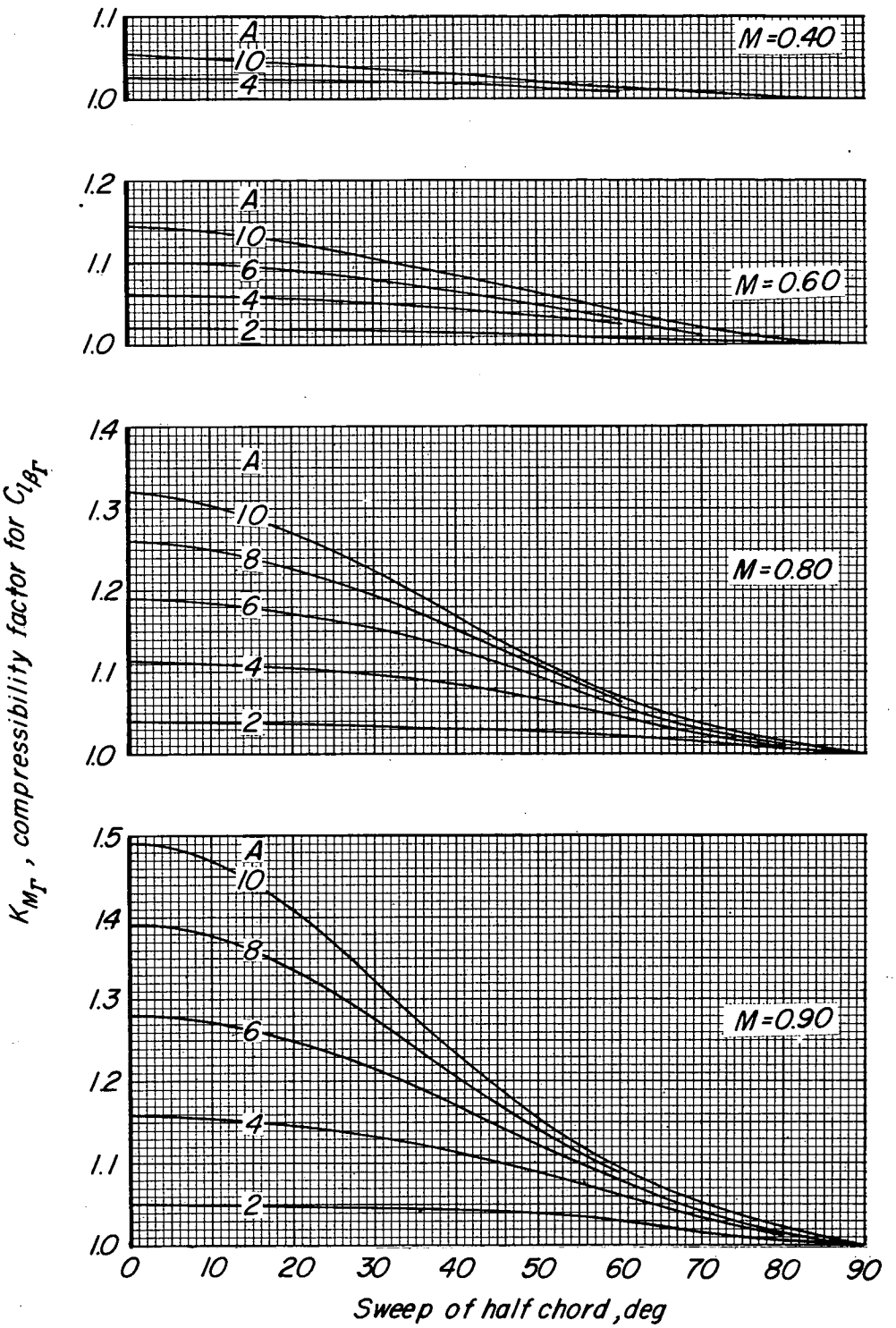

Figure 12.- Compressibility correction factor for the wing-dihedral contribution to rolling moment due to sideslip for finite-aspect-ratio wings.

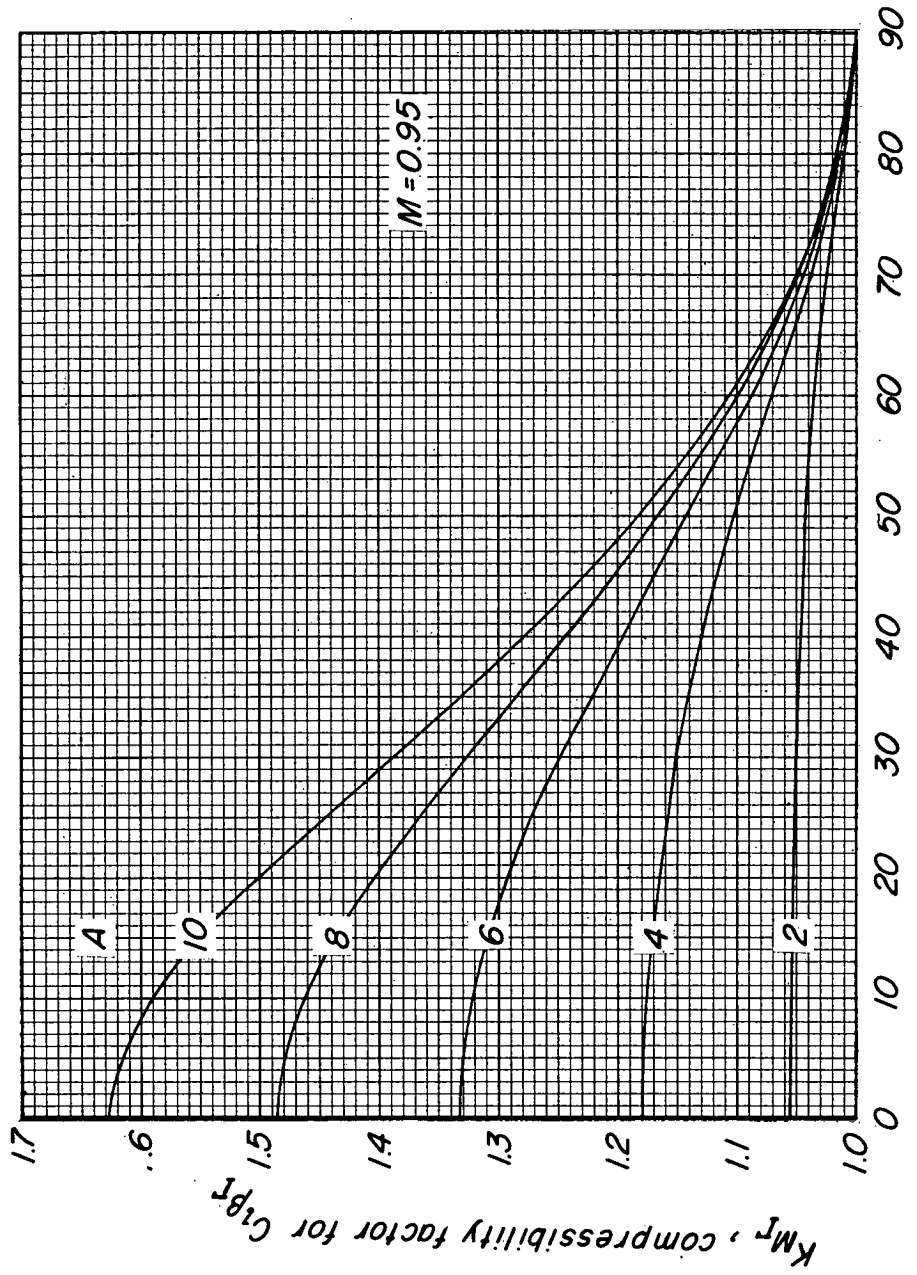

Figure 12.- Concluded.

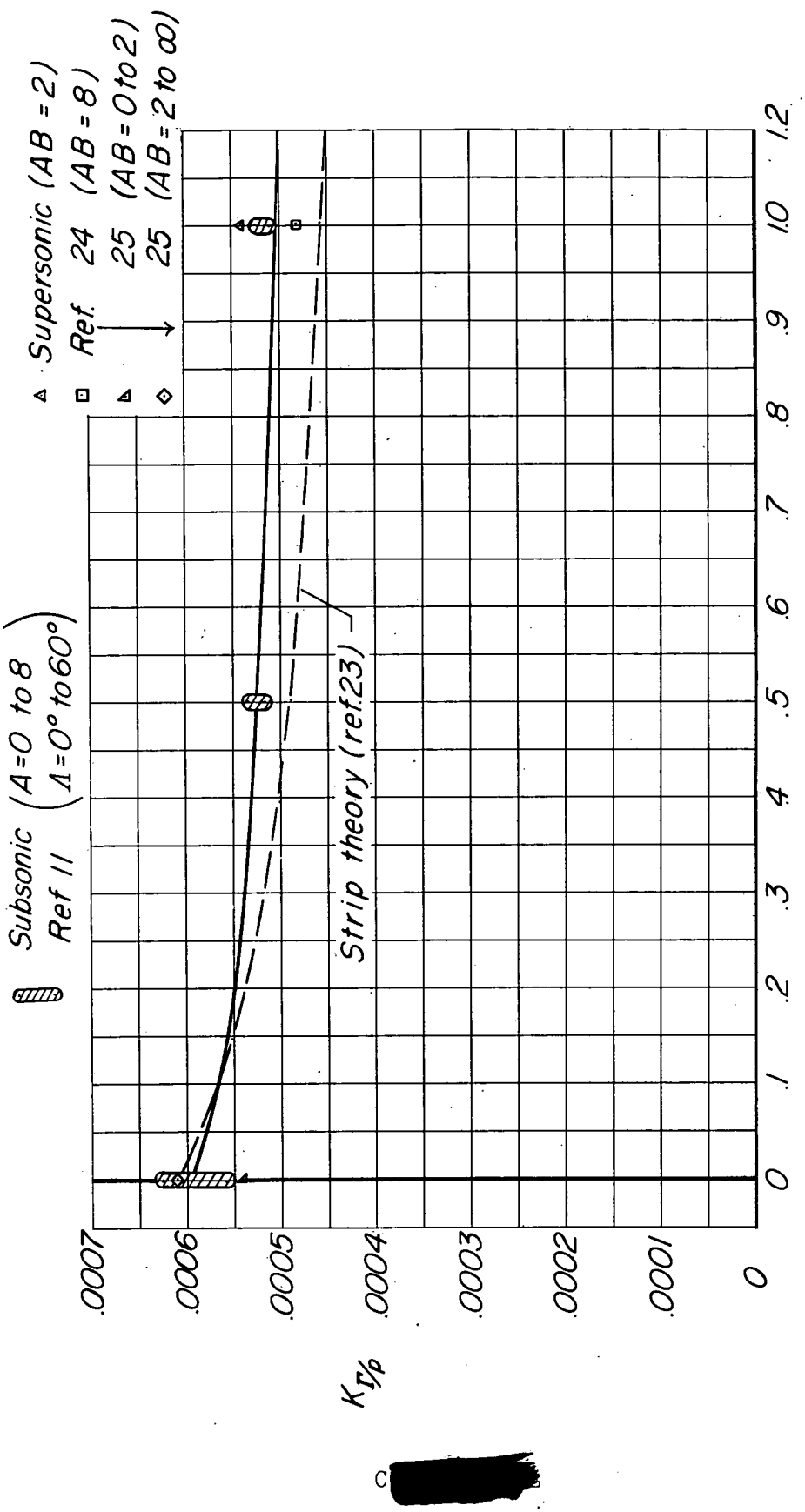

Figure 13.- Variation with taper ratio of the correction factor used in estimating $C_{l_{\beta_\Gamma}}$ from experimental damping in roll.

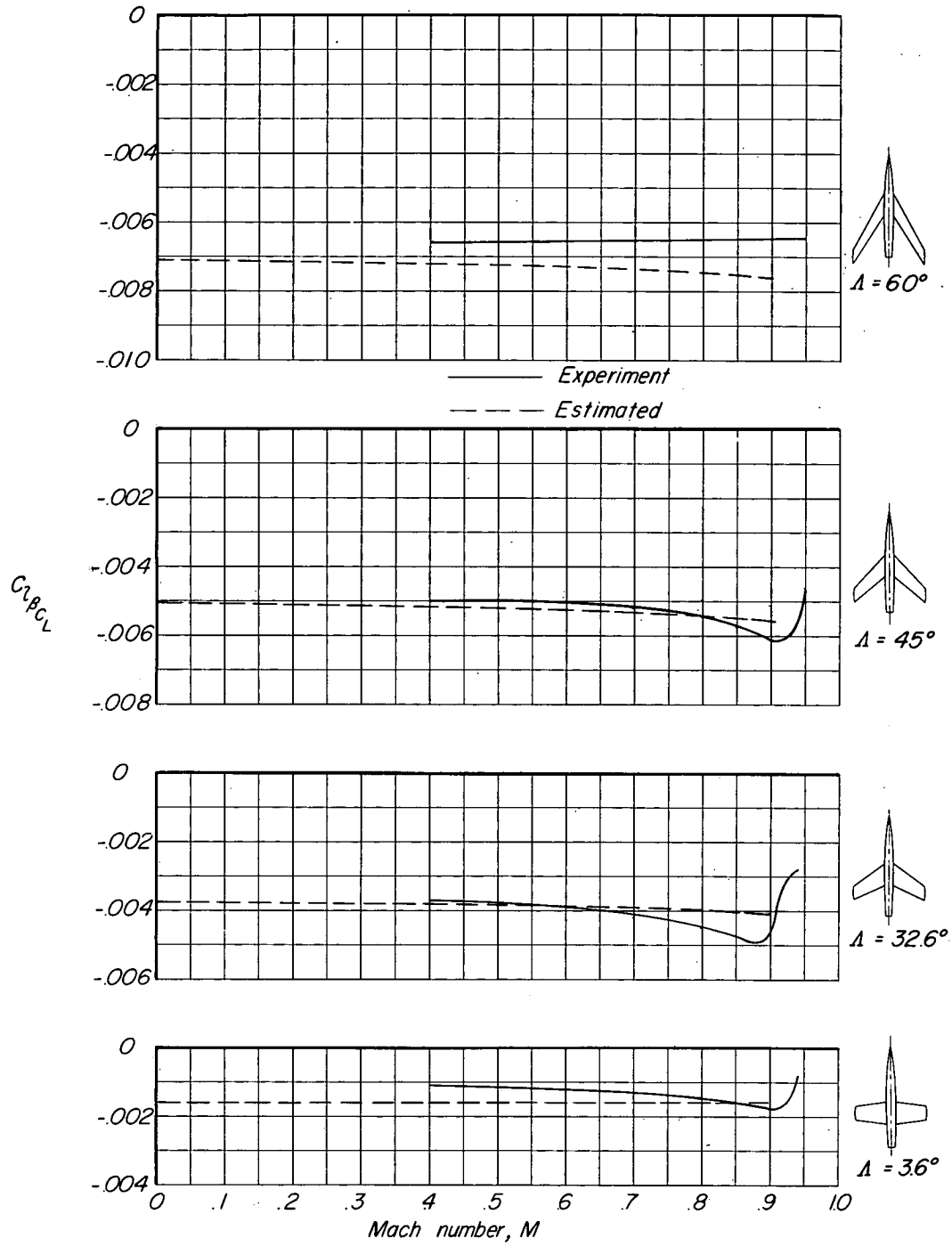

(a) Effect of sweep. A = 4; λ = 0.6.

Figure 14.- Comparison of experimental and estimated rolling moment due to sideslip showing effects of Mach number and wing plan form. $C_L < 0.2$, NACA 65A006 airfoil sections (except where noted). (β in degrees.)

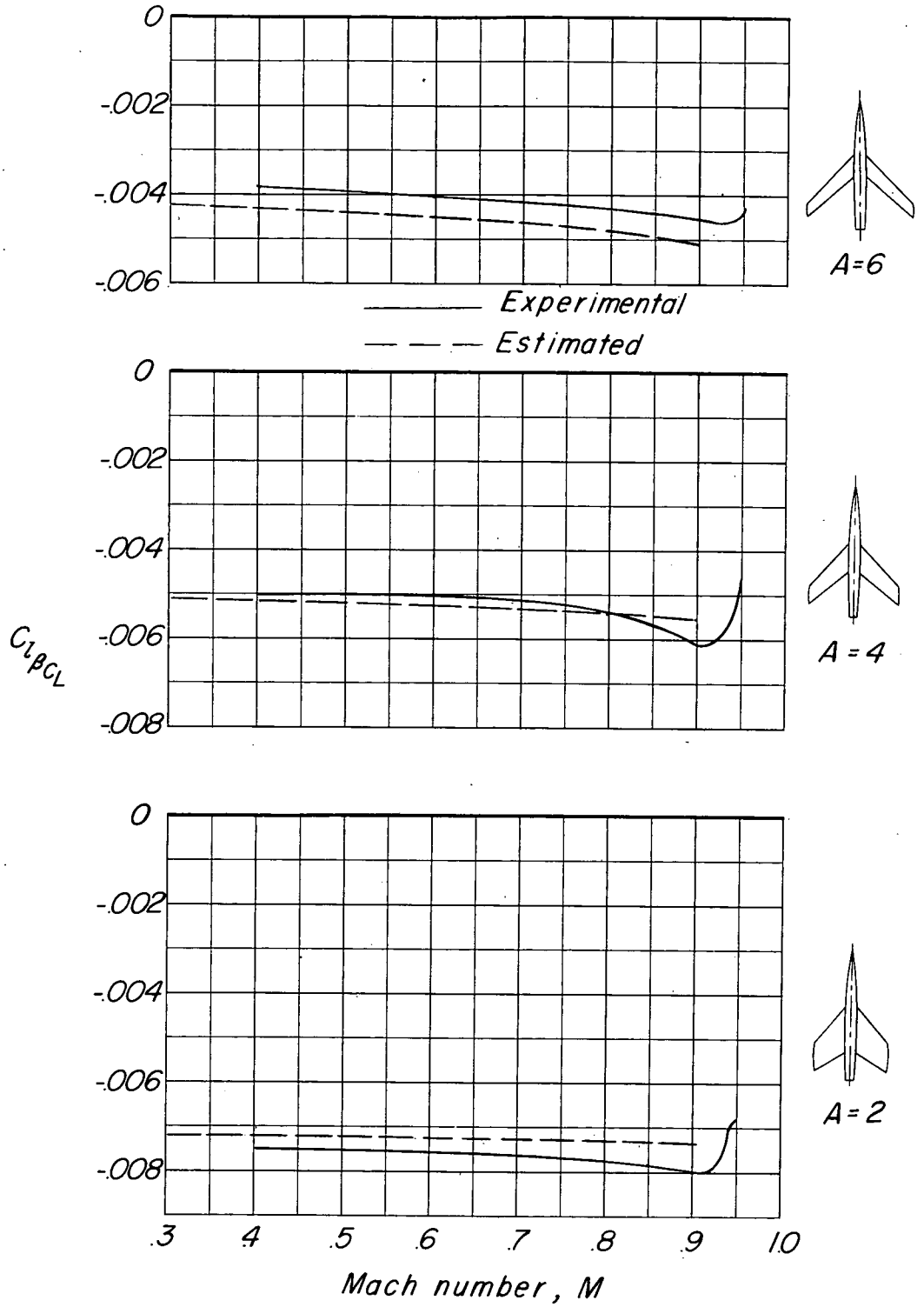

(b) Effect of aspect ratio. $\Lambda = 45^\circ$; $\lambda = 0.6$.

Figure 14.- Continued.

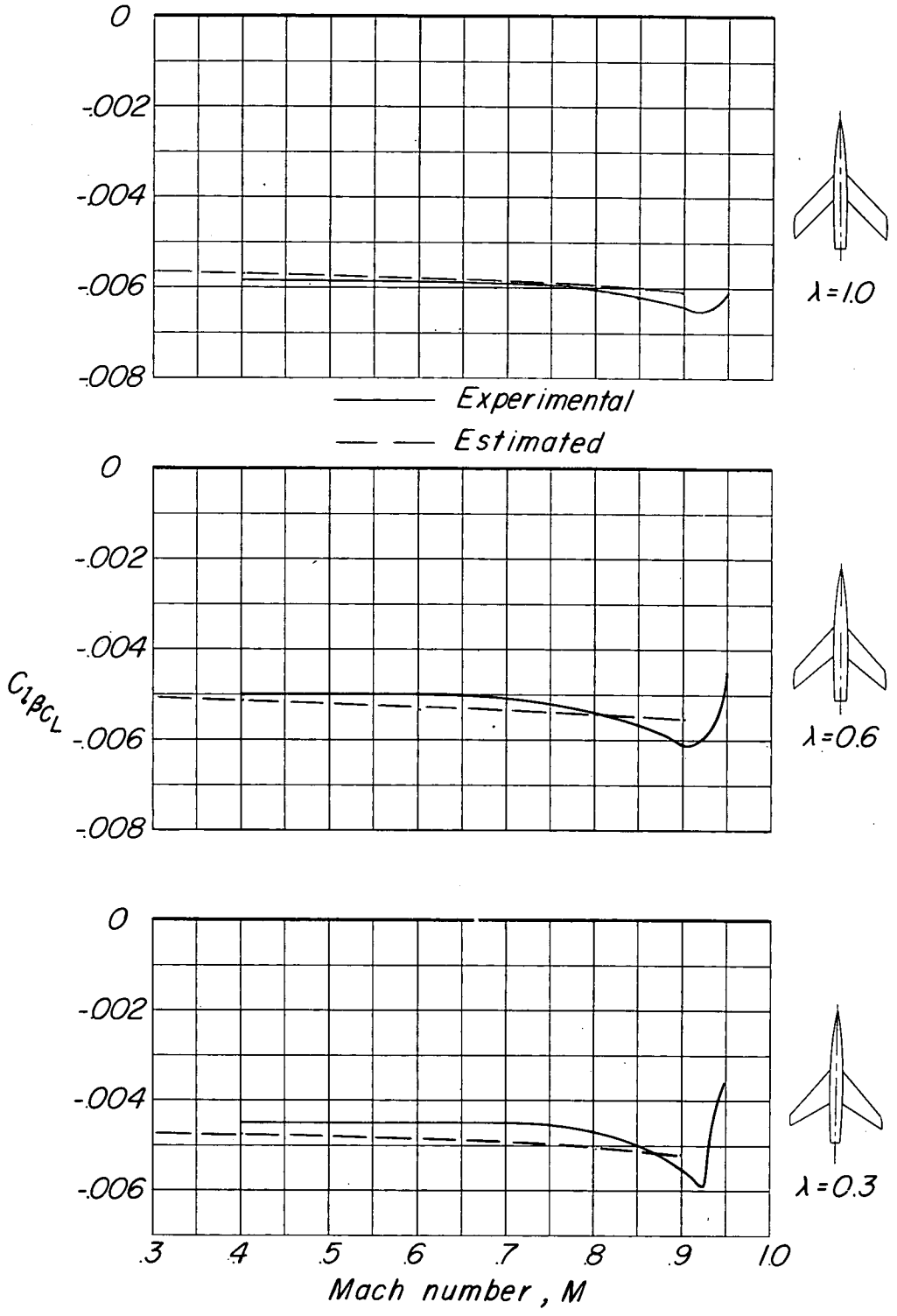

(c) Effect of taper ratio. $\Lambda = 45^\circ$; $A = 4$.

Figure 14.- Continued.

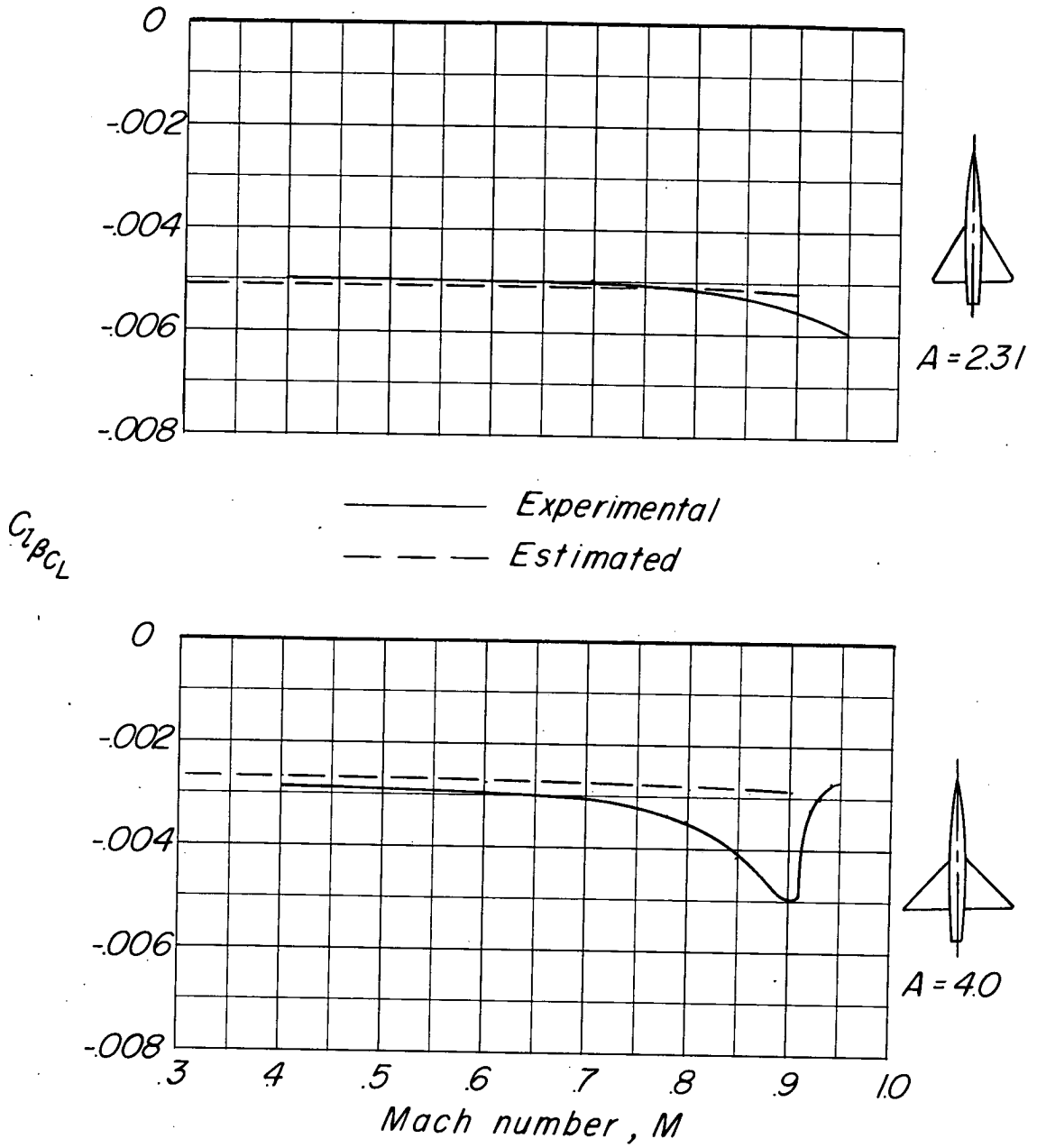

(d) Delta wings (NACA 65A003 airfoil sections for A = 2.3 wing).

Figure 14.- Concluded.

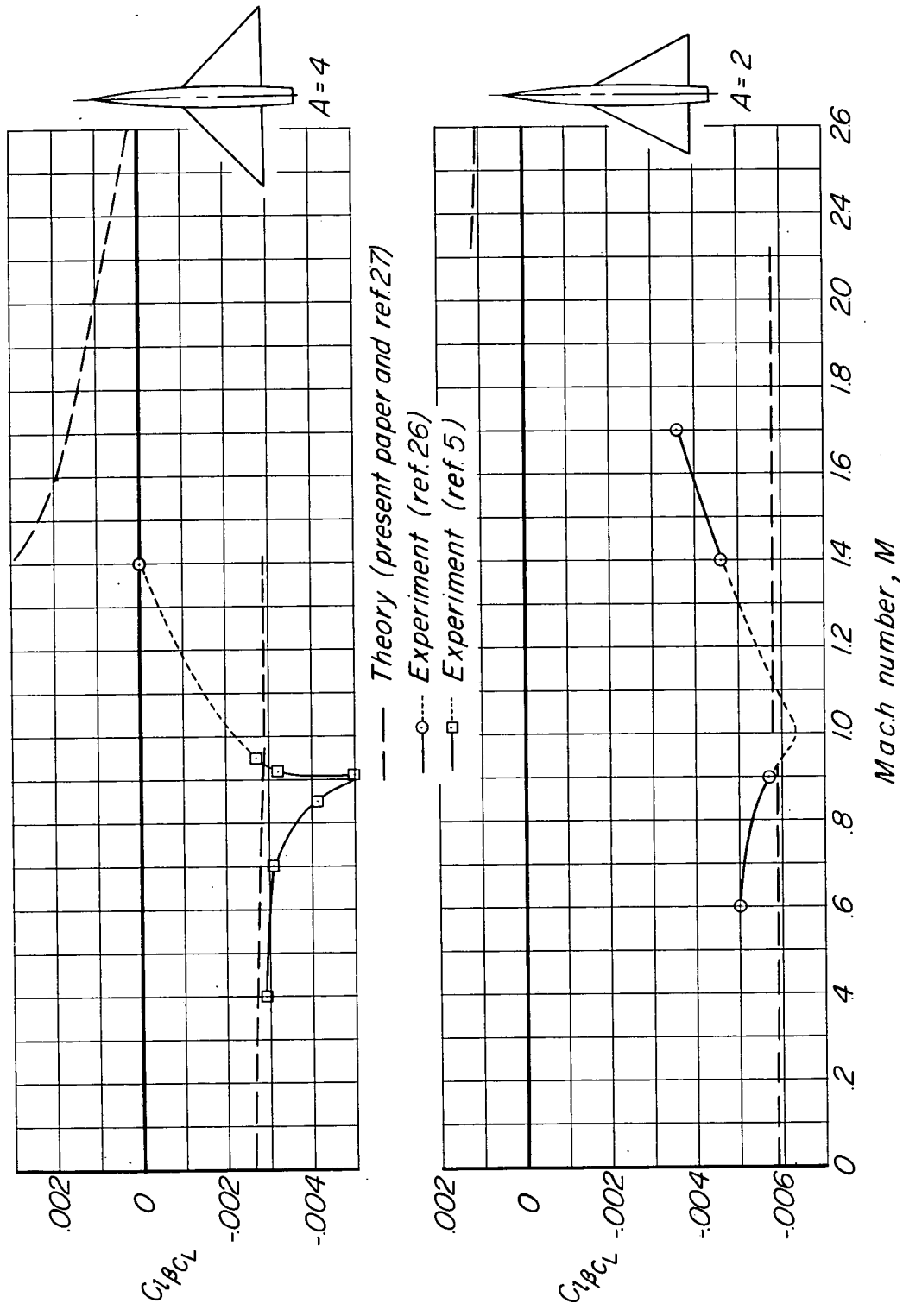

Figure 15.- Comparison of experimental and estimated rolling moment due to sideslip through the transonic Mach number range for two delta wings. (β in degrees.)

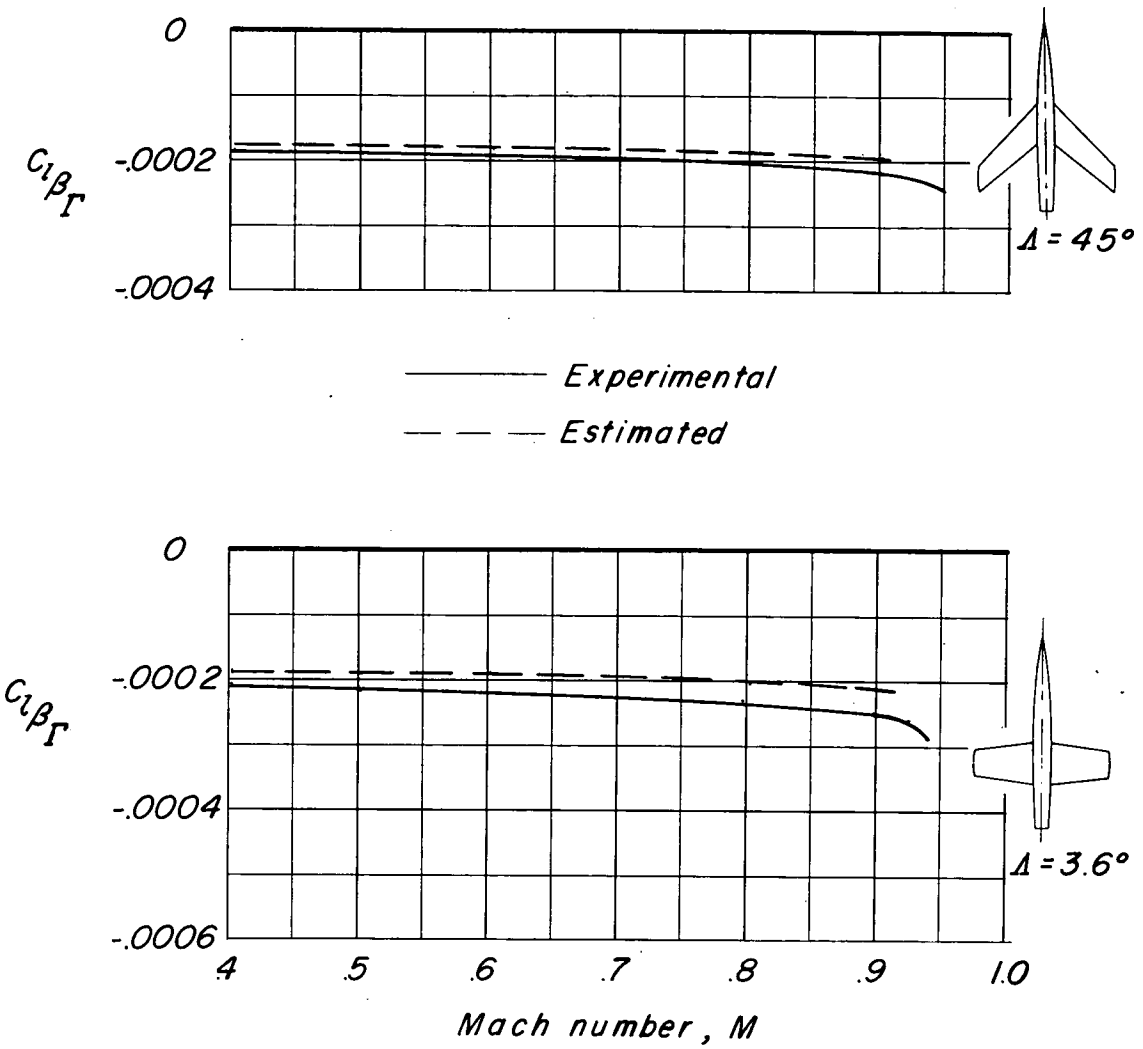

Figure 16.- Comparison of experimental and estimated contribution of wing dihedral to rolling moment due to sideslip through the subsonic Mach number range. $C_L < 0.2$; A = 4; $\lambda = 0.6$; NACA 65A006 airfoil sections. (β in degrees.)

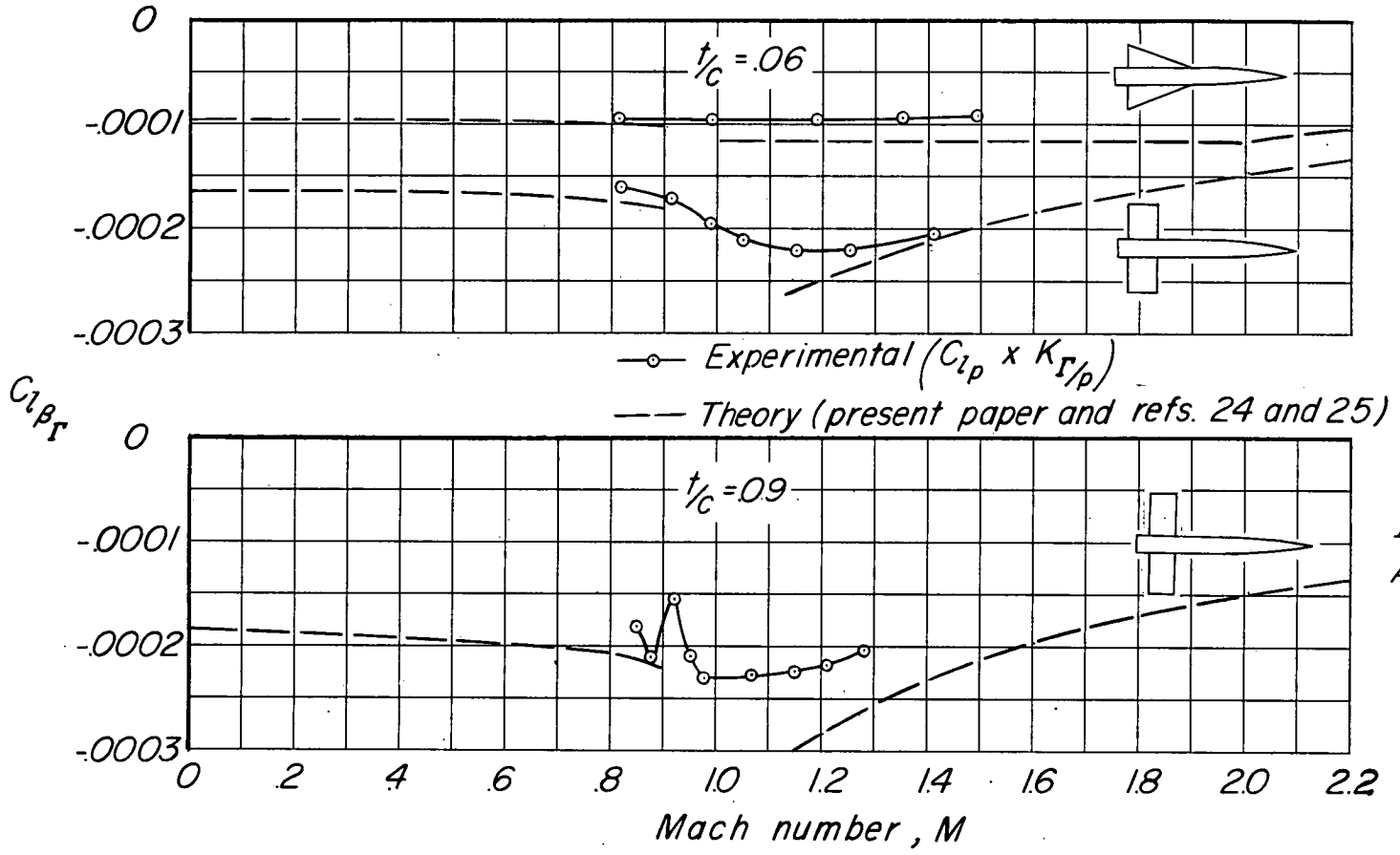

Figure 17.- Variation of the dihedral contribution to rolling moment due to sideslip through the transonic Mach number range as determined from theory and damping in roll of rocket-powered models. (β in degrees.)

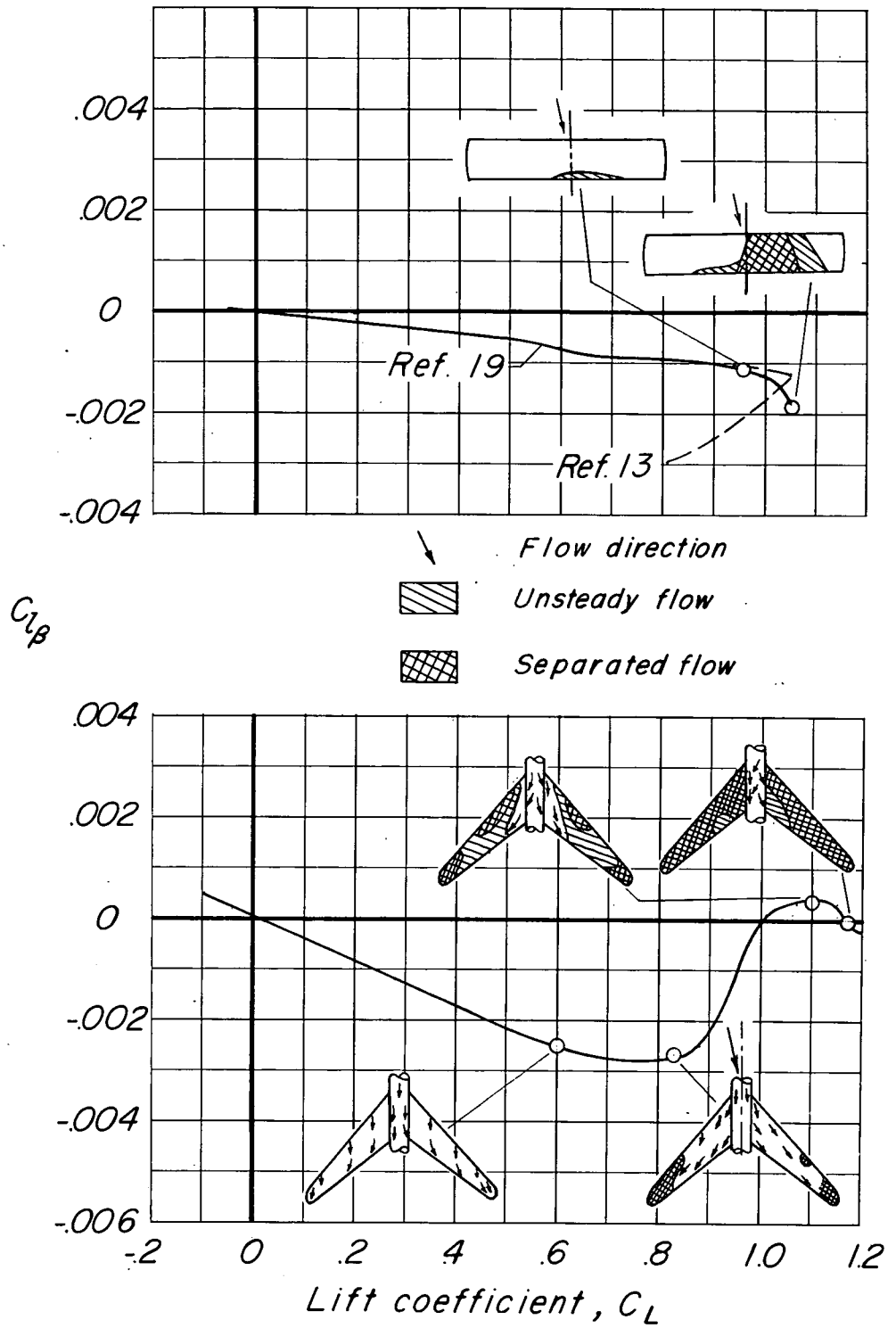

Figure 18.- Low-speed test results illustrating typical effects of wing sweep on the variation of rolling moment due to sideslip with lift coefficient. (β in degrees.)

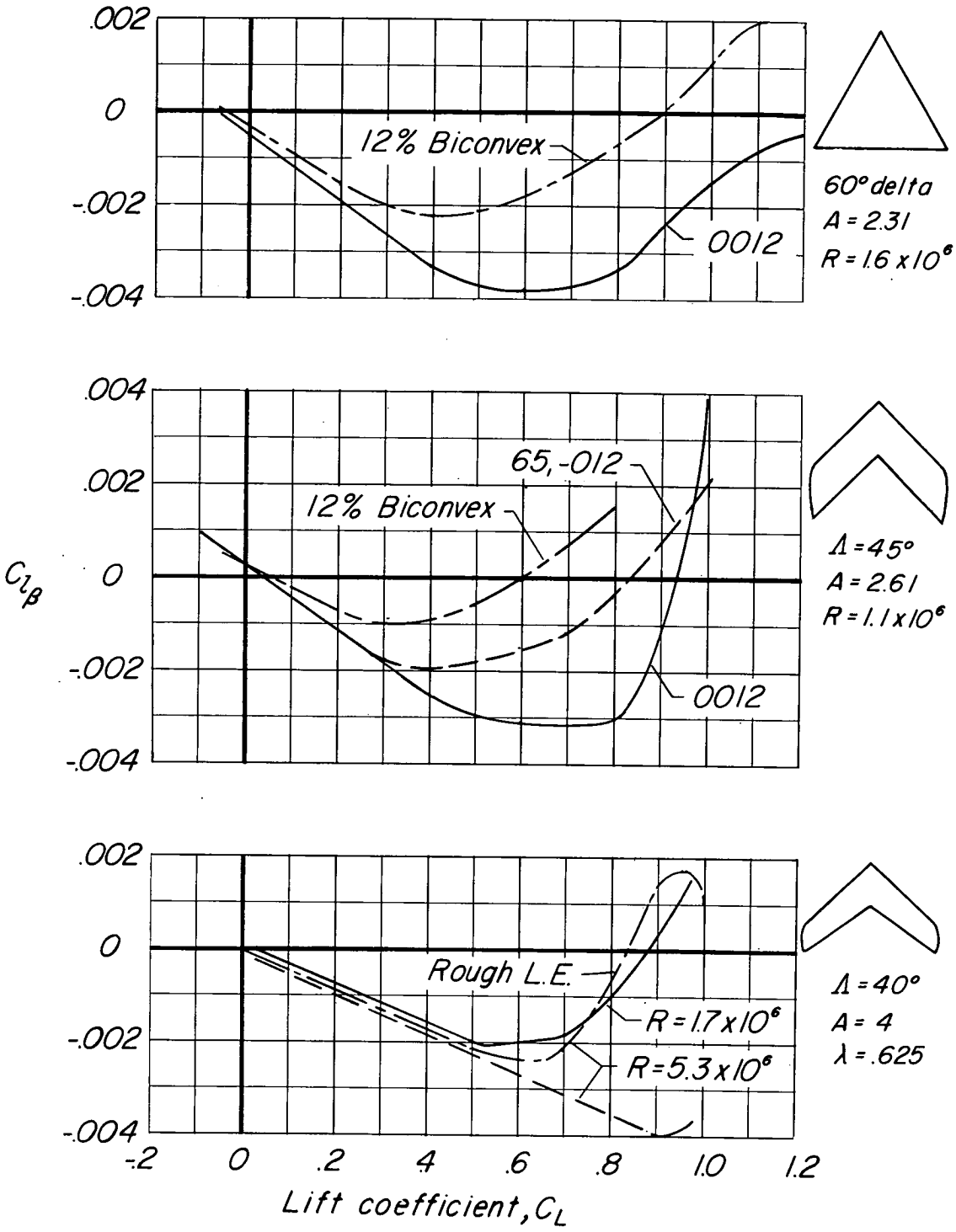

Figure 19.- Low-speed test results showing effects of leading-edge radius and Reynolds number on the variation of rolling moment due to sideslip with lift coefficient. (β in degrees.)

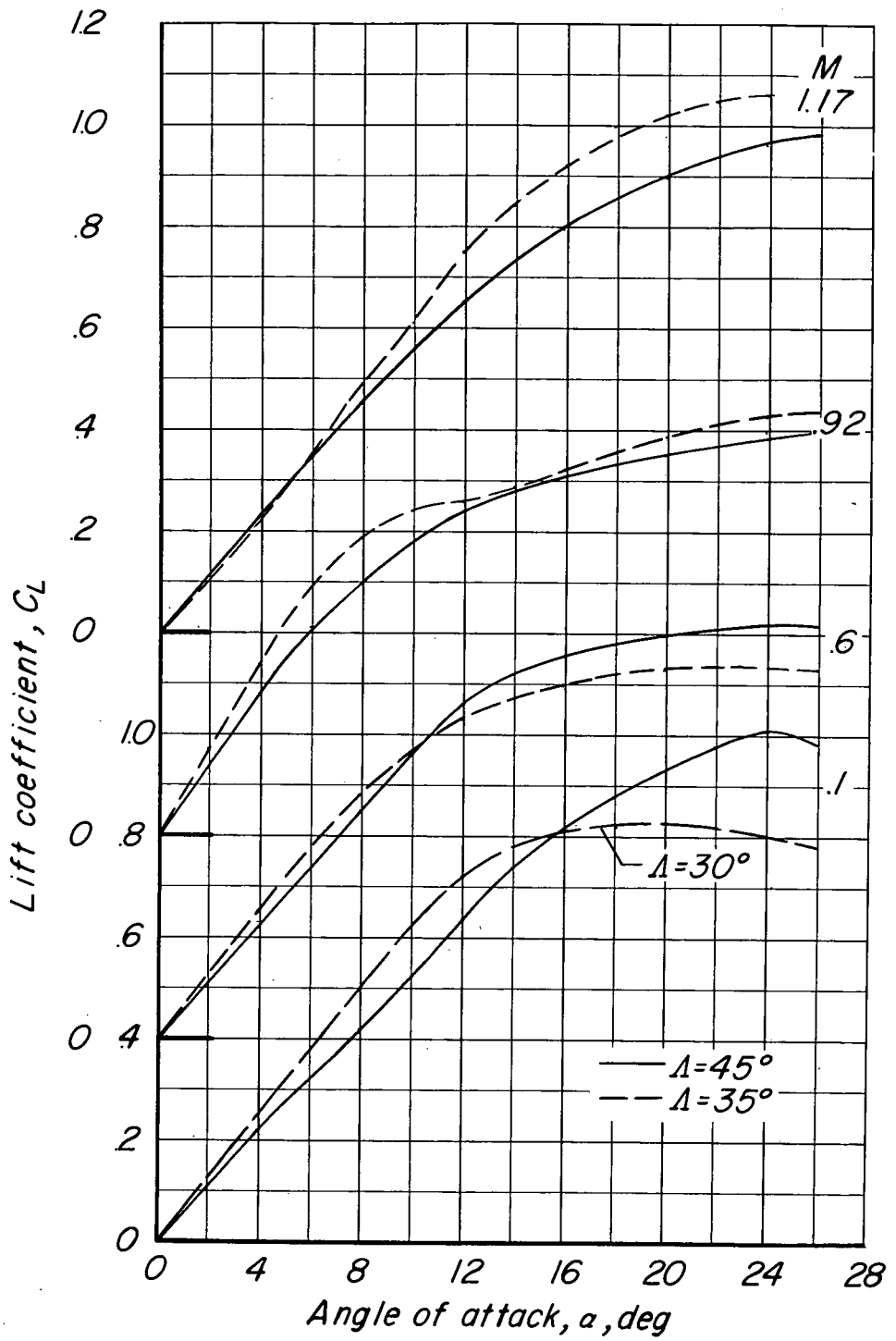

Figure 20.- Test results for two sweep angles illustrating the probable effects of Mach number on the lift characteristics of the leading and trailing wing panels of a 40° swept wing at 5° sideslip. Data from references 33 and 34.

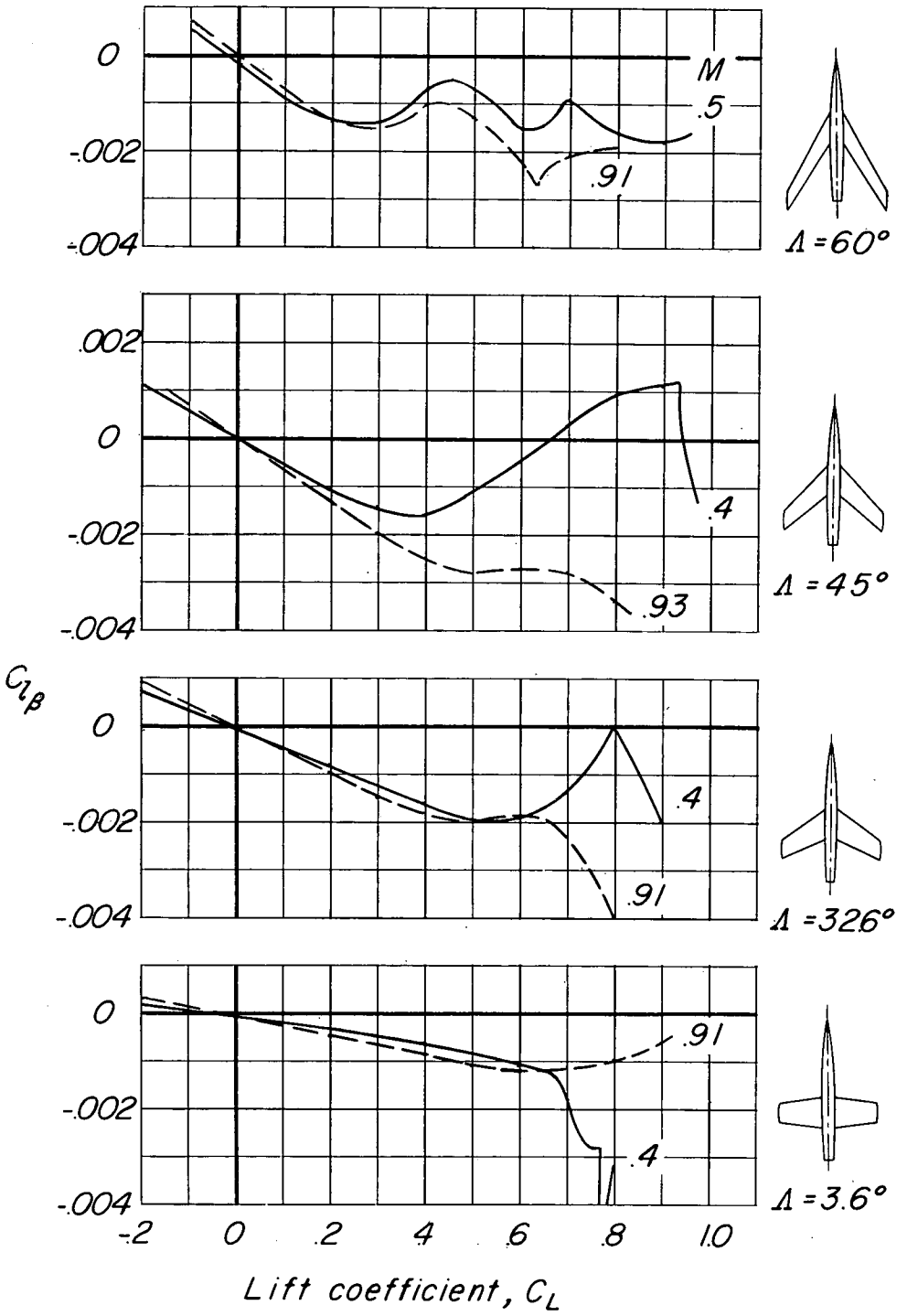

(a) Effect of sweep. A = 4; λ = 0.6.

Figure 21.- Experimental variation of rolling moment due to sideslip with lift coefficient showing effects of Mach number and wing plan form. (β in degrees.)

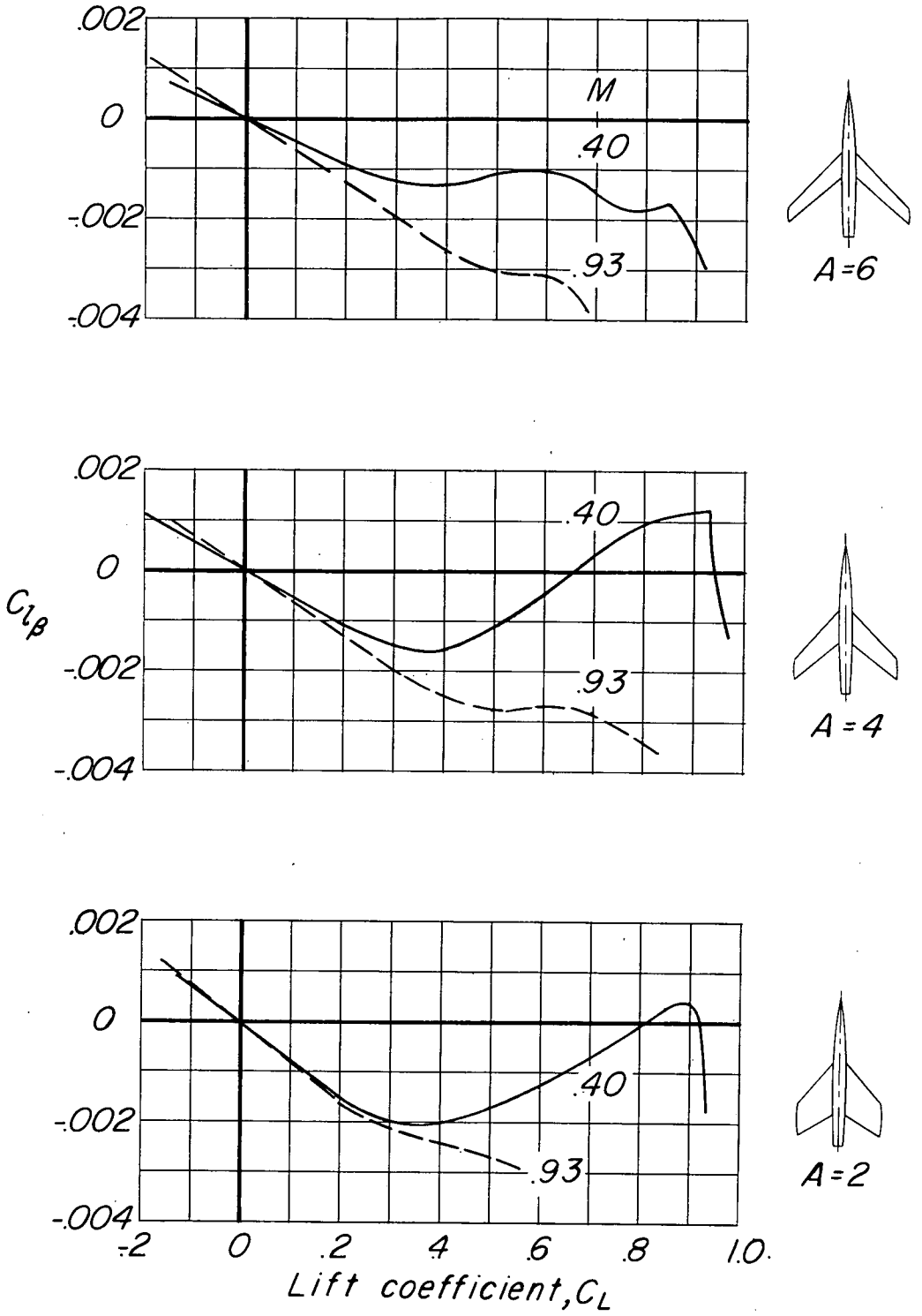

(b) Effect of aspect ratio. $\Lambda = 45^\circ$; $\lambda = 0.6$.

Figure 21.- Continued.

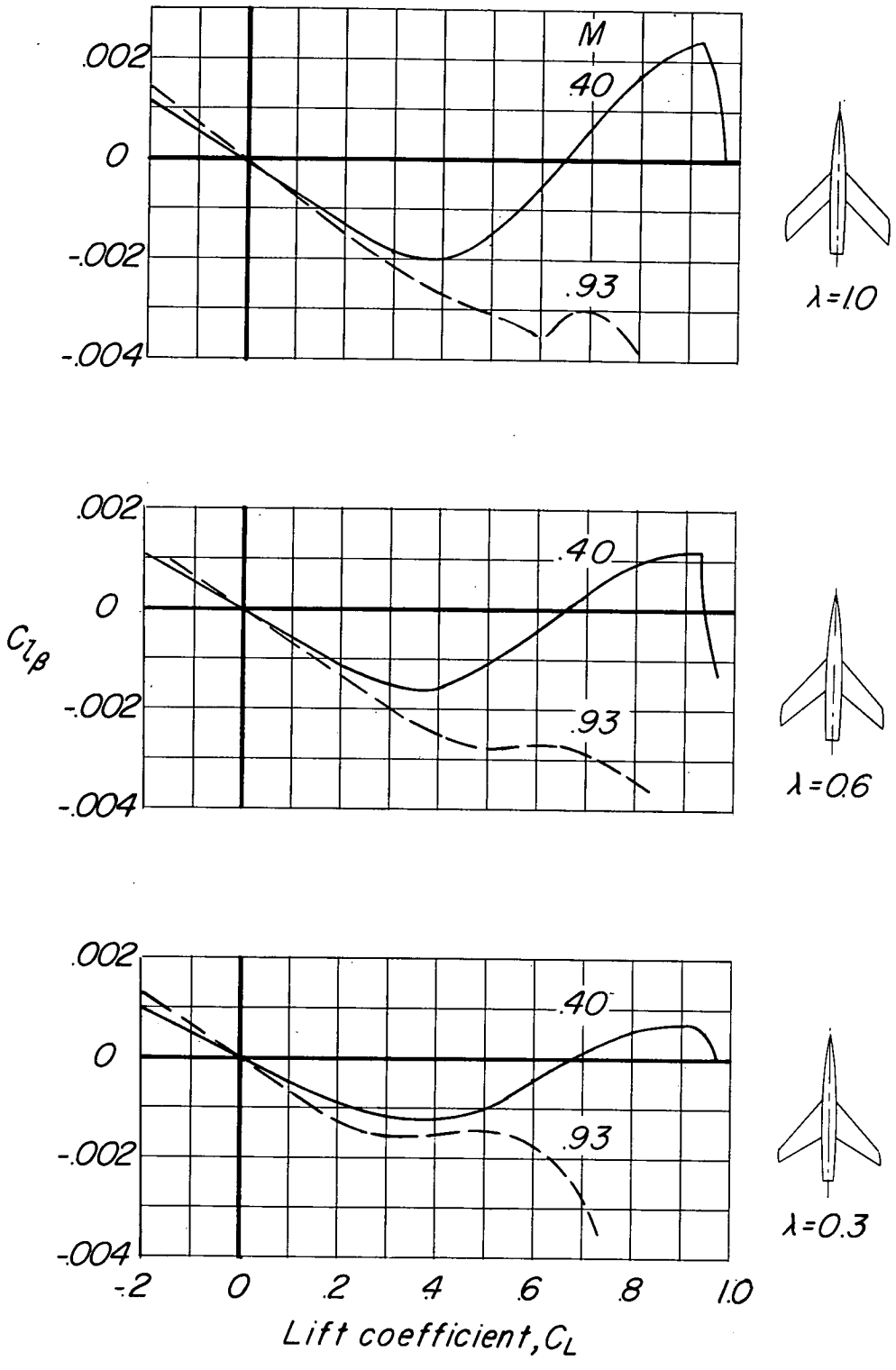

(c) Effect of taper ratio. A = 4; Λ = 45°.

Figure 21.- Concluded.

	○ ◇	□	△	◺	◊ ⌂	⌂
A	2 6	4	3	4	4	Obtained from a number of low speed results
λ	.6	.6	.5	0	.3 10	
t/c	.06	.06	.04	.06	.06	
Ref.	2	1	unpub-lished	5	3	

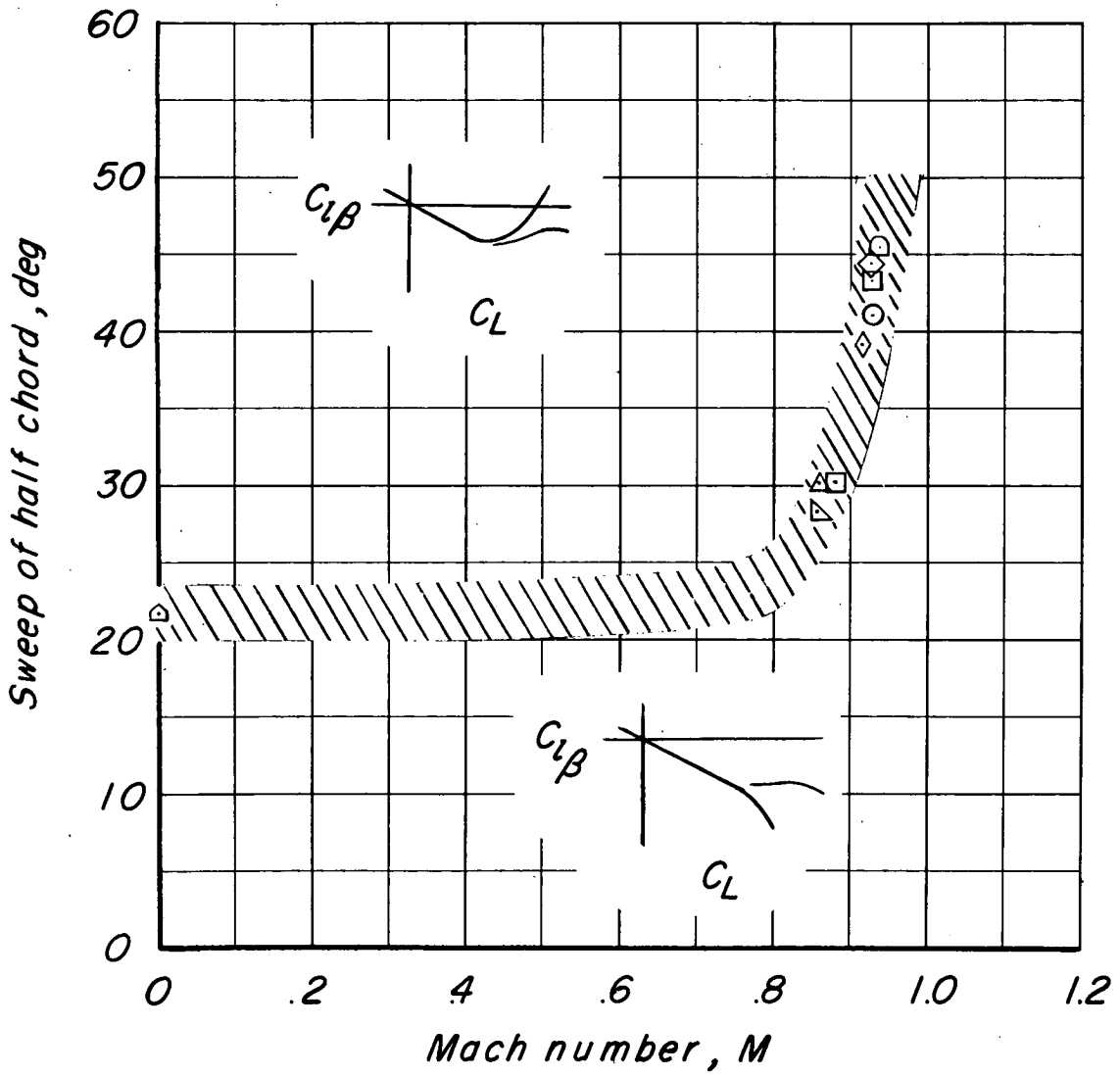

Figure 22.- Boundary of wing sweep and Mach number separating two types of experimental C_{l_β} variations with lift coefficient.

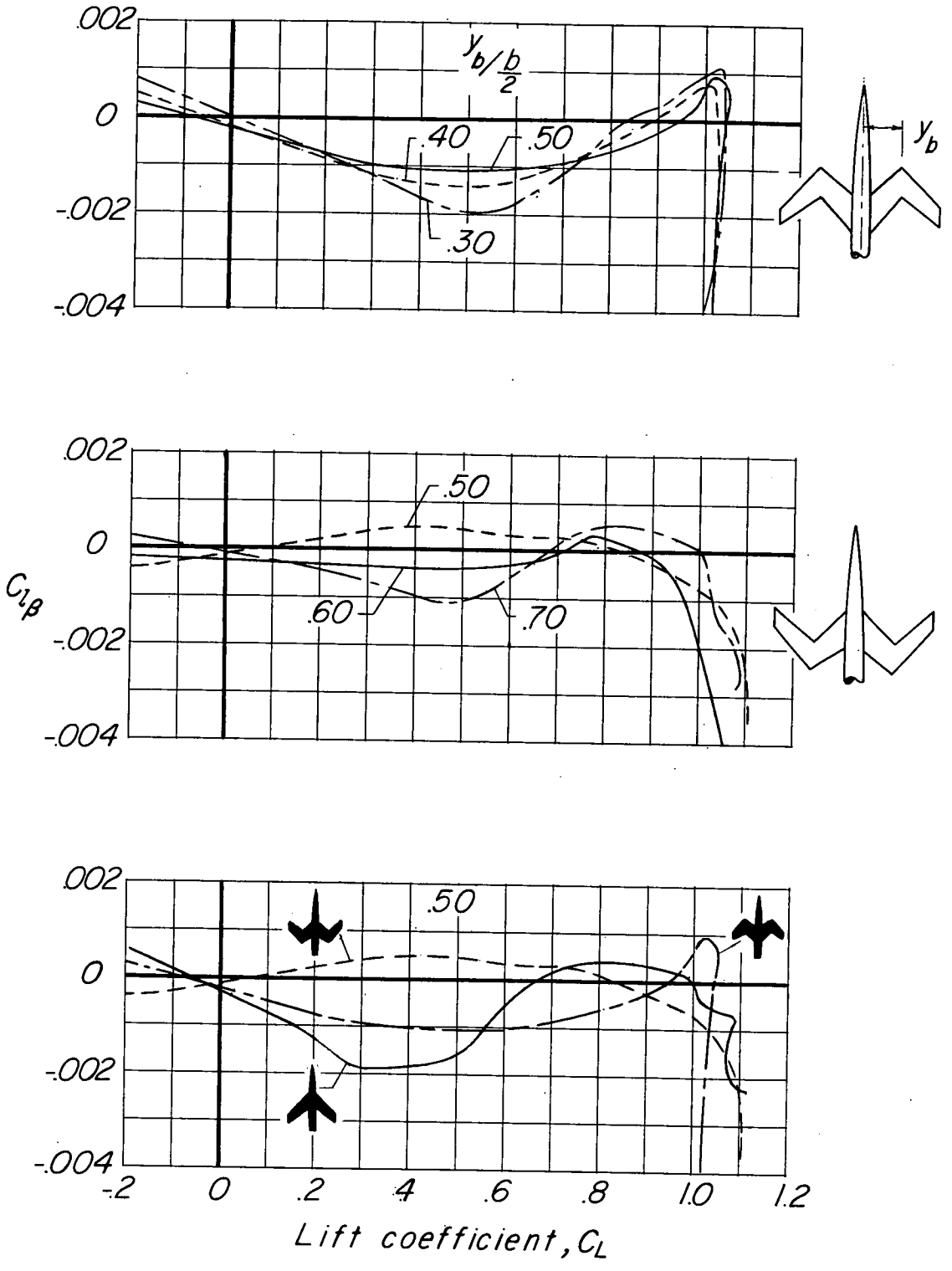

Figure 23.- Low-speed test results for M- and W-wing plan forms showing effects of plan form and location of spanwise sweep discontinuity on rolling moment due to sideslip through the lift range. (β in degrees.)

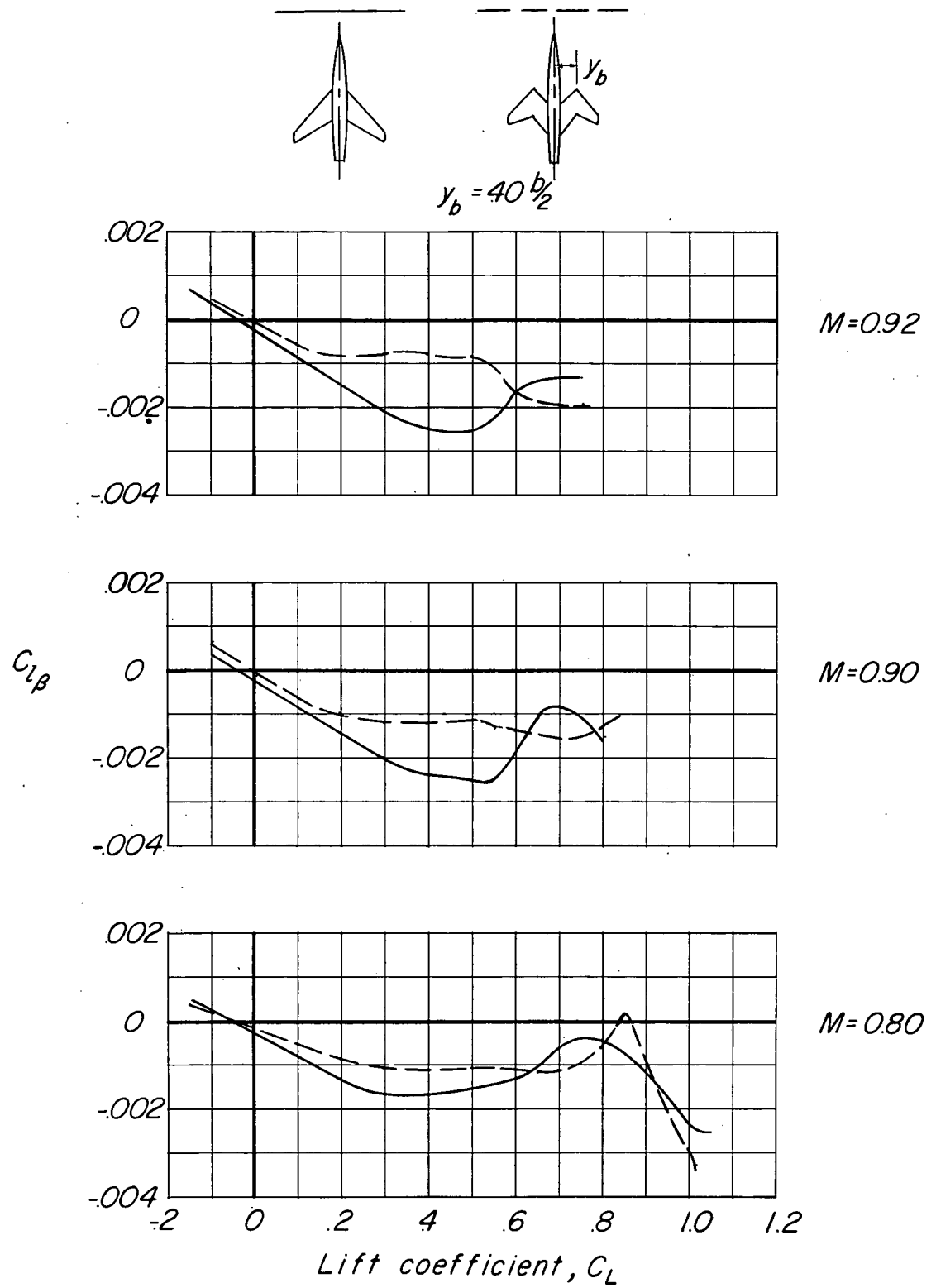

Figure 24.- Effect of a composite wing plan form on rolling moment due to sideslip at high subsonic Mach numbers. $\Lambda = 45^\circ$; $A = 4$; $\lambda = 0.3$. (β in degrees.)

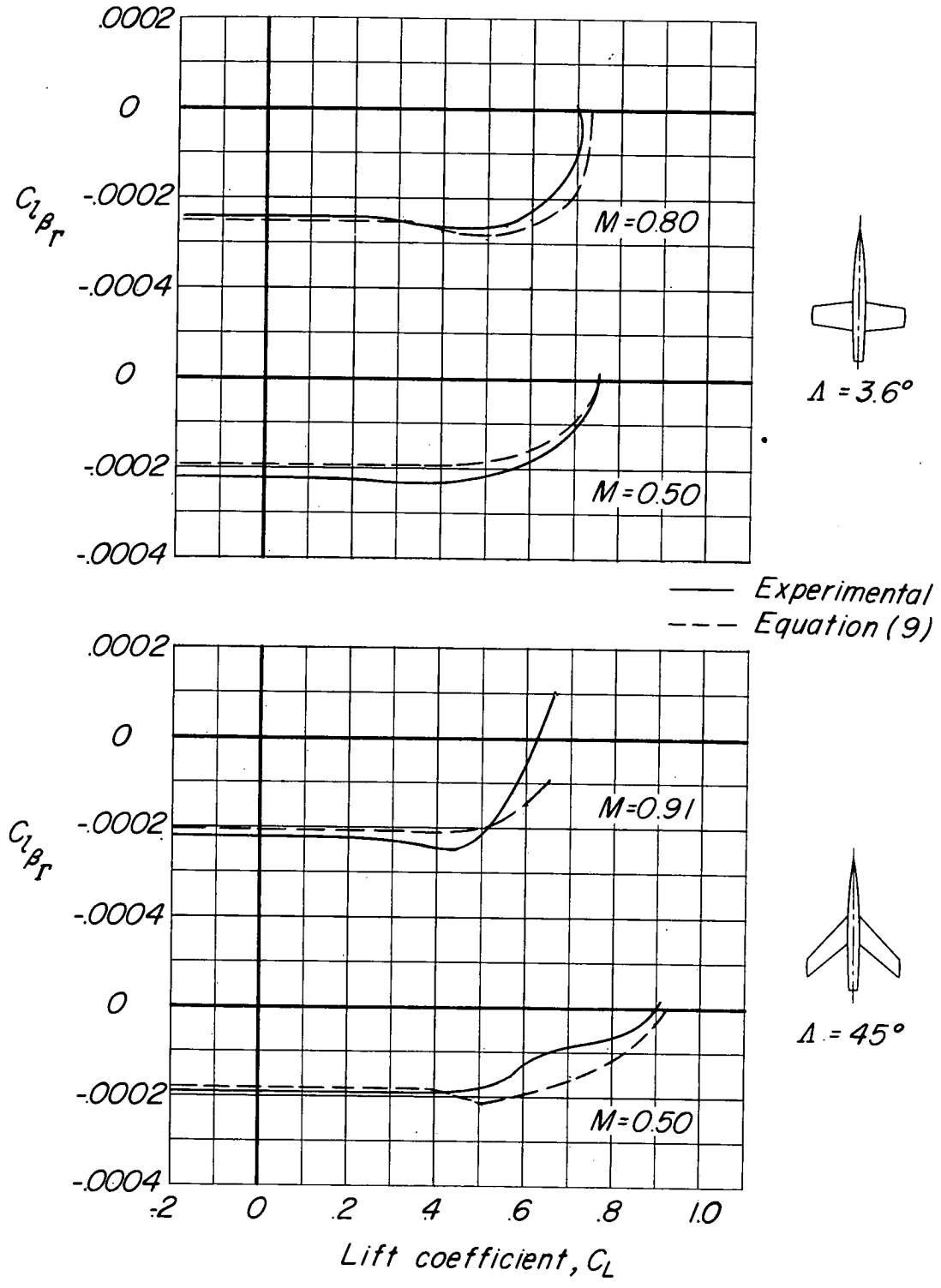

Figure 25.- Comparison of experimental and estimated variation with lift coefficient of the dihedral contribution to rolling moment due to sideslip showing effects of sweep and Mach number. A = 4; λ = 0.6. (β in degrees.)

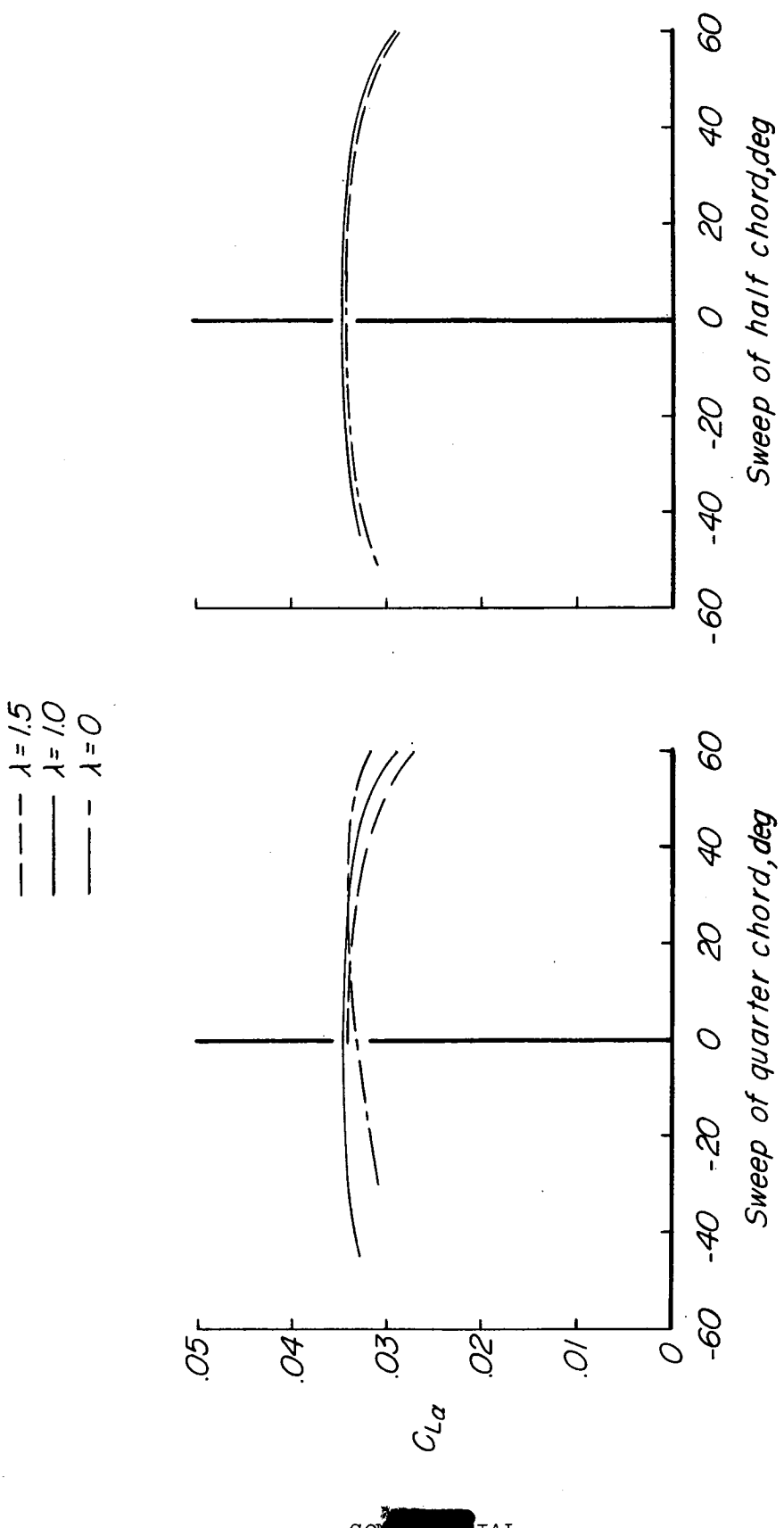

(a) A = 1.5.

Figure 26.- Variation of C_{L_α} with sweep; Weissinger 15-point method. (α in degrees.)

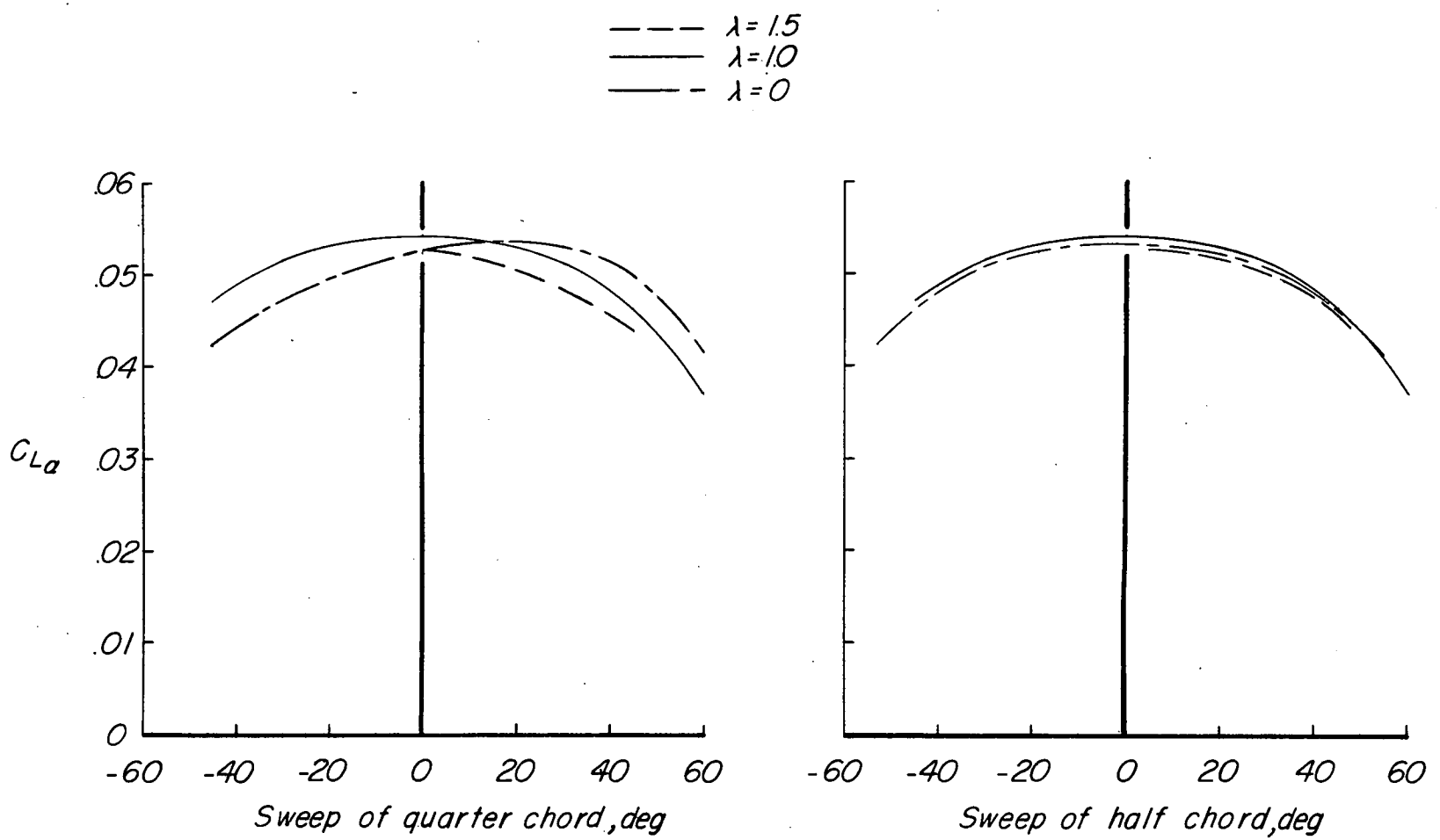

(b) A = 3.0.

Figure 26.- Concluded.

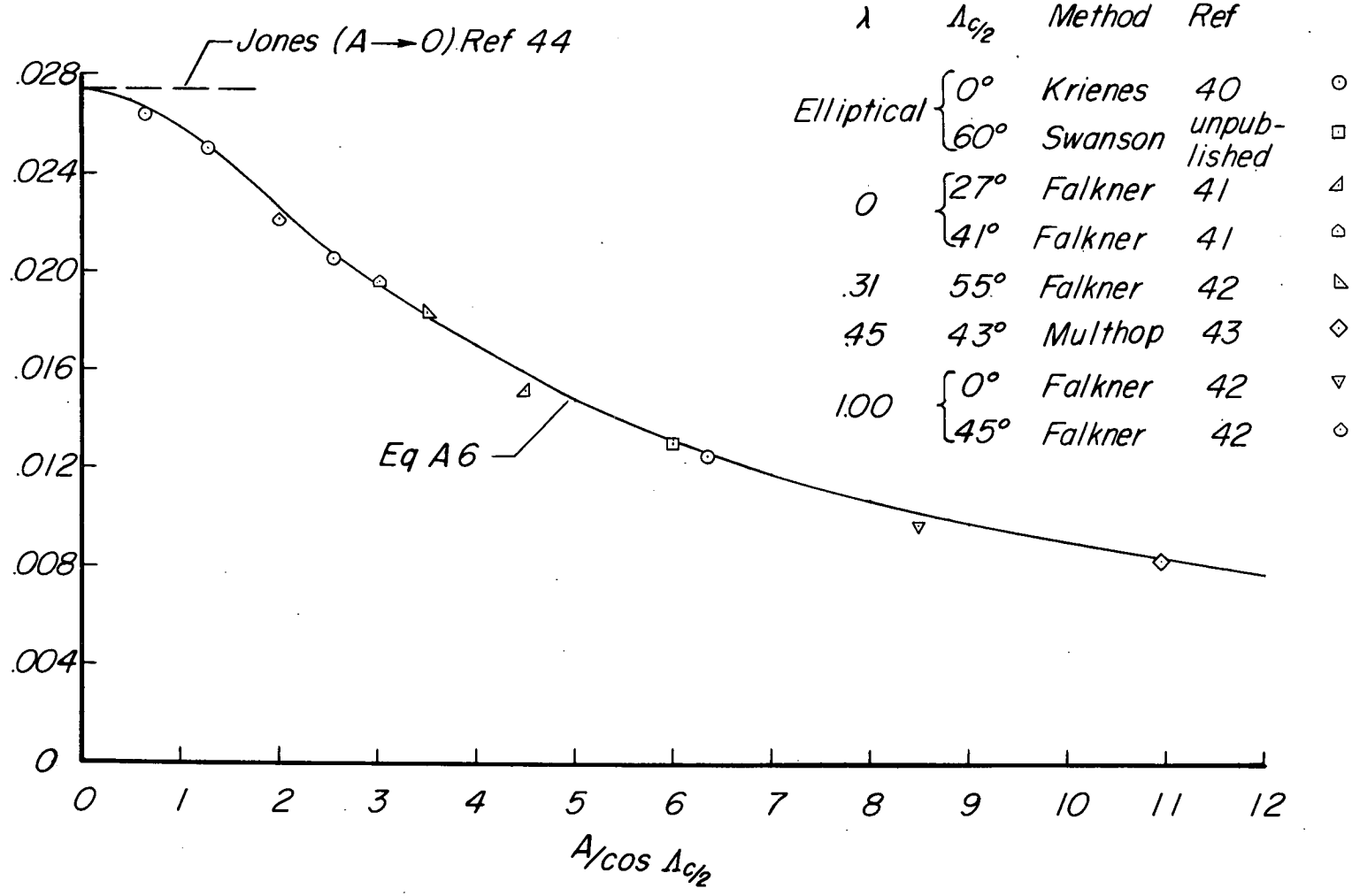

Figure 27.- Variation of $C_{L_\alpha/A}$ with $A/\cos \Lambda_{c/2}$ as determined by several methods. M = 0. (α in degrees.)

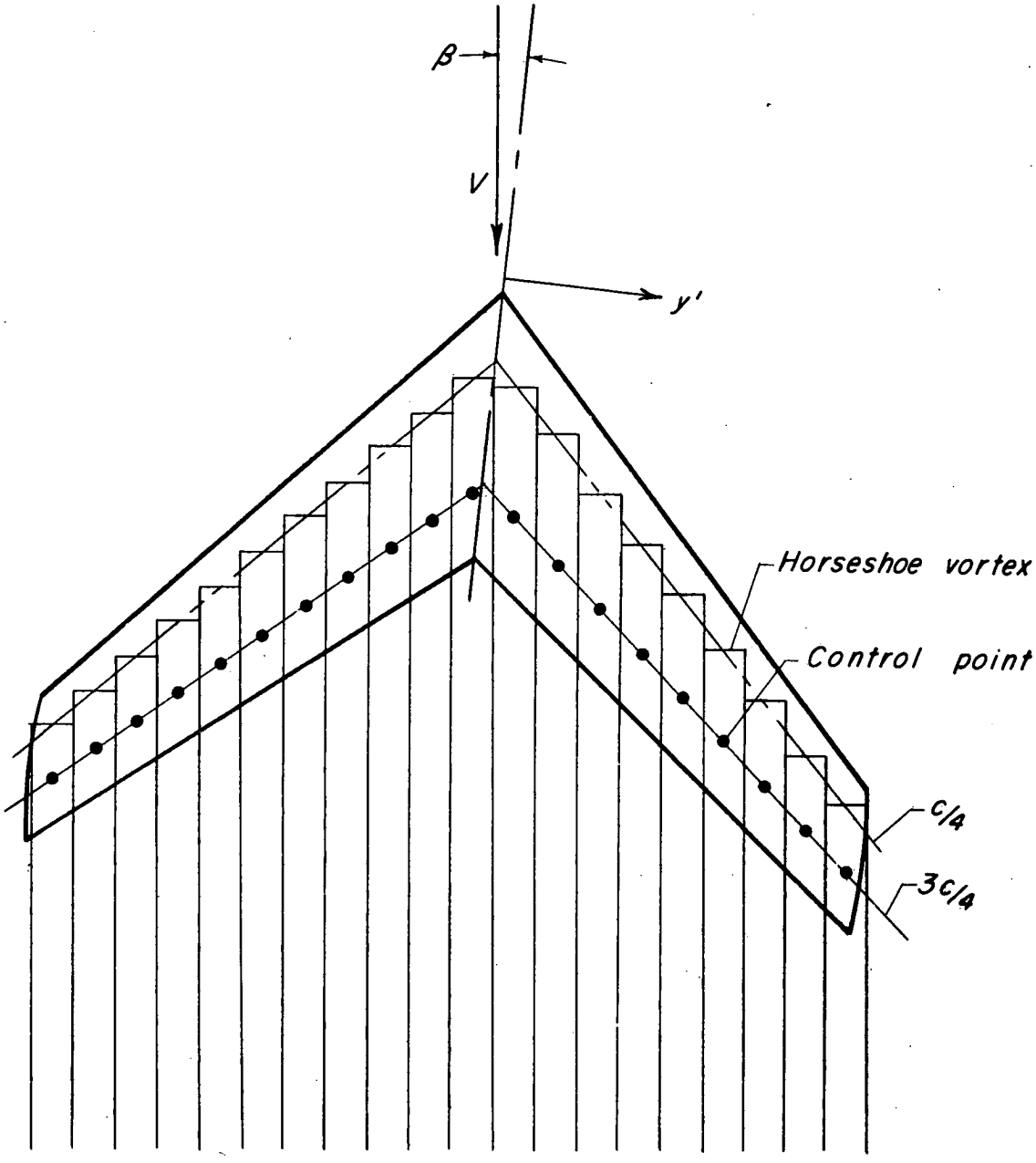

Figure 28.- Vortex system used in estimating rolling moment due to sideslip for isolated wings.

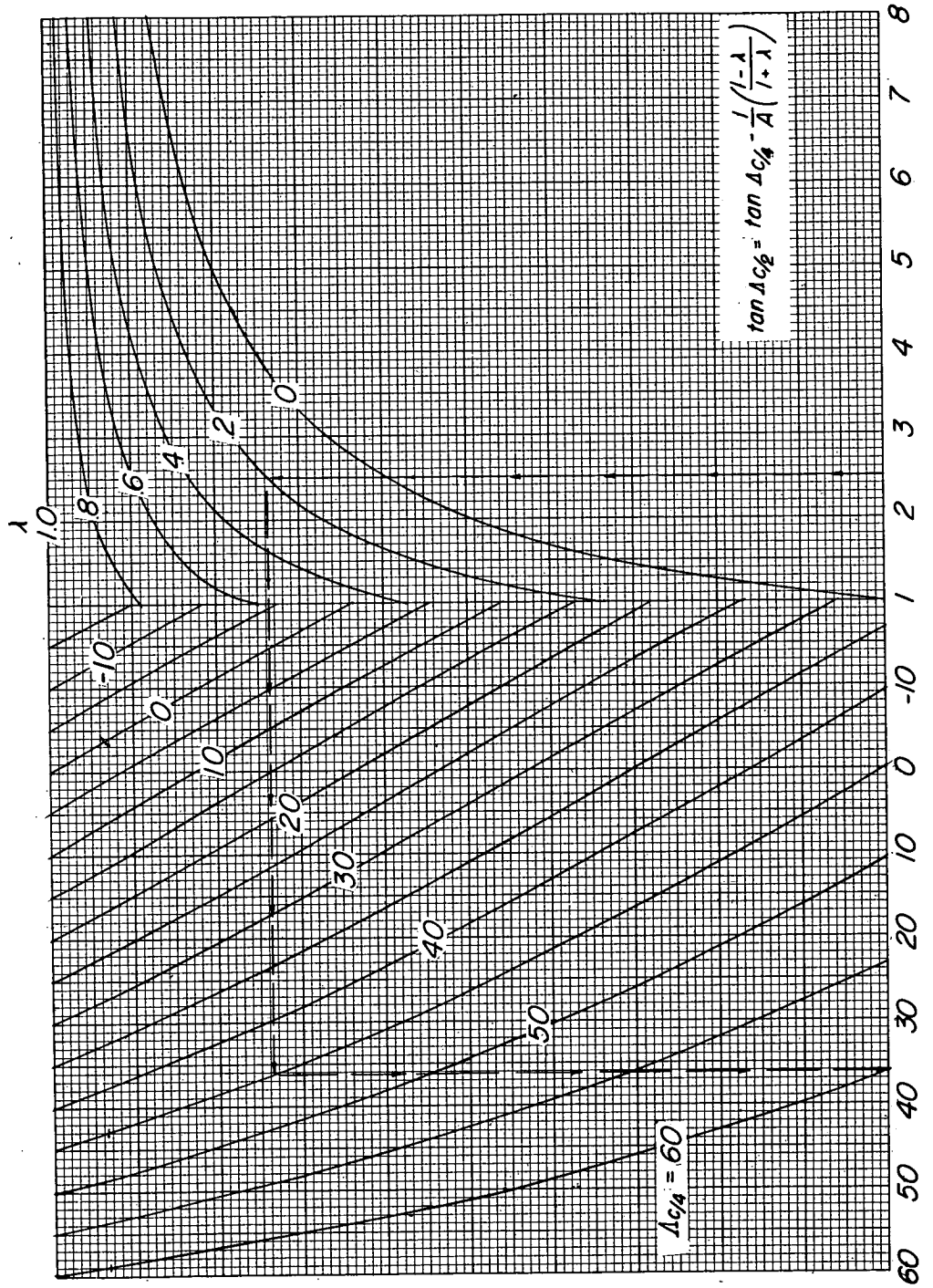

Figure 29.- Nomograph for converting quarter-chord sweep angles to sweep of the half chord.